

Design rules for the chemically fueled self-assembly and disassembly of peptides

Kun Dai

Vollständiger Abdruck der von der Fakultät für Chemie der Technischen Universität München zur Erlangung des akademischen Grades eines

Doktors der Naturwissenschaften (Dr. rer. nat.)

genehmigten Dissertation.

Vorsitzender: Prof. Dr. Matthias Feige
Prüfer der Dissertation: 1. Prof. Dr. Job Boekhoven
2. Prof. Dr. Cathleen Zeymer

Die Dissertation wurde am 14.03.2022 bei der Technischen Universität München eingereicht und durch die Fakultät für Chemie am 12.05.2022 angenommen.

Nothing in life is to be feared, it is only to be understood. Now is the time to understand more, so that we may fear less.

Marie Curie

Nichts im Leben muss man fürchten, man muss es nur verstehen. Jetzt ist es an der Zeit, mehr zu verstehen, damit wir weniger Angst haben.

Marie Curie

Abstract

Biology uses molecular self-assembly to form structures like the cytoskeleton and cell wall. The function of these structures is often regulated through chemical reaction cycles like phosphorylation and dephosphorylation cycles. For example, the ability to assemble and disassemble can be regulated by one reaction cycle at the expense of a high-energy chemical reagent like ATP or GTP. Inspired by nature, man-made chemical reaction cycles that regulate dynamic assemblies have been developed for imitating behaviors associated to living ones and thereby constructing material with unique properties. This thesis aims to develop the design rules in chemically fueled self-assembly with a special focus on the assembly and disassembly.

The thesis starts with an introduction into chemically fueled self-assembly, followed by an example from biology to elucidate the importance of developing chemically fueled self-assembly. After, I summarize the man-made chemical reaction cycles developed to regulate self-assembly and the design strategies to couple those to self-assembly. The final section of the introduction demonstrates other unwanted possible outcomes driven by chemical reactions, i.e., precursor assembles before the addition of fuel, a chemically fueled reaction cycle without self-assembly or kinetically trapped assembly.

In the first experimental chapter of this thesis, i.e., chapter 2, design rules are being developed to avoid these unwanted outcomes. This chapter demonstrates two approaches to regulate the chemically fueled self-assembly behavior from the assembly aspect. When the attractive interactions are rightly balanced with the repulsive interactions, the result is dissipative self-assembly. However, when the repulsive interactions are too strong, no assembly will take place in response to fuel. In contrast, when repulsive interaction is too weak, the assembly is permanent and not dynamic. I generalize the design rules for various peptides and rationalize the different peptide behavior in the context of their energy landscapes.

Chapter 4 demonstrates how different disassembly pathways affect the peptides' behaviors in a chemically fueled reaction cycle. The molecular designs of the peptides are chosen such that they vary in their propensity to form β -sheets and their solubility. The peptides behaviors are controlled from almost non-assembly with chemically fueled reaction cycle, formation of colloids that disassemble when fuel is depleted (chemically fueled self-assembly), to colloids that transition into fibers as fuel depletes (chemically fueled kinetically trapped assembly). The different disassembly pathways are qualitatively understood by the precursor's co-assembly ratio with the product. With this mechanism, we can tune the time colloids transition to fibers by the amount of fuel. After these two experimental chapters, I complete this thesis with a concluding chapter and a chapter which lists my publications.

Zusammenfassung

Die Biologie nutzt die molekulare Selbstorganisation, um ihre Strukturen wie das Zytoskelett und die Zellwand zu bilden. Die Funktion dieser Strukturen wird oft durch chemische Reaktionszyklen wie Phosphorylierungs- und Dephosphorylierungszyklen reguliert. Beispielsweise kann die Fähigkeit zum Auf- und Abbau durch einen Reaktionszyklus auf Kosten eines hochenergetischen chemischen Reagens wie ATP oder GTP reguliert werden. Inspiriert von der Natur wurden künstliche Reaktionszyklen entwickelt, die dynamische Anordnungen regulieren und die Verhaltensweisen von Lebewesen nachahmen. Dadurch können künstliche Materialien mit einzigartigen Eigenschaften konstruiert werden. Diese Arbeit zielt darauf ab, Designregeln in der durch chemische Kraftstoffe angetriebenen Selbstorganisation aufzustellen. Ein besonderer Fokus wird auf die Assemblierung und die Demontage der Strukturen gelegt.

Die Arbeit beginnt mit einer allgemeinen Einführung in die chemisch angetriebenen dissipativen Selbstorganisation, gefolgt von einem Beispiel aus der Biologie, um die Bedeutung der Entwicklung der chemisch angetriebenen dissipativen Selbstorganisation zu verdeutlichen. Anschließend fasse ich die künstlichen chemischen Reaktionszyklen zusammen, die entwickelt wurden, um die Selbstorganisation zu regulieren. Es wird dabei insbesondere auf die Designstrategien eingegangen, wie man die Reaktionszyklen an die Selbstorganisation koppelt. Der letzte Abschnitt der Einführung zeigt andere unerwünschte Ergebnisse, die durch chemische Reaktionen resultieren können. Das sind beispielsweise Selbstassemblierungen ohne die Zugabe von Brennstoff, chemisch angetriebene Reaktionszyklen ohne Selbstorganisation oder kinetisch gefangene Anordnungen.

Im ersten experimentellen Kapitel, d.h. Kapitel 2, werden Designregeln entwickelt, um diese Szenarien zu unerwünschte vermeiden. Dieses Kapitel veranschaulicht zwei Ansätze zur Regulierung des chemisch angetriebenen Selbstorganisationsverhaltens und nimmt dabei Bezug auf den Mechanismus der Assemblierung. Wenn die anziehenden Wechselwirkungen mit den abstoßenden Wechselwirkungen richtig ausbalanciert sind, ist das Ergebnis eine chemisch angetriebene, dissipative Selbstorganisation. Wenn jedoch die abstoßenden Wechselwirkungen zu stark sind, findet keine Selbstassemblierung statt, obwohl Kraftstoff verbraucht wird.

Wenn die abstoßende Wechselwirkung dagegen zu schwach ist, ist die Anordnung dauerhaft und nicht dynamisch. Ich verallgemeinere die Designregeln für eine Vielzahl an Peptiden und rationalisiere das unterschiedliche Peptidverhalten im Kontext ihrer Energielandschaften.

Kapitel 4 zeigt, wie verschiedene Zerlegungswege das Verhalten der Peptide in einem chemisch angetriebenen Reaktionszyklus beeinflussen. Die molekularen Designs der Peptide sind hierbei so gewählt, dass sie in ihrer Neigung zur Bildung von β -Faltblättern und ihrer Löslichkeit variieren.

The peptides behaviors are controlled from almost non-assembly with chemically fueled reaction cycle, formation of colloids that disassemble when fuel is depleted (chemically fueled self-assembly), to colloids that transition into fibers as fuel depletes (chemically fueled kinetically trapped assembly).

Das Verhalten der Peptide wird fast ausschließlich von chemisch angetriebener Nicht-Assemblierung, Bildung von Kolloiden, die sich zerlegen, wenn der Brennstoff erschöpft ist (chemisch angetriebene Selbstorganisation), bis hin zu Kolloiden, die bei Brennstoffmangel in Fasern übergehen (chemisch angetriebene kinetisch gefangene Anordnung), gesteuert. Die unterschiedlichen Zerlegungswege werden qualitativ durch das Co-Assemblierungsverhältnis des Vorläufers mit dem Produkt beschrieben. Mit diesem Mechanismus kann die Zeit, in der die Kolloide in Fasern übergehen, durch die Menge an Brennstoff eingestellt werden.

Nach diesen beiden experimentellen Kapiteln schließe ich diese Arbeit mit einer Zusammenfassung und einer Liste mit Veröffentlichungen ab.

Abbreviations

A		Alanine
ADP		Adenosine diphosphate
AMP		Adenosine monophosphate
ATP		Adenosine triphosphate
CAC		Critical aggregation concentration
D		Aspartic acid
E		Glutamic acid
EDC		1-Ethyl-3-(3-dimethylaminopropyl) carbodiimide
F		Phenylalanine
Fmoc		Fluoren-9-ylmethoxycarbonyl
G		Glycine
GTP		Guanosine triphosphate
GDP		Guanosine diphosphate
hr		hour
L		Leucine
LCD		Liquid-crystal display
min		minute
Nap		Naphthoxyacetyl
PKA		Protein kinase A
R		Arginine
S		Serine
TFA		Trifluoroacetic acid
UV		Ultraviolet
Y		Tyrosine

Table of Contents

1. Design of chemically fueled self-assembly	1
1.1 Molecular self-assembly.....	2
1.1.1 In-equilibrium self-assembly.....	2
1.1.2 Out-of-equilibrium self-assembly	3
1.1.3 Chemically fueled self-assembly	3
1.2 The unique properties of chemically fueled self-assembly.....	5
1.3 How to design chemically fueled self-assemblies	7
1.3.1 Design of chemical reaction cycles	7
1.3.2 Coupling assemblies with chemical reaction cycles.....	13
1.4 Other outcomes driven by chemical reactions	20
1.4.1 Energy landscape for other outcomes.....	20
1.4.2 Precursor assemblies	21
1.4.3 Chemically fueled reaction cycle without self-assembly	23
1.4.4 Chemically fueled kinetically trapped assembly.....	25
1.5 Conclusion and Outlook	27
2. The aim of this thesis.....	28
3. Regulating chemically fueled peptide assemblies by molecular design.....	30
4. Morphological transitions in chemically fueled self-assembly	68
5. Conclusion and Outlook.....	97
6. Further publications	99
7. Acknowledgments	100
8. References.....	102

1. Design of chemically fueled self-assembly

Self-assembly describes the process in which the disordered components form an organized structure driven by the interactions between the components themselves.¹⁻⁵ When the disordered components are molecules, the process is called molecular self-assembly.⁶ The formation of the molecular self-assembly structures is the result of non-covalent interactions, such as hydrogen bonding, π - π stacking, electrostatic interactions, hydrophobic effects, van der Waals interactions, and others.^{4,6,7} With these interactions, various structures can be built, such as fibers⁸⁻¹⁰, vesicles^{11, 12}, micelles^{13, 14}, and colloids¹⁵. Some essential and common materials can be created, such as liquid crystals¹⁶ in LCD (liquid crystal display)^{17, 18} and supramolecular hydrogels in biomedicine.¹⁹

Molecular assemblies are vital to life. Bilayer membranes, ribosomes and nucleic acid transcription machinery are all formed through molecular self-assembly. In some cases, the assemblies are regulated by the rule of thermodynamics, which occurred in- or close-to-equilibrium. In other instances, the assemblies are controlled by non-equilibrium self-assembly to support dynamic processes, such as the dynamic exchange of substance. These functions are governed by kinetics and continuously dissipate energy with chemical reactions.¹ For example, the self-assembly of tubulin is driven by the hydrolysis of GTP.²⁰ By mimicking such non-equilibrium self-assembly as found in biology, we can create materials with unique functions, which cannot be achieved in equilibrium. These unique functions include the ability to self-heal.²¹ However, most of the molecular assembled materials developed so far are far from those observed in biology. It is still challenging to translate such properties into fully synthetic materials. Furthermore, understanding these out-of-equilibrium behaviors will help us imitate life-like behavior and help us uncover the origin of life, or even synthesize life from the bottom-up.

In this chapter, I will introduce what molecular assembly is, including the chemically fueled self-assembly. I will explain why we focused on chemically fueled self-assembly, how to design chemically fueled self-assembly and other outcomes in designing chemically fueled self-assembly.

1.1 Molecular self-assembly

In this section, I will introduce the different types of molecular self-assembly according to the relative stability of the assembled structure, the building blocks and the precursors in the energy landscape. From a thermodynamic perspective, the self-assembly can be classified into three categories, e.g., 1. in equilibrium self-assembly (Figure 1A); 2. out of equilibrium self-assembly (Figure 1B); 3. chemically fueled self-assembly.

Understanding the energy landscape can be one essential step when designing building blocks to attain desired molecular self-assembly. The detailed description of each type of assembly will be explained in the following sections.

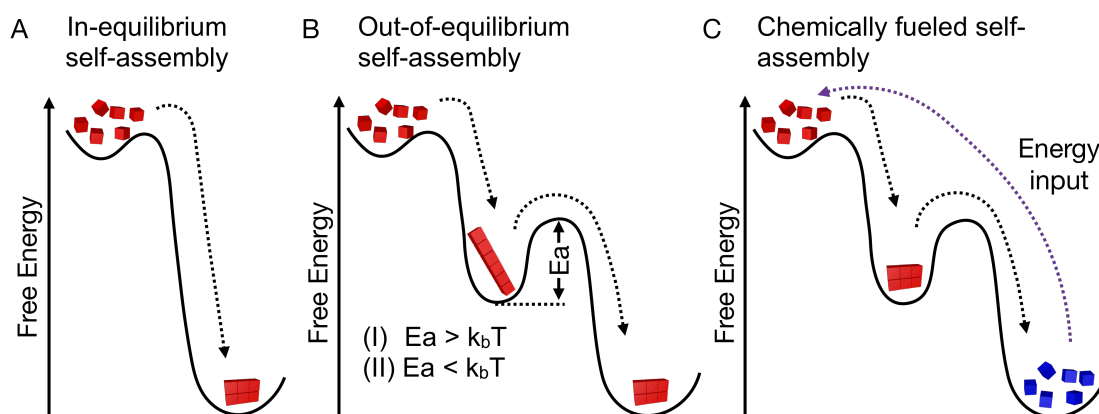


Figure 1: Schematic free energy landscape of different self-assembly processes. **A)** In-equilibrium self-assembly; **B)** Out-of-equilibrium self-assembly: (I) kinetically trapped self-assembly and (II) metastable self-assembly; **C)** Chemically fueled self-assembly.

1.1.1 In-equilibrium self-assembly

In-equilibrium self-assembly is the most explored method of creating assemblies. Scientists have created countless self-assembled materials,²²⁻²⁴ such as the assembly of metal-organic frameworks (MOF) for gas storage and separation applications,²⁵⁻²⁷ assembly of liquid crystals in LCD.^{17, 18} In-equilibrium self-assembly occurs when the self-assembled state is in the global minimum of the energy landscape, while the unassembled building blocks are in a higher energy state (Figure 1A). In other words, the assembly is a process that gains free energy and thus is thermodynamically favored.⁴ In the assembly state, the building blocks can be exchanged dynamically with those in

solution, but the rates are equal; therefore, there is no net flow of energy, and the system can stay stable for a long time.²⁸ The exchange property mentioned above plays a vital role in the assembly process because this process provides a chance for the system to find the global minimum, and therefore, the thermodynamically most-favored state. The rate of exchange is strongly dependent on the strength of the interactions between the building blocks. For example, spherical micelles assemble with weak interactions so that the exchange can occur at a relatively high rate.²⁹ In contrast, the bilayer of phospholipids is formed with strong interactions, leading to orders of magnitude lower exchange rates and much weaker dynamics.³⁰

Furthermore, the exchange property allows the in-equilibrium self-assembly to change the assembled structure with external stimuli such as changes in temperature, pH levels, or adding salt. These external stimuli can change the energy landscape's global minimum, therefore changing the structure, possibly even leading to disassembly.

1.1.2 Out-of-equilibrium self-assembly

Out-of-equilibrium self-assembly occurs when the assembled building blocks are not in the lowest state in the energy landscape, but they are at a local minimum state which is higher than the global minimum (Figure 1B). The assembled building blocks are trying to find the global minimum as it is the thermodynamically favored state. Thus, there are two different scenarios: i.e. (I) kinetically trapped assembly and (II) metastable assembly. The two different assemblies are dependent on the energy barrier (E_a) that the local minimum state should overcome to reach the global minimum. If the energy E_a is higher than the energy that the system has (k_bT , Boltzmann constant (k_b), and temperature (T)), the building blocks have no chance to exchange with the surroundings and remain stable in this state, which is called kinetically trapped assembly. If the energy E_a is relatively low, the energy available (k_bT) in the system can help the building blocks leap from the local minimum to the global minimum. That means the building blocks can exchange with the surroundings but at a very slow rate, which we call metastable assembly. For both assemblies, external stimuli such as sonication and heating may change the original state.^{31, 32}

1.1.3 Chemically fueled self-assembly

The final type of assembly I will discuss is dissipative out-of-equilibrium self-assembly, which is a process in which the assembly exists out-of-equilibrium driven by the transduction of energy (Figure 1C). When the energy is a chemical fuel, we call it

chemically fueled out-of-equilibrium self-assembly or chemically fueled self-assembly as a brief name. Specifically, a precursor resides in the global minimum and cannot self-assemble. Only upon activation through a chemical reaction is it transferred to an activated building block that resides in a higher position in the energy landscape. In this higher state, the activated building block can self-assemble and gains energy upon doing so. That assembly is thus represented by a local minimum state in the energy landscape. However, this assembled structure is not stable since another reaction for deactivation brings the activated building blocks to the precursors.

The fuel-driven self-assembly continuously undergoes this pathway until all fuel has been converted. When all activated products transfer back to the precursor, the reaction will stop, and the total system returns to the start global minimum state. If the energy input is constant, we can assume that the number of activated building blocks will keep the system in the assembled state.^{33, 34}

In essence, chemically fueled self-assembly is self-assembly coupled to a catalytic reaction cycle that continuously converts chemical fuel and comprises a minimum of two reactions, i.e., one activation and one deactivation reaction. In the activation reaction, a non-assembled precursor reacts or binds with the fuel yielding a product in an activated state for assembly. Deactivation reaction: the product is intrinsically unstable and reverts to the precursor. As a consequence, the self-assembly is regulated by the product concentration. When the activated building block (product) concentration is above the critical aggregation concentration (CAC), self-assembly occurs (Figure 2). The driving force of the reaction cycle is the conversion of energy to waste. Besides the chemical fuel, light can also be used as an energy source. The most significant advantage of using light as energy is that the waste in this case is heat, which usually does not interfere with the reaction cycle or assembly process. However, chemical fuel as energy is more relevant to biology.³⁵

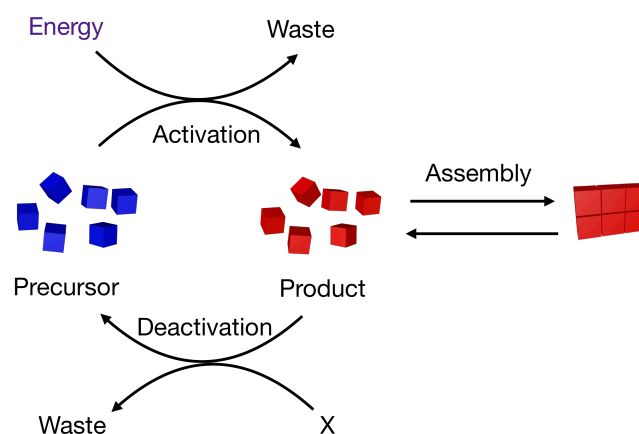


Figure 2: Scheme of a chemical reaction cycle driven by energy.

In the next section, I will introduce chemically fueled self-assembly examples found in biology and explain why the chemically fueled self-assembly is the focus of this thesis.

1.2 The unique properties of chemically fueled self-assembly

The field of chemically fueled self-assembly is in its infancy. However, biological examples include the chemically fueled self-assembly of actin filaments, intermediate filaments and microtubules driven by guanosine triphosphate (GTP)- or adenosine triphosphate (ATP)-fueled chemical reaction cycles. The hydrolysis of GTP or ATP kinetically controls the assembly's dynamic behavior, thus regulating a cell's internal organization, shape, motility and life cycle.^{20, 36} As the largest cytoskeletal components, microtubules are driven by the hydrolysis of GTP and contribute to cell trafficking, cell signaling, cell division and proliferation.^{20, 36} As a result, deregulation of microtubule function can lead to neurodegenerative diseases, including amyotrophic lateral sclerosis, hereditary spastic paraplegia, Alzheimer's disease, and Parkinson's disease.^{37, 38}

Dynamic microtubules are controlled by the continuous activation and deactivation of the molecular building block, tubulin. Tubulin is a heterodimer comprising an activated α - and a β -tubulin. Upon binding with GTP as chemical fuel, the α - and β -tubulin are activated. With two molecules of GTP bound, each tubulin is activated and the activated tubulin can form protofilaments by supramolecular polymerization (Figure 3).²⁰ The microtubules are composed of 13 filaments connected in parallel and transversely to produce a rigid hollow tube with a diameter of 25 nm.³⁹ Since capping proteins stabilize the microtubules on one end of the tube, the growth and shrinkage can only occur on the other end. When the activated tubulin dimer is hydrolyzed from GTP-bound to guanosine diphosphate (GDP)-bound tubulin, with a delay, the stabilizing cap is lost, and the microtubules will quickly shrink, known as a catastrophe-phase. When the activation is faster than the deactivation, the microtubules grow.^{20, 40} Consequently, when the GTP is in high or low concentration, the formation of activated tubulin would be faster or slower than deactivation of the tubulin, leading to the growth or shrinkage of microtubules. By tuning the GTP concentration, biology can regulate the shrinkage and growth of microtubules, i.e., with kinetic control. In other words, the assembly and disassembly are not constant but rely on the concentration of chemical fuels, which is drastically different from self-assembly under thermodynamic control. This feature offers unique properties, such as the ability to self-heal damaged microtubules. Furthermore, the disassembled tubulin can be recycled rapidly and perform a role in other self-assembled structures. The microtubule self-assembly is a typical example of

chemically fueled self-assembly, in which GTP is used as a fuel to drive the reaction and control the assembly. In biology, examples like the formation of microtubules driven by a chemically fueled reaction cycle are numerous. Exploration of this field helps to increase our understanding of mechanisms in some diseases, and can further offer a pathway to the synthesis of life and build functional materials controlled in space and time that are adaptivity or even self-healing. Therefore, scientists have put some effort into building chemically fueled self-assemblies in recent years, and I will introduce some of them in the following sections.

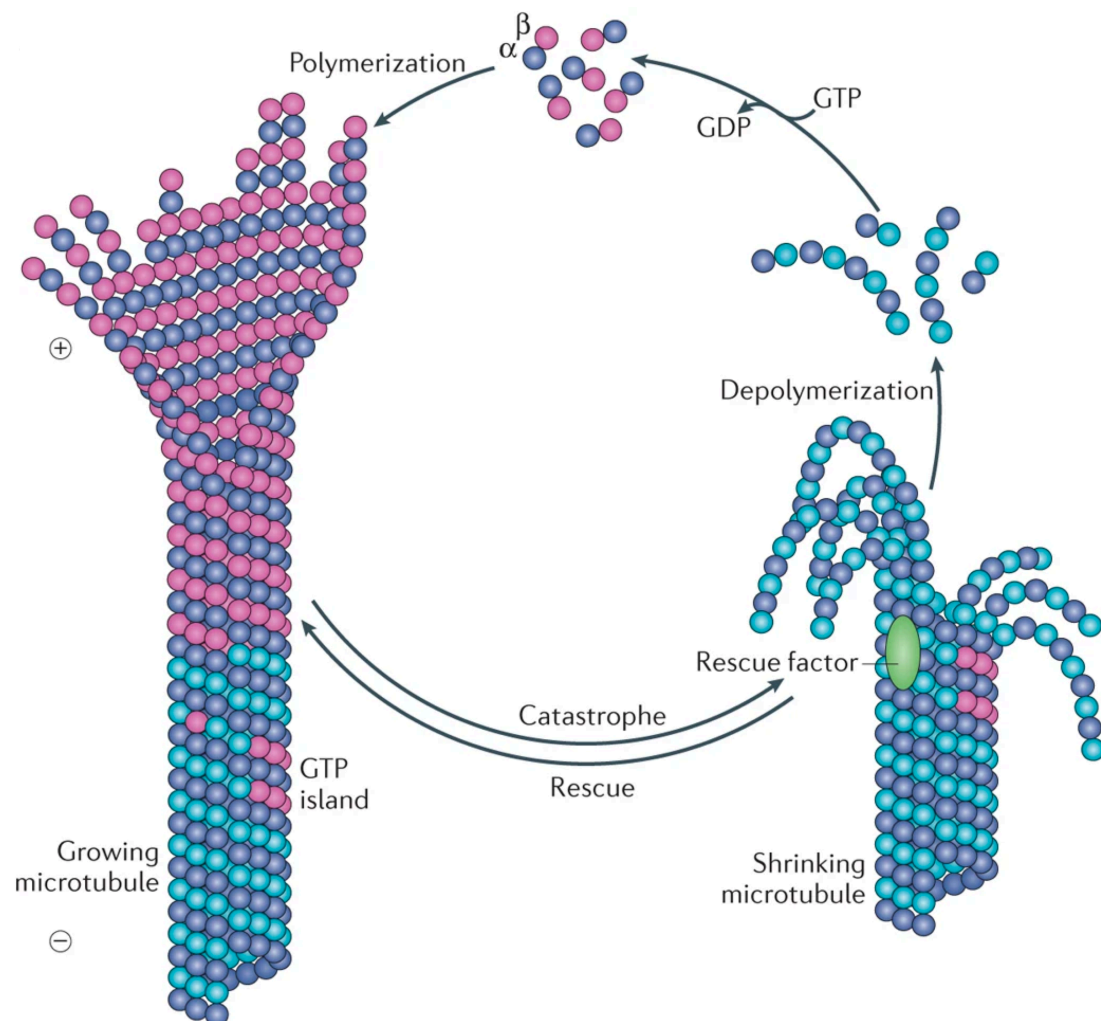


Figure 3: The cycle of tubulin assembly and disassembly is fueled by hydrolysis of the GTP bound to β -tubulin, enabling microtubules to switch between catastrophes and rescues.²⁰ Reprinted from reference {20} by permission from the Nature Publishing Group, a division of Macmillan Publishers Limited. Copyright © 2015.

1.3 How to design chemically fueled self-assemblies

In the previous two sections, I have introduced what chemically fueled self-assembly is, and why we should focus on it. In this section, the design of chemically fueled self-assembly will be discussed. Firstly, I will focus on the design of chemical reaction cycles (section 1.3.1). Next, I demonstrate how to couple the self-assembly process to these chemical reaction cycles (section 1.3.2). I will close with two different strategies to induce chemically fueled self-assembly, *i.e.*, the charge abolishment strategy and the transient linker strategy.

1.3.1 Design of chemical reaction cycles

Generally, the chemical reaction cycle comprises two reactions, e.g., an activation and deactivation reaction. In the activation reaction, the non-assembled precursor is activated by a reaction with a chemical fuel. In the deactivation reaction, the activated product reverts to the precursor. The two reactions have to occur in the same conditions, such as the same temperature, pH level, and solvent. The activation and deactivation should work independently and avoid side reactions. Furthermore, the background of fuel consumption should be much slower than the reaction in the presence of precursors.^{34,41} Fuel can play a direct or indirect role in the chemical reaction cycle. In the direct role, the fuel directly react with the precursor and be transferred to waste. If it is an indirect role, the fuel will not react with precursors, and not produce waste.^{42,43} According to these requirements, in 2010, van Esch and coworkers reported the first example of dissipative out of equilibrium self-assembly driven by a chemical reaction cycle.⁴⁴ During the last decade, chemists, biologists and material scientists have been inspired to build more dynamic systems, creating more chemical reaction cycles to drive the dissipative self-assembly. Because of the significant importance of peptide assembly in biology and material science,⁴⁵⁻⁴⁷ I will mainly focus on reaction cycles involving peptides as precursors.

1.3.1.1 Hydrolysis of ester driven reaction cycle

As one of the most efficient catalysts, enzymes have been explored by Ulijn and coworkers to build the transient formation of an amide bond system^{48,49} (**Figure 4**). They chose one amino acid as a precursor, such as L-tyrosine amide (Y-NH₂), one acyl donor tyrosine methyl ester as fuel to react with the precursor. In the presence of the

digestive enzyme, α -chymotrypsin, the corresponding dipeptide (Nap-YY-NH₂) rapidly formed, liberating methanol as waste in the hydrolysis of the ester. Meanwhile, the deactivation occurs with the same enzyme, which slowly catalyzes the breaking of the amide bond in the aqueous media generating the original precursor and a carboxylic acid as waste. Under the same conditions but without this enzyme, this reaction cycle cannot work. The chemical reaction cycle can be regulated by changing pH and enzyme concentration. In a follow-up study, they expand the usability of this chemical reaction cycle by using different types of amino acid-precursors.⁴⁹

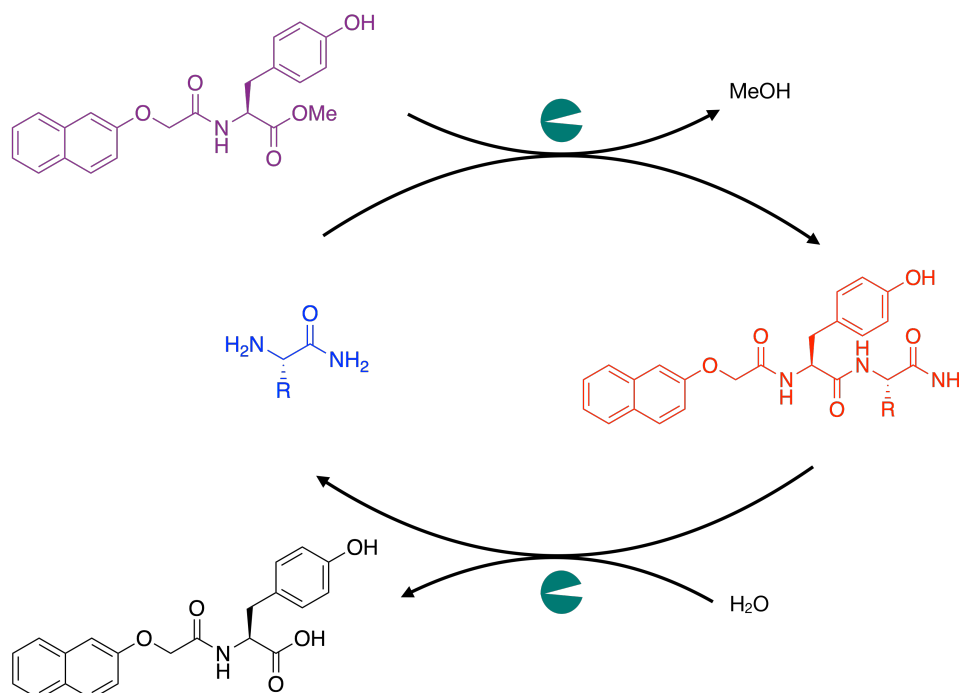


Figure 4: General scheme of the chemical reaction cycle which is driven by the hydrolysis of the methyl ester-based fuel (purple). An amino acid (precursor-blue) reacts with methyl ester-protected amino acid (fuel-purple) in the presence of chymotrypsin, connecting the two molecules via an amide bond (product-red) and releasing MeOH as waste. The deactivation is also catalyzed by the same enzyme in the presence of water. The precursor (blue) is then recovered and the corresponding carboxylic acid is liberated as waste. Adapted with permission from reference {48}. Copyright {2013} American Chemical Society.

1.3.1.2 ATP hydrolysis driven reaction cycle

The hydrolysis of ATP, like in biology, is also used as the energy source to drive chemical reaction cycles.⁵⁰⁻⁵⁷ As an example, I will discuss one of the artificial examples based on peptide-derivative precursors reported by Hermans and co-workers

(Figure 5).⁵³ For the activation reaction, they use ATP as fuel. The enzyme protein kinase A (PKA) phosphorylates two serine amino acids on the precursor, in this case, a symmetric peptide derivative conjugated to a peptide–perylene diimide derivative (PDI). The activation reaction changes the precursor’s overall charge from +4 to charge neutral zwitterionic. The change in overall charge induces a change in the morphology of the corresponding supramolecular polymer. While the precursor (PDI) self-assembled into relatively short P-helical fibers, the activated state (p2-PDI) assembled in larger M-helical fibers.

For the deactivation reaction, a second enzyme, λ -protein phosphatase (λ PP) is used to dephosphorylate the product p2-PDI back to the precursor PDI releasing inorganic phosphate as waste (Figure 5). This elegant example mimics biological behavior to some degree since phosphorylation and dephosphorylation cycles support many living behaviors in biology.⁵⁸ However, the P_i is an inhibitor for the enzyme in the deactivation of p2-PDI, which means many refuel cycles will slow down even stop the deactivation. As a result, they built a continuous stirred membrane reactor by a constant influx of fuel to exchange the fraction time by time.

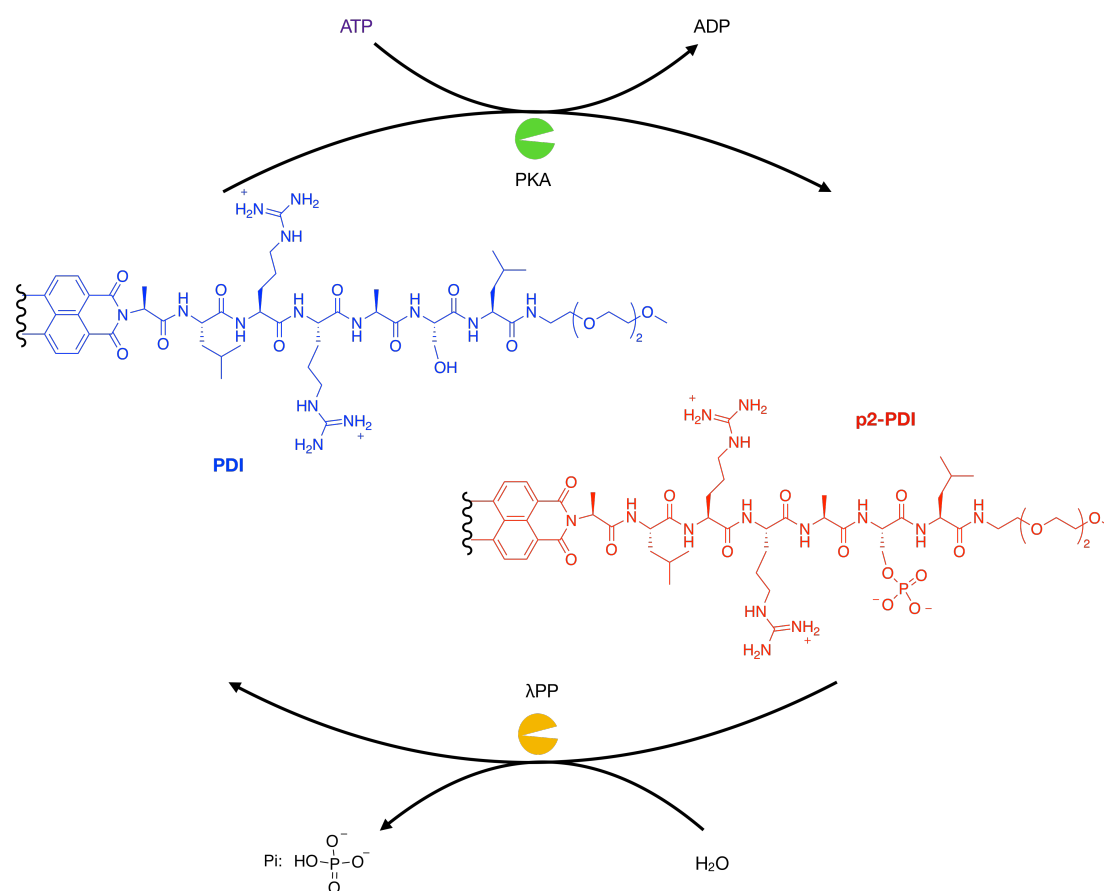


Figure 5: General scheme of the chemical reaction cycle, which is driven by ATP hydrolysis. In an enzyme (PKA) catalyzed reaction, peptide-based compound PDI

(precursor-blue) transfers to p2-PDI (product-red) in the presence of ATP (fuel, purple). The p2-PDI can be deactivated back to the original PDI with the other enzyme (λ PP) in the presence of H_2O realizing inorganic phosphate as waste. Adapted from reference {53} by permission from Springer Nature Ltd., Copyright © 2017.

1.3.1.3 Reduction-oxidation reaction cycles

When designing chemical reaction cycles, redox reactions are also an option to drive dissipative self-assemblies,⁵⁹⁻⁶² in which the fuel is usually an oxidizing agent while a reducing agent is required for the deactivation reaction. For example, the Guan group designed a chemical reaction cycle driven by hydrogen peroxide (H_2O_2) as an oxidizing agent for the activation, and dithiothreitol (DTT) as a reducing agent for the deactivation (Figure 6).⁶³ In the activation reaction, a cysteine precursor is oxidized to its corresponding disulfide dimer for assembly. In the presence of DTT, the deactivation converts the disulfide dimer to the original precursor. The chemical reaction cycle is pH and fuel-concentration sensitive, which allows for the regulation of the reaction rates. However, the reaction rates are relatively slow in comparison with other examples reported.

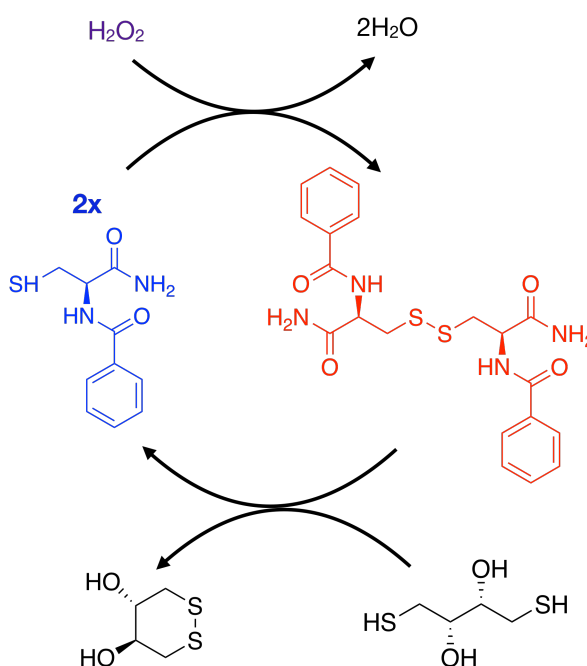


Figure 6: General scheme of the chemical reaction cycle, which is driven by oxidizing and reducing agents. A cysteine-based compound (precursor in blue) reacts with H_2O_2 (fuel in purple) to build the disulfide product (red). The deactivation occurred in the presence of dithiothreitol, which transfers the activated building block to the start

compound. Adapted from reference {63} by permission from the Wiley-VCH Verlag GmbH & Co. KGaA, Copyright © 2020.

1.3.1.3 Carbodiimide driven reaction cycle

Recently, Boekhoven⁶⁴ and Hartley⁶⁵ introduced a chemical reaction cycle driven by hydration of carbodiimides as a fuel. The source of carbodiimide can be N-cyclohexyl-N'-(2-morpholinoethyl)carbodiimide-methyl-p-toluenesulfonate (CMC), N,N'-Diisopropylcarbodiimide (DIC) and ethyl-3-(3-dimethylaminopropyl)carbodiimide (EDC), but the latter is most used. In this reaction, a carboxylate-carrying precursor is activated and converted to an anhydride or active ester. Meanwhile, the transient product is deactivated by reaction with water, which means that the deactivation occurs spontaneously. Furthermore, this chemical reaction cycle can work at a broad temperature range, compared with the temperature-sensitive reaction cycle using enzymes. The carbodiimide-driven reaction cycle⁶⁶⁻⁷¹ has further advantages. One of which is the fact that the carboxylic acid group is common and abundant that a wide range of precursors can be used, such as peptides,^{72, 73} nanoparticles,⁷⁴ polymers^{66, 75-78} and small organic molecules.⁷⁹ This provides an excellent platform for researchers to explore chemically fueled self-assemblies.⁸⁰⁻⁸⁵

One pioneering example is from the Boekhoven group.⁶⁴ The authors used fluoren-9-ylmethoxycarbonyl-(Fmoc-) amino acids or peptides containing a dicarboxylate group as precursors. All precursors are dissolved in aqueous buffer at pH 6, a pH value higher than the precursors' pKa. Upon EDC addition, a precursor with two anionic carboxylate groups converts into an uncharged anhydride liberating one molecule of EDU as waste. The loss of the two negative charges gives the anhydride a chance to self-assembly due to the lower solubility (Figure 7). I will discuss the assembly process in the next section. As mentioned above, the deactivation reaction occurs spontaneously since the anhydride product is intrinsically unstable in water and will hydrolyze to the precursor. The assembly structure can be regulated by the R group, and the lifetime of the reaction cycle can be tuned by the concentration of fuel.

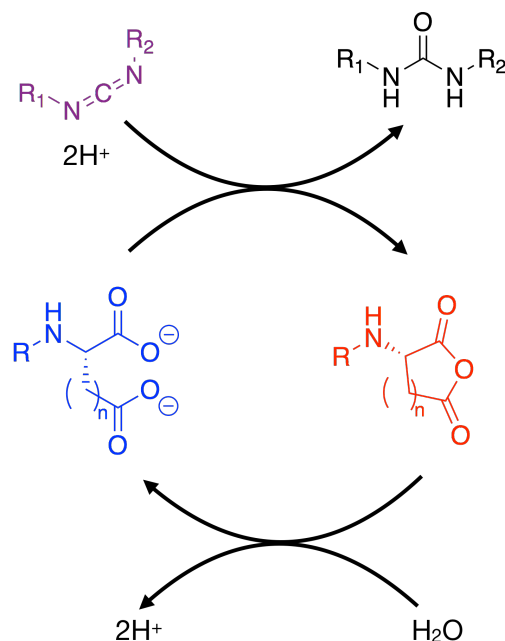


Figure 7: A chemical reaction cycle driven by the hydration of carbodiimides. Amino acids and short peptides containing a dicarboxylic group precursor (blue) react with carbodiimide fuel (purple) to their corresponding anhydride product (red). The anhydride spontaneously reacts with water back to the original dicarboxylic acid. Adapted from reference {64} by permission from Springer Nature Ltd., Copyright © 2017.

Besides the di-carboxylic group reported by Boekhoven and coworkers, other examples in the literature applied the same strategy but used a single carboxylic group as precursors.^{85, 86} In this case, the consumption of EDC connects, via an intramolecular reaction, two precursor molecules into a symmetric anhydride. The corresponding anhydride reverts to the precursor spontaneously by the hydrolysis in water, similarly to the above example.

As we mentioned above, the hydration of carbodiimides can be used to drive the formation of anhydrides and also the formation of active esters.⁸⁷ In the case of the latter, the chemical reaction cycle requires the presence of a second nucleophile apart from the original carboxylic acid precursor. The lifetime of the transient product can be easily tuned over several orders of magnitude. For example, the intramolecular anhydrides have a 1s to 10 s half-life,^{64, 79, 88} and NHS-esters have a 100 s of half-life time,⁸⁹ while nitrophenol esters can reach 10000 s.⁹⁰ The short half-lives can be used for fast responses in molecular machines, while the longer half-lives can be applied for molecules to nucleate for molecular assemblies.

Das and coworkers⁸² reported the formation of activated esters driven by EDC consumption. In this example, a carboxylate precursor containing a histidine residue (blue) reacts with a second nucleophile, p-nitrophenol (NP) in the presence of EDC. As a result, an activated ester (red) is formed which hydrolyze in water to the precursor (Figure 8).^{82, 83} It is important to highlight the role of the histidine in this chemical reaction cycle. The histidine cooperatively catalyzes the formation (playing as a base) and breaking of the ester bond (shuttling protons and influencing the local pH) during the activation reaction. The rate of deactivation can be controlled by the pH value, and the highest activity is at pH=6.5.

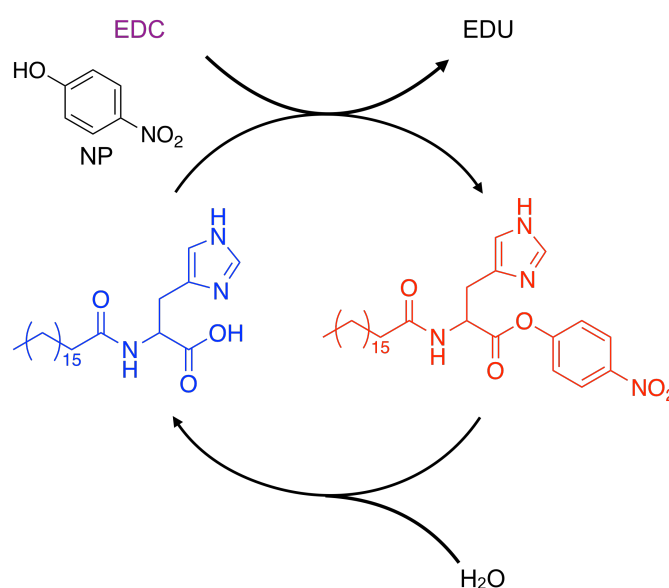


Figure 8: General scheme of the chemical reaction, which is driven by EDC. The precursor (blue) and one nucleophile p-nitrophenol are converted to an ester (red) driven by EDC. Adapted from reference {82} by permission from the Wiley-VCH Verlag GmbH & Co. KGaA, Copyright © 2019.

As shown above, scientists have put much effort into developing different chemical reaction cycles, making it possible to mimic life behaviors and potentially create functional materials. Based on the reaction cycles, how to create dissipative assemblies from chemical reaction cycles will be introduced in the following section.

1.3.2 Coupling assemblies with chemical reaction cycles

I have introduced what chemically fueled self-assembly is, why I focused on it, and how to design chemical reaction cycles that can drive self-assembly. In this section, I focus on how to regulate assemblies with these chemical reaction cycles. The main goal

is to find soluble precursors and toggle the rate of activation and deactivation to control the assemblies.

There are two main design strategies in regulating chemically fueled assemblies: 1. The charge abolishment strategy that transiently negates or decreases precursors' charges; 2. the transient linker strategy that combines two non-assembling precursors to one product. The detailed examples will be introduced in the following sections.

1.3.2.1 Two strategies to couple reaction cycles to self-assembly

Researchers have developed multiple reaction cycles that convert chemical fuel into transiently activate a building block (see section 1.3.1). This raises the question of how can we couple the formation of assemblies to chemical reaction cycles? In one strategy, the charge(s) of the precursor are abolished by a chemical reaction cycle, transferring to a less- or non-charged transient product. The loss of these charges decreases the solubility of the product and the repulsive interactions between them. In other words, the increase of interactions leads to self-assembly. The deactivation converts the product back to the precursor. The re-installment of charges upon deactivation drives the disassembly and re-solubilize in the solvent (Figure 9A). The second strategy is by linking two non-assembling components to form a new product during the activation reaction. The increasing attractive interactions between molecules gives the system more chance to assemble into the desired structure. In the deactivation, the chemical bond will be broken from the product and release the precursors. The re-decrease of interactions will disassemble the structure (Figure 9B). The following section will describe the design strategies in specific examples.

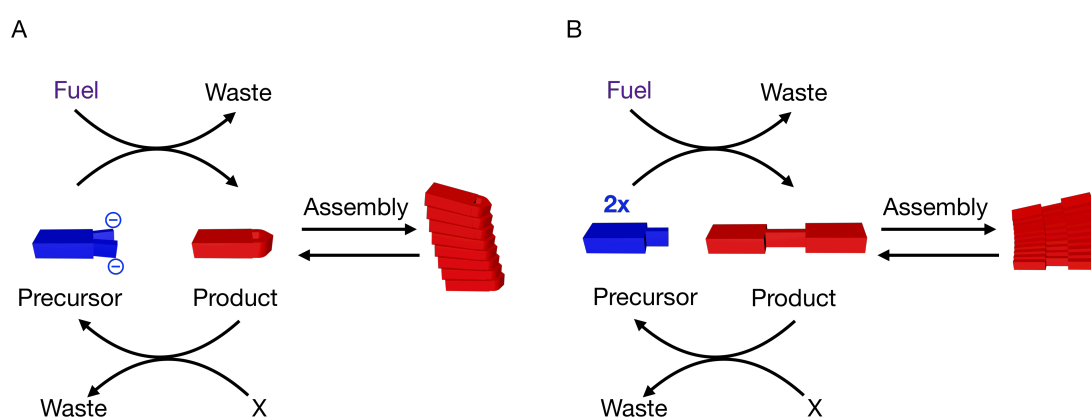


Figure 9: The strategies to couple a reaction cycle to self-assembly. **A)** Charge abolishment strategy that transiently negates or decreases charges of a precursor to activated building blocks for assembly. **B)** Transient linker strategy that transiently combines two non-assembling precursors into an activated product that can assemble.

1.3.2.2 Charge abolishment strategy

One of the strategies to induce chemically fueled self-assembly is charge abolishment, which means negation or decrease of the charges from the precursors to the products.^{51, 64, 72} The less- or non-charged products tend to assemble due to the loss of repulsive interactions. From the product to precursor, the appearance of charges in molecules leads to a re-increase of repulsion interaction, thus disassembly.

Boekhoven and co-workers⁶⁴ used the charge abolishment strategy converting a dicarboxylic precursor into a less- or non-charged anhydride using EDC as fuel (see section 1.3). The differences in precursor design induced different types of self-assembly in response to the addition of fuel. For instance, when fuel was added to a solution of Fmoc-D (D stands for aspartic acid) in an aqueous buffer, the precursor was activated to its corresponding anhydride and assembled into spherulites (Figure 10B-left). As an application, the transient assembled spherulites are used as self-erasing inks (Figure 10C). The time of the temporary message encoded with the assemblies can be controlled by fuel concentration. Similarly, when Fmoc-E (E stands for glutamic acid) is used as a precursor, the EDC fuel drives the formation of colloids instead (Figure 10B-middle). One interesting behavior of this peptide is the self-protection mechanism during the deactivation process found when the anhydride is located in the colloids. The deactivation process, in which hydrolysis only occurs in solution but not in the colloids, follows a zero-order rate.⁹¹ With increasing forming beta-sheet propensity, Fmoc-AAD (A stands for alanine) formed fibers with the addition of fuel EDC (Figure 10B-right). The fibers consecutively entangle to form hydrogels, and the lifetime of the hydrogel can be controlled by the EDC concentration as observed by rheology (Figure 10D). To sum up, the authors created different transient assembled structures and functional materials by using the charge abolishment strategy.

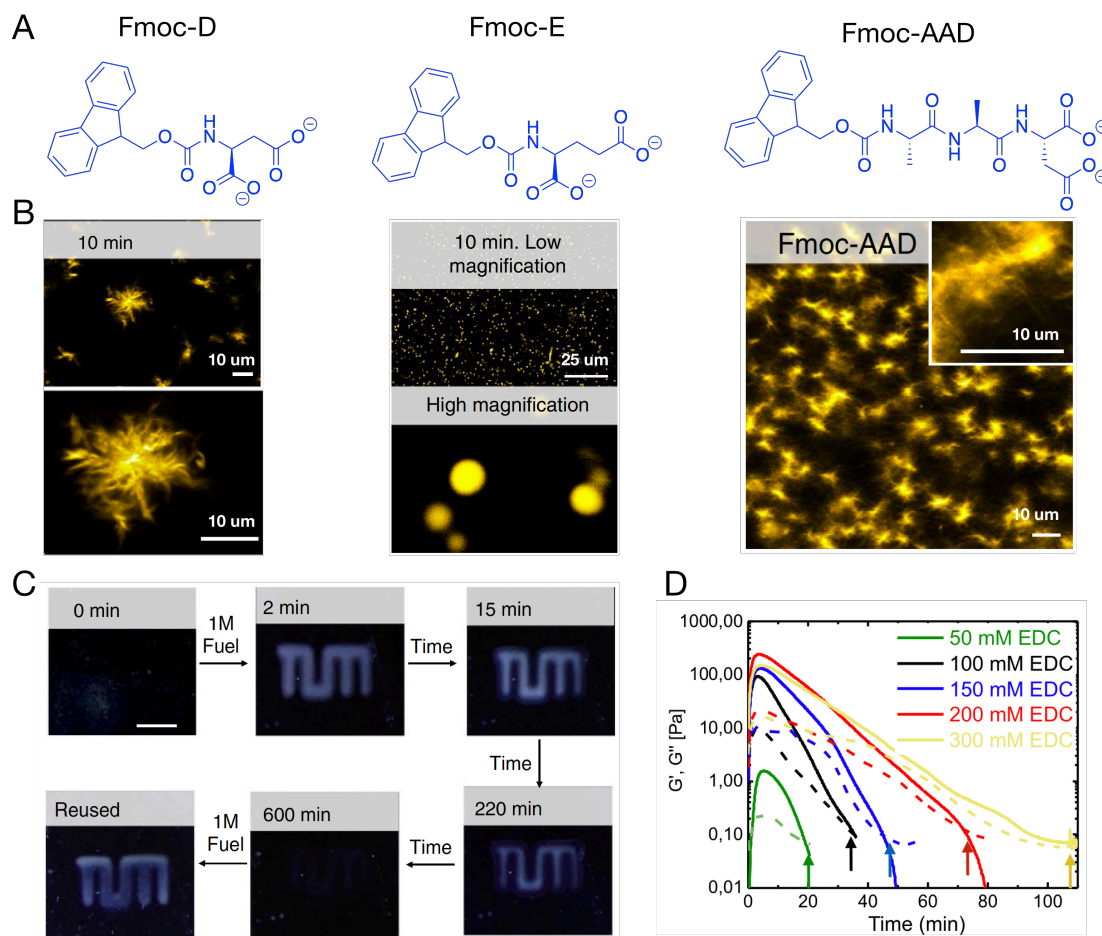


Figure 10: Dissipative self-assembly driven by EDC. **A)** List of precursors used to form different assembled structures. **B)** Confocal micrograph of transient self-assembled structures formed upon fuel addition. **C)** Fmoc-D assemblies used as temporary inks. **D)** Representative rheology time sweeps of Fmoc-AAD hydrogels when using different EDC concentrations. Solid lines represent the storage modulus (G'), dashed lines represent the loss modulus (G''), and arrows indicate the crossover point. Adapted from reference {64} by permission from Springer Nature Ltd., Copyright © 2017.

1.3.2.3 Transient linker strategy

The other possible strategy is the transient linker strategy. In this case, two non-assembled components are combined when activated by one chemical fuel.^{48, 49, 63, 79, 85} In some cases, the precursor can combine with itself, and in other cases, the precursor is connected with the fuel or with a second nucleophile. The product can interact stronger with each other in comparison to the precursor, leading to the formation of assemblies. In the deactivation, the linking bond is broken and the precursor is released resulting in disassembly.

In an early example, Ulijn and co-workers⁴⁸ designed a chemical reaction cycle driven by the hydrolysis of ester and catalyzed by an enzyme (Figure 11A). They used the non-assembled Y-NH₂ as a precursor, and an ester compound acyl donor tyrosine methyl as fuel. In the presence of an enzyme, NAP-YY-NH₂ was produced by combining these two components. In the presence of the same enzyme, the amide bond in the product is hydrolyzed to produce the original precursor. The stronger interactions in the transient products led to the assembly of a transient gel (Figure 11B). The gel formed after 1 min and transferred back to a transparent solution after 8 h. The fibers formed in a large amount at 30 minutes and disassembled after 8 h (Figure 11C). The amount of enzyme can control the hydrogel lifetime from 1000 minutes to 200 minutes. However, the system can only be refueled three times, after which the product could not reach the critical gelation concentration (CGC). The author assumed it was related to the accumulation of Nap-Y-OH leading to the yield reduction.

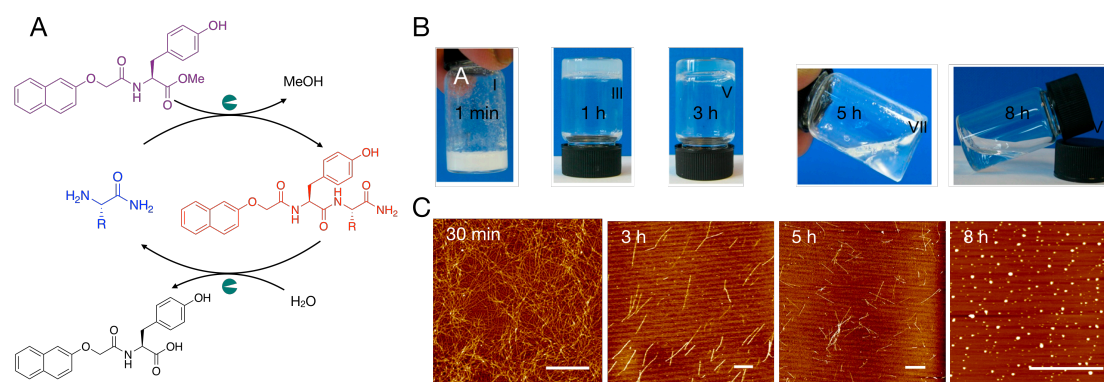


Figure 11: Dissipative self-assembly driven by hydrolysis of the ester. **A)** A brief reaction of the precursor Y-NH₂ to product NAP-YY-NH₂. **B)** Photographs of the gel of Nap-YY-NH₂ at 1 min, 1 h, 3 h, 5 h, and 8 h after the reaction. **C)** AFM photographs of the assembly structure at 30 min, 3 h, 5 h, and 8 h (scale bar, 2 μm). Adapted with permission from reference {48}. Copyright {2013} American Chemical Society.

Another classic example that used the transient linker strategy is the one already mentioned in section 1.3.1.3 reported by Guan and co-workers.⁶³ The oxidizing agent, H₂O₂, was responsible for the linkage between two precursors leading to one transient disulfide-based peptide (Figure 12A). The product can assemble into fibers, and lead to the formation of a transient transparent hydrogel. After all products reverting to the precursors, the hydrogel converted back to a solution (Figure 12B). The dynamic growth and shrinkage of fibers can be observed from confocal laser scanning microscopy (CLSM) (Figure 12C), which is very similar to the observation in van Esch and coworkers' work.⁹² These fibers' growth and shrinkage driven by chemical fuel are

reminiscent of the formation and degradation of the microtubules driven by GTP, which is described in section 1.2.

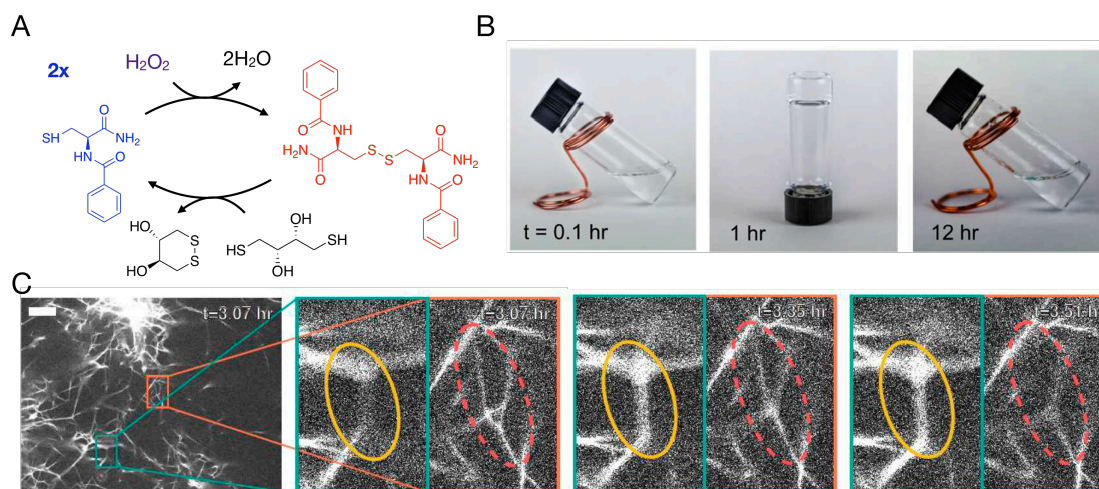


Figure 12: Dissipative self-assembly driven by H_2O_2 . **A)** brief reaction of the precursor to the product. **B)** Photographs of the gel of Nap-YY-NH₂ at 0.1 hr, 1 hr, and 12 h after fuel addition. **C)** CLSM photographs of dynamic assembly of fibers over time. Yellow solid circles indicate growing fibers are, and red dash circles indicate shrinking fibers. The scale bar is 20 μm . Adapted from reference {63} by permission from the Wiley-VCH Verlag GmbH & Co. KGaA, Copyright © 2020.

The example previously mentioned from Das and coworkers (section 1.3.1.3 carbodiimide-driven reaction cycle) is also an example that can be included in the present section. In this case, the linkage between the precursor and the second nucleophile (NP) is responsible for the assemblies' formation.^{82, 83} The precursor (Figure 13A) is an amphiphilic molecule that contains a carboxylic group, necessary for the carbodiimide reaction cycle and a histidine residue that plays a key role in catalyzing the formation and rupture of the ester bond. In the activation reaction, the histidine plays a role as a base to push the alcohol and carboxylic acid to form an ester. The formation of ester upon fuel addition between the precursor and the second nucleophile results in self-assembly. In the deactivation reaction, it serves a catalytic role to shuttle protons and influences the local pH, prompting the hydrolysis of the ester bond. Right after the addition of EDC, a hydrogel forms from the solution and transitions to the solution after 30 minutes (Figure 13C). Amyloid-like fibrils can be observed from TEM after the addition of EDC but significantly decrease with time (Figure 13D). Notably, there is no ester formation if the histidine is replaced by phenylalanine, proving the histidine group's catalytic effect. In the deactivation reaction, the presence of assemblies is crucial for the catalytic role of the histidine. The

cooperative effect of the proximally located histidine in the assemblies is responsible for the catalytic activity of such an imidazole group in the hydrolysis reaction.

This elegant example shows not only how the chemical reaction cycle can control the assembly formation but interestingly also how the assemblies can influence the chemical reactions involved. They also choose another histidine peptide derivative Ac-H17LVFFA21E-NP as a precursor (Figure 13B), the addition of EDC leads to the formation of the ester bond with 4-nitrophenol. The esters also formed amyloid-like fibrils structures (Figure 13E). Varying the concentration of the precursors and nucleophile NP can result in different lifetimes of the transient gels. Finally, they tested the electrical transport properties of the amyloid network from this system. They found a transient enhancement current density corresponding to the assemblies (Figure 13F).⁸³

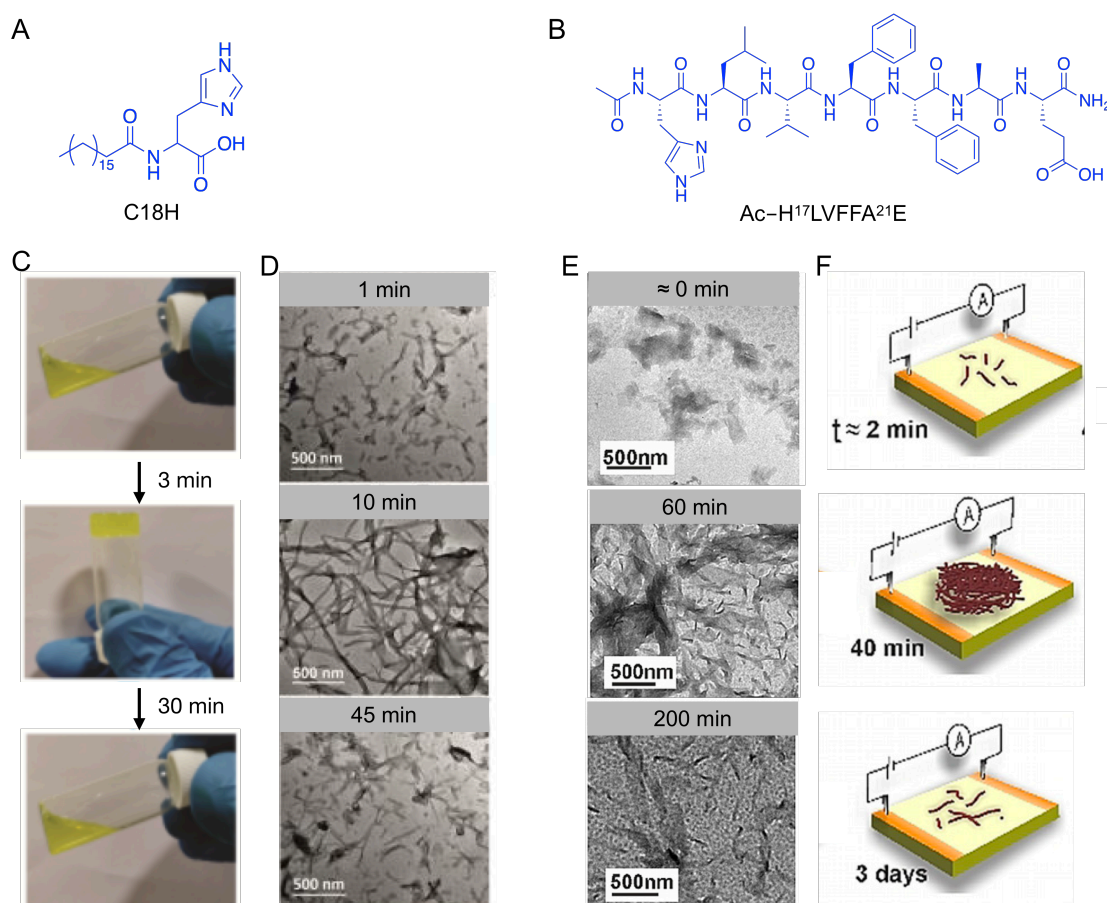


Figure 13: Dissipative self-assembly driven by EDC. **A, B)** List of peptides precursors used for assembly. **C)** TEM of C18H as precursor after fuel addition at different time intervals. **D)** Images of C18H in the presence of NP and EDC in different periods. **E)** TEM of Ac-H¹⁷LVFFA²¹E as precursor after fuel addition at different time intervals. **F)** Schematic representations of devices prepared by drop-casting the ester product of different time points. A, C and D adapted from reference {82} by permission from the Wiley-VCH Verlag GmbH & Co. KGaA, Copyright © 2019. B, E and F adapted from

reference {83} by permission from the Wiley-VCH Verlag GmbH & Co. KGaA, Copyright © 2020.

1.4 Other outcomes driven by chemical reactions

We have discussed different strategies to create chemically fueled self-assemblies, and the unique properties have been described. However, some other outcomes can occur when designing self-assemblies. For instance, the precursor self-assembles before the addition of fuel, or assembly does not occur upon activation, or the assembly can remain kinetically trapped even after all the fuel is depleted. The last one represents one of the biggest problems when designing chemically fueled self-assemblies. Here I explain the mechanisms for having these unwanted outcomes rather than chemically fueled self-assembly from an energy point of view and illustrate the different scenarios with examples reported in the literature.

1.4.1 Energy landscape for other outcomes

In the first scenario, the precursor self-assembles without the fuel addition (Figure 14A). Before the addition of fuel, the low solubility of the precursors or the strong interactions between the molecules result in assemblies. In the energy landscape, the molecules pass from a higher position to the local minimum state to assembly (discussed in section 1.1.1.). Another usual situation is chemically fueled reaction cycle without self-assembly (Figure 14B). It occurs when even after the addition of fuel, the product is not able to self-assemble and remains in solution. In this situation, although the fuel is added to the system, the precursors try to overcome the energy barrier to a higher position in the energy landscape, but the fuel input is insufficient to help the building blocks do that. As a result, the molecules stay in the global minimum state. The last common scenario typically observed when designing chemically fueled self-assembly is the kinetic trapping of the assembled molecules. It is similar to the kinetically trapped self-assembly described in section 1.1.2, but the difference is the fuel input. The addition of fuel helps the precursors from a global minimum state to occupy a higher energy position in the energy landscape. The activated building block would gain energy when moving to the assembly state, which is in a local minimum state, but after the fuel depletes, these activated building blocks cannot revert completely to the precursor state, resulting in a kinetically trapped assembly. That is to say, the product molecules are kinetically trapped in the assembly (Figure 14C). In most scenarios of chemically fueled kinetically trapped assembly, the activated building blocks can

transfer back to the precursors, but there is one lower energy barrier to the local minimum state, in which the activated building blocks will drop into the lower energy barrier rather than the local minimum state. Although all products change to precursors, part of the precursors will be kinetically trapped in the assembly (Figure 14D).

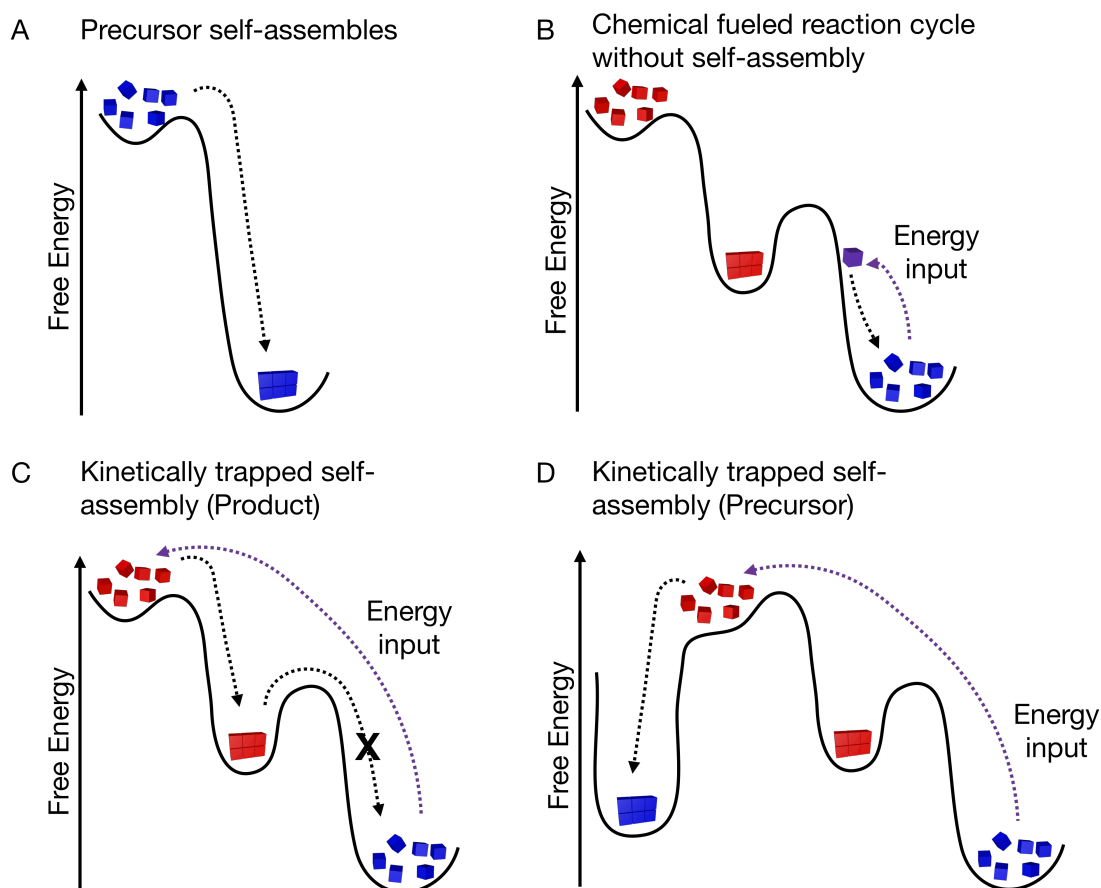


Figure 14: Schematic free energy landscape of different self-assembly processes in one chemical reaction cycle. **A)** Precursor self-assembles. **B)** Chemically fueled reaction cycle without self-assembly. **C)** Kinetically trapped self-assembly (Product). **D)** Kinetically trapped in self-assembly (Precursor).

1.4.2 Precursor assemblies

One of the possibilities is that precursors assemble directly before the addition of fuel. It is one significant assembly, but also one outcome that scientists would like to avoid when designing chemically fueled self-assembly.

One example is from Haldar's work.⁸⁵ The transient linker strategy is used in their work, which connects two molecules of benzyloxycarbonyl-L-phenylalanine to one product for assembly. However, the precursor (Figure 15A) was not well-soluble in the solvent

(10% DMSO in H₂O). Above 4 mg mL⁻¹, the precursor formed a gel without the addition of fuel (Figure 15B), as further proved by the strain sweep experiment (Figure 15C). At the microscopic level, the formation of the spherulites is confirmed. The way to solve this problem concerning the assembly of precursors, is to decrease the concentration of the precursors or change the solution environment. In this example, when the author tried to decrease the precursor concentration below 4 mg mL⁻¹, the peptide was still not completely soluble, and precipitates formed.

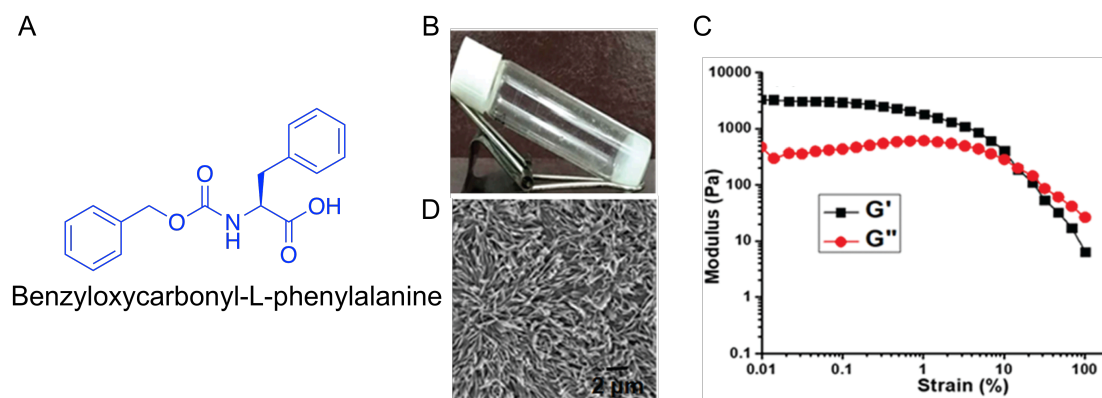


Figure 15: Benzyloxycarbonyl-L-phenylalanine assembly before the addition of fuel. **A)** The structure of benzyloxycarbonyl-L-phenylalanine. **B)** Photographs of the gel formation before the addition of fuel. **C)** Strain sweep experiment of the hydrogel from the precursor (the black line represents G' and the red line G''). **D)** FE-SEM photographs of the precursor dried hydrogel. Adapted from reference {85} by permission from The Royal Society of Chemistry, Copyright © 2021.

Hermans and co-workers also reported an example in which the precursor assembles⁵³. Precursor PDI transfers to the transient p2-PDI product in this system and the process is regulated by phosphorylation and dephosphorylation reactions (Figure 5). However, the precursor PDI can also assemble into supramolecular polymers, which is confirmed by ultraviolet-visible-light spectra. While the precursor (PDI) self-assembled into relatively short P-helical fibers, the activated state (p2-PDI) assembled in larger M-helical fibers. The addition of fuel to this particular dissipative system reorganizes the supramolecular assemblies rather than driving the system from solution to a self-assembled state.

In Das's cooperatively catalysis system, they showed that when they chose precursors as Ac-K¹⁷LVFFA²¹E-NH₂ (KE) and Ac-K₁₇LVFFA₂₁L-NH₂ (KL) (Figure 16A and 16B) in 10:1 ratio respectively and dissolved them in 20% v/v DMSO/water, the precursors can assemble to fibrils without any fuel addition. These fibrils grow and

entangle over time (Figure 16C) and after 24 hours, they form a self- a self-supporting gel that stands for days (Figure 16B).⁸³

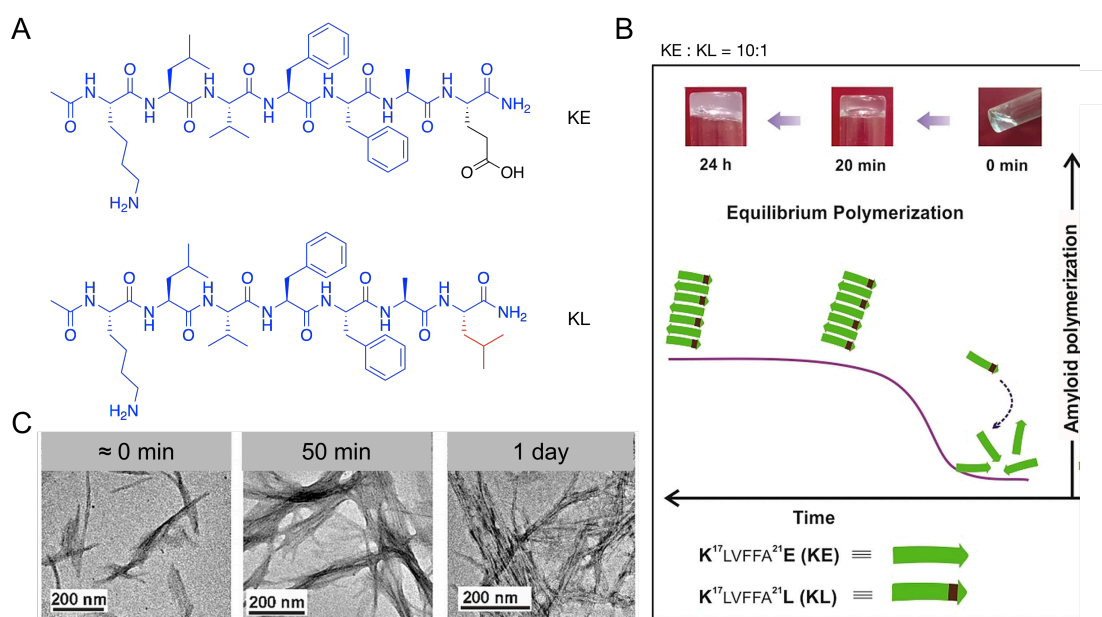


Figure 16: KE/KL (10/1) assembly before the addition of fuel. **A)** The structure of KE and KL. **B)** equilibrium amyloid polymerization. **C)** TEM of the mixture of KE and KL at different time intervals. Adapted from reference {83} by permission from the Wiley-VCH Verlag GmbH & Co. KGaA, Copyright © 2019.

1.4.3 Chemically fueled reaction cycle without self-assembly

Besides the situation that precursor assembles before the addition of fuel, non-assembly after the fuel addition (chemically fueled reaction cycle without self-assembly) is also very common in the design of a chemically fueled reaction cycle.

One example is from Ulijn and coworkers. They reported the non-assembly in the fuel-driven reaction cycle (Figure 17A).⁴⁹ They use the transient linker strategy that combines two peptides to one tripeptide with stronger interactions to assembly (Figure 17B). A range of precursors X-NH₂ (X=tryptophan (W), leucine (L), valine (V), serine (S), threonine (T)) has been tested. They are all well-soluble in sodium phosphate buffer at pH 8 (Figure 17C). After adding fuel and enzyme, the corresponding products are not detected, indicating the transient products are either of a very short existence and immediately hydrolyzed or are not generated. As a result, all of these precursors showed no gelation (Figure 17D). Only when the precursors were changed to F-NH₂ and Y-NH₂ (where F stands for phenylalanine and Y for tyrosine), the appearance of assembly into fibers was detected.

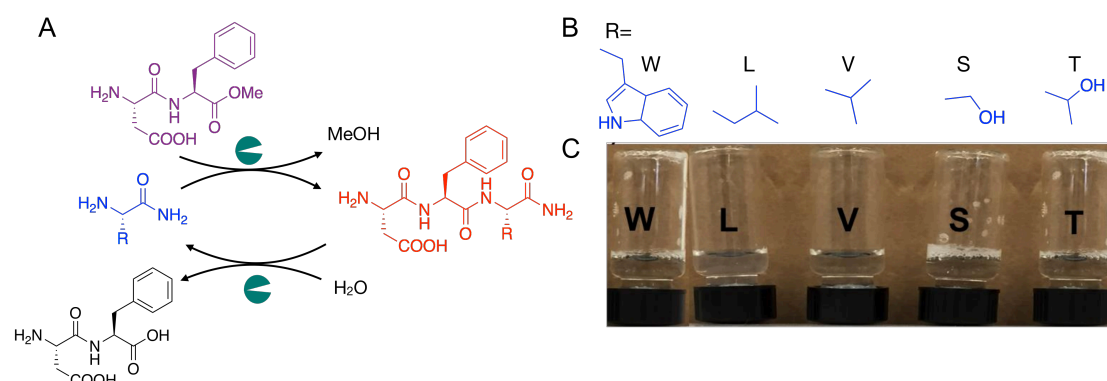


Figure 17: Peptide showed no assembly after the addition of fuel. **A)** One brief reaction scheme of the precursor amino acid with the ester to one tri-peptide. **B)** Structure of R group in the amino acid as precursors. **C)** Photograph of different amino acids in response to the ester fuel and enzyme. Adapted from reference {83} by permission from the Wiley-VCH Verlag GmbH & Co. KGaA, Copyright © 2015.

In one work from Das group,⁸² histidine-based compounds and nucleophile 4-nitrophenol (NP) are dissolved in the solvent, the addition of EDC and catalysis of histidine will drive the formation of ester for assembly. However, adding EDC cannot result in the assembly when the precursor is C2H (Figure 18A). This is proved by the weak signal in CD spectra (Figure 18B) and no network from TEM (Figure 18C).

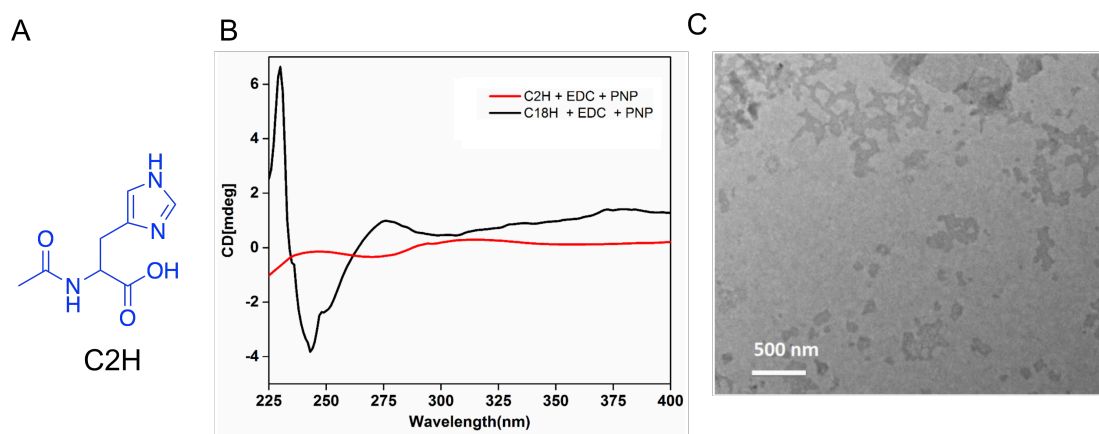


Figure 18: Peptide showed no assembly after the addition of fuel. **A)** Peptide structure of C2H. **B)** CD spectra of C2H (non-assembly) and C18H (assembly) in the presence of EDC and NP. **C)** TEM of C2H in the presence of EDC and NP. Adapted from reference {82} by permission from the Wiley-VCH Verlag GmbH & Co. KGaA, Copyright © 2019.

1.4.4 Chemically fueled kinetically trapped assembly

Kinetically trapped self-assembly can seriously damage the dynamics of chemically fueled self-assembly, and the unique properties of materials such as self-healing and adaptivity will lose. As a result, it is one result that scientists would like to avoid in research of chemically fueled self-assembly. In one case, the transient product cannot completely transfer back to the precursor after fuel is depleted; thus, part of the structure cannot be disassembled. The product is kinetically trapped in the assembly.

In Ulijn's work⁴⁸, a transient linker strategy is used to create chemically fueled self-assembly. When using the precursor as Y-NH₂, they successfully get the dissipative assembly described in the last section (Figure 19A). However, when the precursor change to F-NH₂, only one -OH group less, the product NAP-YF-NH₂ can form but cannot completely transfer back to the precursor. After fuel depletes, 30 % of the product is still in the system, which is kinetically trapped in the gel (Figure 19B).

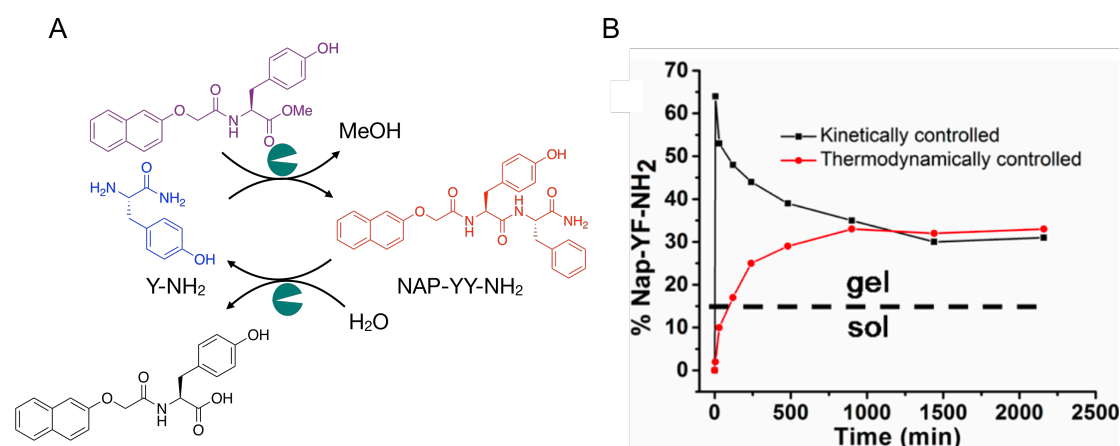


Figure 19: Peptide showed no assembly after the addition of fuel. **A)** One brief reaction scheme of the precursor Y-NH₂ and F-NH₂ to product NAP-YY-NH₂ and NAP-YF-NH₂ respectively. **B)** Reactions of Nap-Y-OMe (black line) with F-NH₂. Adapted with permission from reference {48}. Copyright {2013} American Chemical Society.

In a final unwanted scenario, after the consumption of all fuel, all of the products transfer back to the precursors, but the available thermal energy cannot overcome the strong interactions between precursors, leading to the precursor remaining kinetically trapped in the assembly. Only heat, sonication and some other extra stimuli have chances to rescue the precursors from kinetically trapped state to solution.

One example of precursor remaining kinetically trapped in the assembly is from EDC-fueled chemical reaction cycle. When the non-assembled precursors are Fmoc-AVD and Fmoc-AVE (Figure 20A), even if all of the transient products have been deactivated

back to the precursors, some precursor remains kinetically trapped in the assemblies. This kinetic trapping is caused by the precursor molecules not having sufficient energy to disassemble from the fibers. From a macroscopic level, these two peptides form hydrogel upon application of fuel, and after fuel depletion, the assembled gel becomes weaker. However, some gel can still be observed, where the precursor is still in the assembled state (Figure 20B). From the microscopic level, there is no assembly from both precursors before the addition of fuel. After 100 mM of fuel addition, the fuel drives the precursors to their corresponding anhydrides, leading to the assembly of fibers. After 24 h, when all of the anhydrides transfer back to precursors, assembled fibers decrease significantly, but some of the precursors are still kinetically trapped in fibers (Figure 20C and Figure 20D). Only when the author tried to change the amino acid from valine (V) to alanine (A), the decrease of interactions avoid Fmoc-AAD and Fmoc-AAE to kinetically trap.

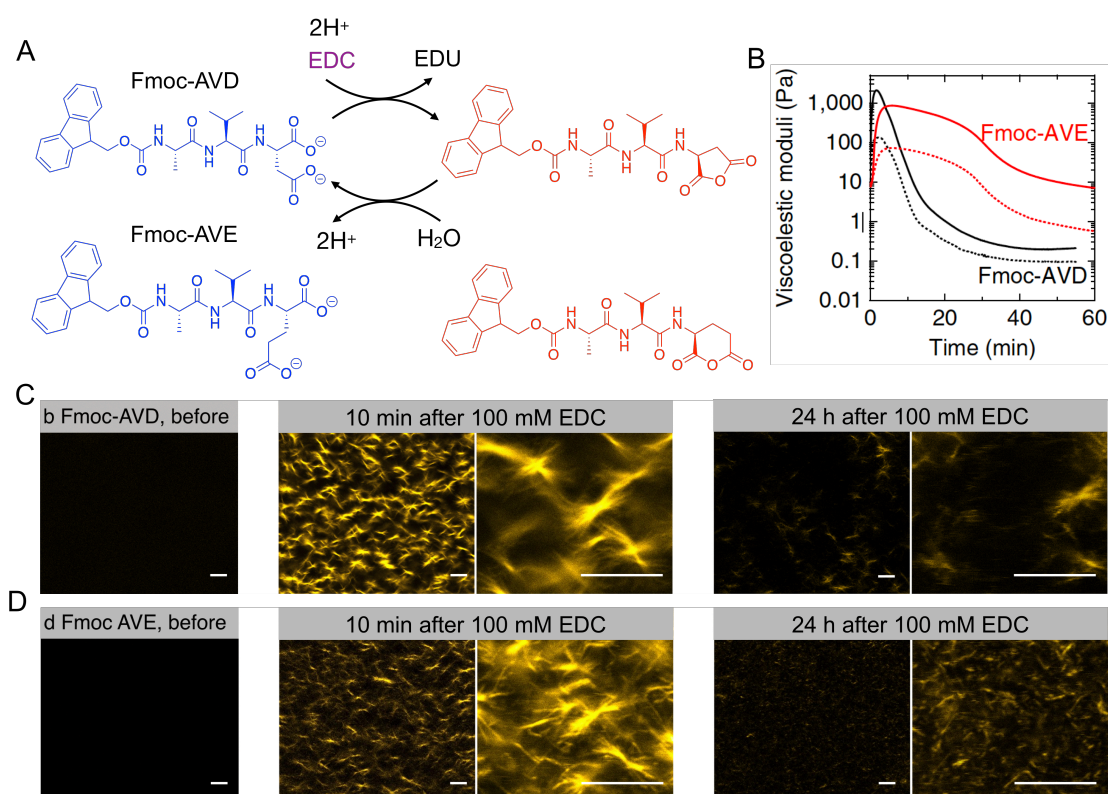


Figure 20: Chemically fueled kinetically trapped assembly from two peptides as precursors. **A)** The brief reaction cycle of Fmoc-AVD and Fmoc-AVE to their corresponding anhydrides. **B)** Rheological time sweeps of gels formed by Fmoc-AVD and Fmoc-AVE precursor in response to EDC. The solid line represents the storage modulus (G'), the dashed line represents the loss modulus (G''). **C)** Confocal micrographs of Fmoc-AVD (**C**) and Fmoc-AVE (**D**) before, 10 minutes and 24 hours

after addition of 100 mM EDC. All scale bars are 10 μm . Adapted from reference {64} by permission from Springer Nature Ltd., Copyright © 2017.

1.5 Conclusion and Outlook

In order to understand biological self-assembled behavior, uncover disease mechanisms, synthesize life from the bottom-up, and further create artificial materials with unique properties, scientists have invested much attention into chemically fueled self-assembly. With the basic principles from biology, many chemical reaction cycles based on peptides have been developed, e.g., ester-driven, ATP-driven, H_2O_2 -driven, carbodiimide-driven reaction cycles, and others. Several strategies have been developed to couple the chemical reaction networks to the formation of assemblies. The abolishment of charges upon activation and the transient linker strategy that combines two molecules are the most common ones. Some exciting behaviors have been explored. The formation of assemblies can also influence the rates in the chemical reaction cycle either through catalysis^{73, 82, 83} or by protecting the product from reaction with water^{64, 79, 91, 93}. Preliminary applications of these unique materials have also been developed, including self-erasing inks,⁶⁴ self-expiring labels,⁸¹ and others. However, the strategies that scientists have developed are still not sufficient. When designing chemically fueled self-assemblies, the researchers encounter several issues usually not desired. The precursor can self-assemble before the application of the fuel or not assemble at all even though a sufficient amount of fuel is added. In other cases, especially when considering the formation of fibers, the assemblies can remain kinetically trapped when fuel is depleted and therefore, the unique properties of dissipative assemblies are often lost. In conclusion, there are still many hurdles to overcome in order to design the perfect dissipative system with which we can mimic the unique properties of their biological counterparts.

2. The aim of this thesis

Life demonstrates ubiquitous far-from-equilibrium assemblies, which are kinetically controlled. Examples include self-assembly of tubulin through the hydrolysis of GTP (fuel) as described in chapter 1.2. Inspired by biological behavior such as the dynamic microtubules, researchers developed synthetic counterparts and mimicked artificial non-equilibrium materials. This has led to exciting new properties that include the ability to tune the material's property in space and time by gradients of reactants, described in chapter 1.3. As concluded from chapter 1, although this field has seen significant development, existing designs sometimes fail because the precursor assembles before fuel addition, or the addition of fuel does not induced self-assembly, or the assembly remains kinetically trapped after fueling, which has been discussed in 1.4. As a result, Most of these examples are serendipitous discoveries because there are no clear design rules. Furthermore, as described in chapter 1, the activation for assembly and deactivation for disassembly proceed through two different pathways for the chemically fueled self-assembly. As two important steps, scientists mainly focus on the activation step, while disassembly has so far not been studied in much detail.

The first aim of this thesis is to develop design rules in the chemically fueled self-assembly. The second aim of this thesis is to awaken researchers' attention to disassembly in the fuel-driven dissipative self-assembly.

In chapter 3, I demonstrate two approaches to control the chemically fueled self-assembly of peptides by molecular design. In one approach, the attractive interactions between peptides are tuned by increasing the number of isoleucine (I) in the peptides, allowing to toggle the fuel-driven behavior from no assembly, chemically fueled self-assembly to precursor self-assembly. In another approach, the repulsive interactions between peptides are tuned, resulting in similar control. The rules of altering the ratio of attractive to repulsive interactions between peptides can be generalized for other peptide sequences. Furthermore, these findings are explained by the energy landscapes of self-assembly.

In chapter 4, the importance of disassembly in fuel-driven assembly is demonstrated. I designed four similar peptides. The molecular designs of the peptides are chosen such that they vary in their propensity to form β -sheets and their solubility. In response to fuel, the more soluble ones form colloids that disassemble when fuel is depleted. However, the more hydrophobic and less soluble ones form colloids that transition to fibers as fuel depletes. The different disassembly pathways are qualitatively understood by the ratio of co-assembly of the precursor with the product. With this mechanism, the time that colloids transition to fibers can be controlled by the amount of fuel.

In conclusion, the thesis aims to develop the design rules in chemically fueled self-assembly concerning both the assembly and the disassembly process. With these design rules, I aim to help this field efficiently design fuel-driven dissipative self-assembly and morphology control.

3. Regulating chemically fueled peptide assemblies by molecular design

Abstract

The past years have witnessed the development of chemically fueled self-assemblies. Inspired by the self-assembly of microtubules by hydrolysis of GTP and formation of actin bundles by conversion of ATP, different chemical reaction cycles and assemblies have been explored, e.g., formation of fibers, droplets, vesicles, liposomes, micelles. However, these exciting discoveries cannot conceal the lack of the design rules behind the chemically fueled self-assemblies. It is still very challenging to efficiently design these dynamic behaviors.

The focus of this work is to generalize the design rules from molecular design. In this work, The peptides' behavior can be toggled by molecular design from no assembly, chemically fueled self-assembly to permanent self-assembly. Specifically, the fuel used in this reaction cycle is 1-ethyl-3-(3-dimethyl aminopropyl) carbodiimide (EDC). A molecular precursor reacts with the high-energy molecule (EDC) to form anhydride, spontaneously deactivated to the precursor simultaneously. The design rules are the balance of attractive interactions and repulsive interactions.

In one approach, the amount of attractive interactions between peptides Ac-F(I)n-D is tuned. The attractive interactions were tuned by the number of isoleucine units, i.e., not self-assemble (Ac-FID-OH) and transiently self-assemble to hydrogel in response to EDC (Ac-FIID-OH) or self-assemble to permanent hydrogel without EDC (Ac-FIIID-OH). These rules can be generalized for Ac-FVnD-OH ($n = 1, 2, 3$ or 4).

In the other approach, the repulsive interactions between peptides are tuned. The addition of salt can decrease the repulsive interactions, i.e., with the addition of salt, the non-assembled peptide (Ac-FID-OH) can undergo self-assembles into transient hydrogel; the dissipative self-assembled peptides (Ac-FIID-OH) will change to self-assembled hydrogel without fuel. In contrast, increasing the repulsive interactions by introducing a second carboxylate at the N-terminus helps the permanent hydrogel (Ac-FIIID-OH) change to transient hydrogel in response to fuel. Furthermore, all these findings are explained in the context of the energy landscapes of self-assembly.

In summary, The simplicity of the peptide design and reaction cycle allows creating some general rules for the self-assembly behavior in response to fuel.

This work has been published:

Title: Regulating chemically fueled peptide assemblies by molecular design

Authors: Kun Dai, Dr. Jennifer Rodon Fores, Caren Wanzke, Benjamin Winkeljann, Alexander M. Bergmann, Prof. Dr. Oliver Lieleg, Prof. Dr. Job Boekhoven

First published: 27 July 2020

Journal: Journal of the American Chemical Society

Publisher: American Chemical Society

DOI: 10.1021/jacs.0c04203

Link: <https://pubs.acs.org/doi/abs/10.1021/jacs.0c04203>

Reprinted with permission from J. Am. Chem. Soc. 2020, 142, 14142-14149.

Copyright 2019 American Chemical Society.

I acknowledge the permission with this reprint from American Chemical Society

This section states the individual work of each author in the publication above Kun Dai designed and conducted all experiments. Jennifer Rodon Fores helped with scientific problems. Caren Wanzke and Alexander M. Bergmann imaged with a cryogenic transmission electron microscope. Benjamin Winkeljann and O. Lieleg carried out and helped analyze the gel properties with top-plate rheology. Kun Dai and J. Boekhoven wrote the manuscript. The work was performed under the supervision and guidance of J. Boekhoven.

Regulating Chemically Fueled Peptide Assemblies by Molecular Design

Kun Dai, Jennifer Rodon Fores, Caren Wanzke, Benjamin Winkeljann, Alexander M. Bergmann, Oliver Lieleg, and Job Boekhoven*

Cite This: *J. Am. Chem. Soc.* 2020, 142, 14142–14149

Read Online

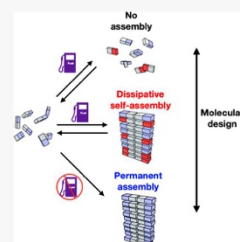
ACCESS |

Metrics & More

Article Recommendations

Supporting Information

ABSTRACT: In living systems, fuel-driven assembly is ubiquitous, and examples include the formation of microtubules or actin bundles. These structures have inspired researchers to develop synthetic counterparts, leading to exciting new behaviors in man-made structures. However, most of these examples are serendipitous discoveries because clear design rules do not yet exist. In this work, we show design rules to drive peptide self-assembly regulated by a fuel-driven reaction cycle. We demonstrate that, by altering the ratio of attractive to repulsive interactions between peptides, the behavior can be toggled between no assembly, fuel-driven dissipative self-assembly, and a state in which the system is permanently assembled. These rules can be generalized for other peptide sequences. In addition, our finding is explained in the context of the energy landscapes of self-assembly. We anticipate that our design rules can further aid the field and help the development of autonomous materials with life-like properties.



INTRODUCTION

The construction of dissipative self-assembling systems aims at the construction of assemblies that possess the dynamic behavior we observe in living systems.^{1–6} Inspired by the self-assembly of microtubules fueled by the hydrolysis of GTP,⁷ or the formation of actin bundles by the conversion of ATP,⁸ researchers have developed chemical reaction cycles that can be used to drive dissipative assembly of small molecules or nanoparticles.^{9,10} In these chemical reaction cycles, an activation reaction converts a precursor molecule into a self-assembling product driven by the irreversible conversion of a high-energy reagent. A deactivation reaction reverts the product to the original precursor spontaneously. Thus, the chemical energy that is obtained by the conversion of the high energy reagent into waste is temporarily stored in a transient modification of the precursor molecule.^{5,11,12} We, and others, refer to the high-energy molecule as a chemical fuel. That chemical change can be used to induce self-assembly. However, due to the transient nature of the product, it will disassemble upon reversion to the precursor. As a consequence of the dynamic interplay between product activation and deactivation, the assembly and disassembly are dynamic too, which results in emerging structures that possess behavior that we typically do not observe in equilibrium. Examples of dissipative assembly include the formation of fibers driven by the hydrolysis of methylation agents,¹³ the formation of supramolecular polymers by the reduction of oxidizing agents^{14,15} or by the hydrolysis of ATP,¹⁶ the formation of active droplets at the expense of a condensing agent,^{17,18} and others.^{19–27} Exciting behaviors observed in these assemblies

contain the dynamic instabilities found in synthetic self-assembled fibers²⁸ and solutions spontaneously oscillated from one self-assembled state to another driven by a chemical fuel.¹⁵

Despite the recent progress in the field, it remains challenging to design molecules in order to ensure that the energy harvested by the chemical reaction cycle is optimally used to induce dynamic assembly. Thus, in this work, we introduce two approaches to control the fuel-driven self-assembly of peptides by molecular design. In one approach, the amount of attractive interactions between peptides is tuned, allowing to toggle the fuel-driven behavior from no assembly, chemically fueled dissipative self-assembly to static self-assembly. In another approach, the repulsive interactions between peptides are tuned, resulting in similar control. We rationalize our findings with the energy landscapes associated with the self-assembly and chemical reaction cycle.

RESULTS AND DISCUSSION

Description of the Chemical Reaction Cycle. In this work, we use a chemical reaction cycle that transiently activates a building block for self-assembly (Figure 1A).^{18,29–31} In the cycle, a molecular precursor reacts with a high-energy molecule

Received: April 17, 2020

Published: July 27, 2020



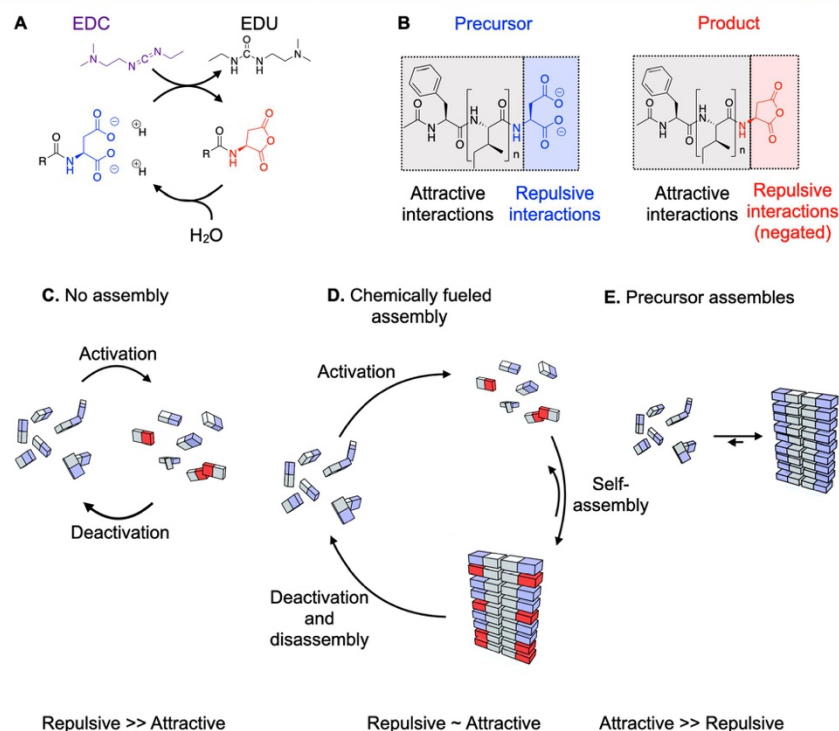


Figure 1. Design strategy for dissipative self-assembly. (A) A chemical reaction cycle is used that comprises an activation and deactivation reaction. In the activation reaction, aspartic acid derivatives react with carbodiimide EDC and are converted to their corresponding anhydride. In the deactivation reaction the aspartic acid anhydride derivative is hydrolyzed. When correctly designed, the transient aspartic acid anhydride can self-assemble, but the aspartic acid derivative cannot. (B) Molecular structure of the precursors and products used in this work. (C–E) The balance between attractive and repulsive interactions can affect the fuel-driven response of the reaction cycle. When the attractive interactions are much weaker than the repulsive interactions, no assembly is formed (C). When the attractive interactions are balanced with the repulsive interactions, dissipative assemblies can form (D). When the attractive interactions are too strong, the precursor can self-assemble without fuel (E).

(fuel) to form a product. That reaction is referred to as the activation reaction. The activation is irreversible; that is, the fuel is irreversibly “burned”. A second reaction spontaneously deactivates the product and yields the precursor. Consequently, the product is metastable with a half-life determined by the deactivation rate.

We used a chemical reaction cycle to regulate the assembly and disassembly of peptides building blocks. In the cycle, aspartic acid derivatives are converted into their corresponding anhydride state by the consumption of a condensing agent, ethyl-3-(3-(dimethylamino)propyl) carbodiimide (EDC). This reaction constitutes the activation reaction. Simultaneously, the anhydride is hydrolyzed. This constitutes the deactivation reaction. When the peptide is correctly designed, its transient anhydride can self-assemble, but the aspartic acid derivative cannot. In effect, the assembly and disassembly of the derivatives is regulated by the formation and hydrolysis of aspartic acid anhydride. We introduced this cycle in previous

work.^{18,25,26,29–32} As a precursor, we used peptides that carry a C-terminal aspartic acid (D). These peptides thus carry two dicarboxylate groups, which are converted into their corresponding cyclic anhydride at the expense of a molecule of carbodiimide (Figure 1A). However, in the aqueous environment, the anhydride product is hydrolyzed back to the precursor, which constitutes the spontaneous deactivation reaction.

Design of the Precursors. Our design strategy for the precursor is to use the loss of negative charges on the carboxylate precursor to induce the self-assembly of the product (Figure 1B). The carboxylates of the precursor have a pK_a in the range of 1.9 and 3.9. Under the employed conditions, the precursors are expected to have an ionic charge of -2 (pH 6, 15 mM precursor, 200 mM 2-(*N*-morpholino)-ethanesulfonic acid (MES) buffer). Moreover, we found in earlier work that, at this pH, the balance of the pH-dependent activation and deactivation is sufficient to ensure the formation

of significant amounts of product.²⁹ In contrast, upon EDC-induced activation, the two carboxylates condense into a charge-neutral anhydride product. Typically, the loss of the two anions is used to regulate the self-assembly behavior of the system to fuel. We categorize the self-assembly behavior in three classes, i.e., fuel is added, and no self-assembly is observed (no assembly, Figure 1C). Fuel is added, and transient assembly is observed (dissipative self-assembly, Figure 1D). The precursor assembles without the addition of fuel (precursor assembles, Figure 1E). While our interest is in chemically fueled dissipative self-assembly, we frequently encounter the other two scenarios (no assembly or precursor assemblies).

The aim of the first part of this study is to understand how attractive interactions can be used to regulate the response of the system to chemical fuel. We tuned the degree of attractive interactions between the molecules in the chemical reaction cycle by varying the peptide segment (Figure 2A). We

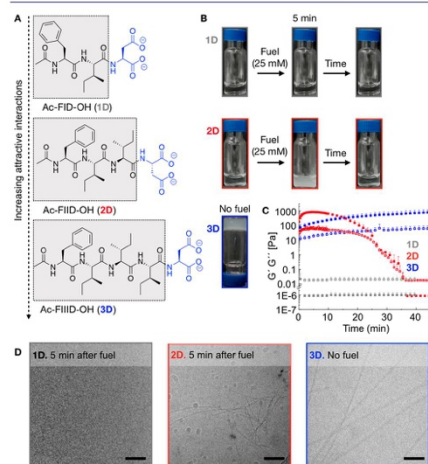


Figure 2. Regulating the response to fuel by tuning the attractive interactions. (A) Molecular structures of peptide 1D, 2D, and 3D used as precursors. (B–D) Assessment of the self-assembly behavior of 1D or 2D before and after the addition of 25 mM fuel and 3D without fuel. (B) Photographs of the solutions. (C) Storage and loss modulus as a function of time. The solid squares represent the storage modulus (G'); open squares represent the loss modulus (G''). Error bars represent the standard deviation of the mean ($n = 3$). (D) Cryo-TEM micrographs. All scale bars correspond to 100 nm. All the experiments were carried out at a peptide concentration of 15 mM, a pH of 6, and in 200 mM MES buffer.

synthesized the precursors Ac-FIID-OH (1D), Ac-FIID-OH (2D), and Ac-FIID-OH (3D), where F stands for phenylalanine, I for isoleucine, and D for aspartic acid. The rationale behind the molecular design is as follows: the aspartic acid is the chemically active unit that switches its degree of electrostatic repulsion by the chemical reaction cycle. In line with recent work by Webber and co-workers,³³ the F and I amino acids were introduced in order to promote fiber formation via π -orbital overlap, hydrogen bond formation, and

hydrophobic interactions. The number of I (1–3) allowed us to test the response of the system with an increasing degree of attractive interactions. Finally, it is worth mentioning that the phenyl group of the F greatly facilitates the characterization of the products of the chemical reaction cycle by HPLC due to its aromatic group. We tested the behavior of the precursors with a thioflavin-T (ThT) assay before the addition of fuel. ThT is a fluorescent dye that drastically increases its fluorescence intensity when bound to structured assemblies like fibers. We found no evidence for fiber formation for 1D and 2D. In contrast, 3D did show an increased intensity, which is evidence of fiber formation before the addition of EDC as fuel (Figure S1).

By analytical HPLC, the evolution of the reaction cycle of precursors 1D and 2D was tested after the application of 25 mM EDC as fuel. Both precursors consumed the 25 mM EDC within 40 min, and the consumption could be fitted with a second-order rate constant (Table S2). The corresponding anhydride was observed within the first minute and peaked between 5 and 10 min before it collapsed until no more anhydride was observed after 40 min (Figures S2, S3, S4). Using a previously described kinetic model,³⁰ we could fit the evolution of relevant reactants in the cycle. That means that we can predict the concentration of each species for every second after the application of fuel. We describe the model in more detail in the Supporting Note 1.

We studied how the emergence and decay of the anhydride affected the macroscopic properties of peptide 1D. We added 25 mM EDC to peptide 1D; however, in all cases, the solution remained optically transparent (Figure 2B). To further verify the lack of assembly in response to fuel, we quantified the turbidity by measuring the absorbance at 600 nm as a function of time in response to 25 and 400 mM EDC (Figure S5B). Neither amount of fuel resulted in increased turbidity. Similarly, a ThT assay did not show an increased signal in response to a large amount of fuel (Figure S6). Rheology measurements showed that 15 mM 1D behaved like a liquid ($G'' \gg G'$) even after the addition of 25 mM EDC (Figure 2C). One can observe a high signal of G' for the first point, which is an artifact caused by the inertia of the measuring system. Finally, cryo-TEM showed no obvious assemblies present in the sample after fueling (25 mM EDC, Figure 2D). Taken together, the data show that peptide 1D does not assemble in response to fuel.

In contrast, 25 mM EDC added to peptide 2D resulted in the rapid formation of a weak turbid hydrogel; that is, within 1 min, the solution turned turbid and viscous (Figure 2B). After around 40 min, the solution regained its original viscosity and transparency. We carried out turbidity measurements by monitoring the absorbance at 600 nm, which could quantify the increased turbidity in response to 25 mM EDC (Figure S5C). It is worth mentioning that when we used up to 400 mM EDC, 2D still underwent transient self-assembly (Figure S5C). Moreover, we found that the duration of the turbidity increased with increasing amounts of EDC (Figure S5C). A ThT assay showed a drastic increase in signal in response to EDC, indicative of beta-sheet formation between the peptides (Figure S6). By means of rheology, we found that 15 mM 2D behaved like a liquid ($G'' \gg G'$) before the addition of 25 mM EDC (Figure S5D), but rapidly converted into an elastic hydrogel after the addition of fuel ($G' > G''$). As the gel formation is very fast, no sol–gel transition is observed upon fuel addition. The increased viscosity was transient, and the

sample was kept in a semistable state before collapsing after 35 min. A cryo-TEM study showed no obvious assemblies before the addition of EDC (Figure S7). However, 5 min after the addition of fuel, we found relatively short fibers (Figure 2D).

To better understand the dissipative self-assembly of peptide 2D, we measured the fiber composition by a ^1H NMR study.³⁰ We used the fact that self-assembled peptides have a reduced transversal relaxation time (T_2), resulting in long correlation times and a broadening of the signal that gets hidden under the baseline. This means that peptides, which participate in the assembly, become NMR-silent, while soluble peptides were NMR-visible. Seven minutes after the addition of 25 mM fuel, we found that roughly 5 mM of the peptide remained in solution. In other words, 10 mM of peptide had assembled into fibers. We used the kinetic model to calculate the amount of product at this point in time and were surprised to observe that only 3 mM of the peptide was in the product state. In other words, if we assume all product was in the fibers, the fibers comprised roughly 70% of precursor, indicating a great amount of coassembly of precursor and product (Figure S8). Taken together, the combined data clearly show that peptide 2D transiently assembles into fibers at the expense of EDC. These fibers comprise both the precursor and the anhydride product.

Finally, we found that peptide 3D was able to assemble into an elastic hydrogel without the addition of EDC (Figures 2B and C, S5A, S6). Moreover, cryo-TEM revealed that the peptide self-assembled into long fibers (Figure 2D). From these observations, we can conclude that the degree of attractive interactions between peptides can regulate the nonequilibrium response of the molecules to a chemical fuel. Peptide 1D, with a relatively low degree of attractive interactions, underwent no assembly in response to fuel (Figure 1; no assembly). Peptide 2D could undergo dissipative self-assembly (Figure 1; dissipative self-assembly). Finally, for the assembly of peptide 3D, no fuel was required (Figure 1; precursor assembles).

Taken together, the data above show that the molecular design of our peptide can affect the response of the system to chemical fuel. We can draw out the following design rules that apply when the energy-dissipating chemical reaction cycle modulates the electrostatic repulsion between peptides. (i) If the attractive interactions are weak, the precursor will not assemble, and the product will not be able to assemble or coassemble with the precursor; that is, no assembly will occur upon fueling the system. (ii) If the attractive interactions are optimized, the peptide will not assemble in the precursor state but in the product state, leading to a coassembly with the precursor. (iii) Moreover, the coassembly will collapse when reverted to the precursor; that is, dissipative self-assembly will occur upon fueling the system. (iv) Finally, when the attractive interactions are too strong, the peptide will assemble in its precursor state; that is, no fuel is required to assemble the system.

In order to generalize our rules, we synthesized Ac-FV_nD-OH, where $n = 1, 2, 3, \text{ or } 4$. We measured the response of these peptides to fuel by turbidity measurements (Figure S9). In line with the data above, the peptides with weak attractive interactions (Ac-FVD-OH and Ac-FVVD-OH) did not show any increased turbidity in response to 25 mM EDC (i.e., no assembly). The turbidity of the solution of Ac-FVVVD-OH did increase, and the solution also became more viscous. Moreover, the increased turbidity and the formation of an elastic hydrogel was transient (i.e., dissipative self-assembly).

Finally, Ac-FVVVD-OH, like 3D, formed a turbid hydrogel prior to the addition of EDC (i.e., the precursor assembled).

Regulating the response of our peptide to fuel by altering the degree of attractive interactions prompted us to study the opposite effect; that is, can we control the peptide's behavior by tuning repulsive interactions? The precursor in our reaction scheme is designed such that it does not assemble because it carries two negative charges that overcome the attractive interactions. We also observed that large amounts of precursor coassemble with the uncharged products. In other words, in the cases where we did not observe fuel-induced self-assembly, the attractive interactions were not sufficiently strong to overcome the electrostatic repulsion between the coassembling precursors. Thus, we reasoned that the addition of salts decreases the Debye screening length and results in a decrease of the electrostatic repulsion between precursors (Figure 3A).³⁴ Namely, additional salt could transition the response of peptides from dissipative self-assembly to a state where the precursor assembles. Moreover, given the fact that precursor and product coassemble to a large degree, the addition of salts could force nonassembling peptides to undergo fuel-driven dissipative self-assembly.

As demonstrated above, peptide 1D did not assemble in response to EDC as fuel when dissolved in 200 mM MES buffer. In contrast, when peptide 1D was dissolved in 200 mM MES buffer with 5 M NaCl, it transiently increased the turbidity in response to 25 mM EDC (Figure 3B), which we could quantify by measuring the absorbance at 600 nm (Figure 3C). A ThT assay demonstrated that peptide 1D with 5 M NaCl did not engage in beta-sheet formation before fuel addition, but did transiently form beta-sheets in response to fuel (Figure S10A,B). The rheology measurements showed only a small increase in the viscoelastic properties upon addition of fuel, but no formation of an elastic hydrogel (Figure S10C). Cryo-TEM revealed that the peptide self-assembled into fibers after the addition of salt in response to the same concentration of fuel (Figure 3E). The above experiments show that the addition of a large amount of salt can change the behavior from a nonassembling peptide to a dissipative assembling peptide.

We showed that without additional salts, peptide 2D could undergo fuel-driven dissipative self-assembly. In contrast, when we added 3 M or more NaCl, the peptide assembled into an elastic hydrogel without the addition of EDC (Figure 3B). We quantified the turbidity by measuring the absorbance at 600 nm (Figure S11A), and we measured the gel stiffness by rheology measurements (Figure 3D). A ThT assay indicated that the hydrogel formation was partially driven by beta-sheet formation (Figure S11B). Moreover, cryo-TEM revealed the presence of fibers without any fuel addition (Figure 3E). We were interested whether the self-assembly behavior of 2D could be modulated by the pH of the solution. We decreased the pH from 6 to 4 by addition of HCl, and the clear solution turned turbid (Figure S12A). The static nature of the assemblies allowed performing a cryo-TEM study (Figure S12B). In contrast, if we increased the pH to 7, we found no more evidence of self-assembly, also in response to 25 mM of fuel. The lack of assemblies is likely a combination of increased charge-charge repulsion between the precursors and a lower maximum anhydride concentration, as the optimal pH of the reaction cycle is pH 6. These combined experiments show that a peptide that transiently assembled driven by a chemical fuel

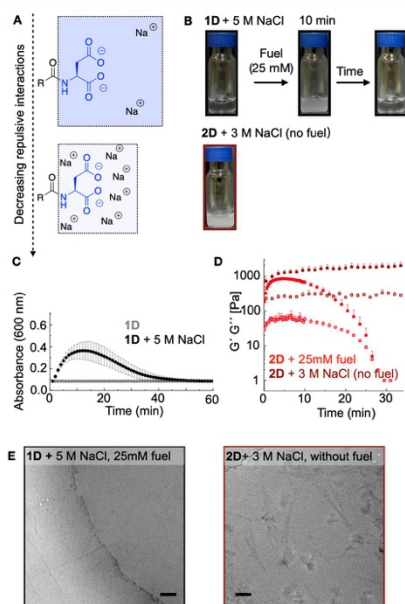


Figure 3. Regulating the response to fuel by tuning repulsive interactions. (A) Schematic representation of screening the repulsive interactions by the addition of salt. (B) Photographs of solutions of peptide 1D (15 mM) with 5 M NaCl before and after the addition of 25 mM of fuel and 2D (15 mM) with 3 M NaCl. (C) Turbidity measurements of 15 mM 1D with or without salt in response to 25 mM of fuel against time. (D) Storage and loss modulus as a function of time, measured by plate–plate rheology of 15 mM 2D with 3 M NaCl or with 25 mM EDC. Solid squares represent the storage modulus (G'); empty squares represent the loss modulus (G''). (E) Cryo-TEM images of the solutions of 15 mM 1D + 5 M NaCl at 10 min after fueling with 25 mM EDC, and 15 mM 2D with 3 M NaCl but without fuel. The error bars represent the standard deviation of the average ($n = 3$). All scale bars correspond to 100 nm. All the experiments were carried out at a pH of 6 and in 200 mM MES buffer.

could be permanently trapped in a self-assembled state by the addition of salt or acid.

From the data above, we can conclude that the response of the peptide can be regulated by controlling the electrostatic repulsion between precursor molecules. However, one could argue that the addition of 5 M of salt is not a particularly elegant design strategy. We thus designed a new peptide class where the increased electrostatic repulsion was encoded in the molecular structure (Figure 4A). We retained the C-terminal aspartate and added an additional aspartate to the N-terminus via a succinic acid spacer, resulting in D^{*}FIID-OH (D2D) and D^{*}FIID-OH (D3D), where D^{*} represents an aspartic acid amidated succinic acid spacer (Figure 4a). Consequently, the attractive interactions of 2D remain roughly equal compared to D2D, but the number of carboxylate groups doubles, which results in an increase in repulsive interactions. We tested the response of these peptides to 25 mM EDC and compared it to

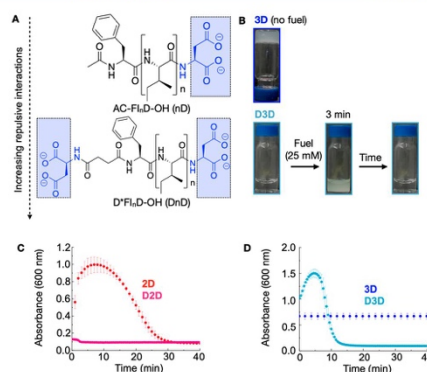


Figure 4. Regulating the response to fuel by tuning repulsive interactions in the molecular design. (A) Schematic representation of increasing the repulsive interactions by addition of charges. (B) Photographs of solutions of peptide 3D (15 mM) without fuel addition and D3D (15 mM) before and after 25 mM fuel addition. (C) Turbidity measurements of D2D (15 mM) and 2D (15 mM) in response to 25 mM fuel against time. (D) Turbidity measurements of D3D (15 mM) in response to 25 mM fuel against time compared with peptide 3D (15 mM) without fuel. Error bars represent the standard deviation of the average ($n = 3$). All the experiments were carried out at a pH of 6 and in 200 mM MES buffer.

the peptides without the additional repulsive interactions, i.e., D^{*}FIID-OH (D2D) versus Ac-FIID-OH (2D) and D^{*}FIID-OH (D3D) versus Ac-FIID-OH (3D). With that, we aim to study whether electrostatic repulsion, now encoded in the peptide design, can be used to regulate the response to chemical fuels.

We described earlier that peptide 3D assembled into a hydrogel without any addition of fuel. In contrast, D3D did not assemble before the addition of fuel, which was proven by a ThT assay measurement (Figure S13). After the addition of fuel (25 mM EDC), the turbidity transiently increased (Figure 4B,C). The fuel-driven self-assembly of D3D was further confirmed by the transient formation of beta-sheets (Figure S14E). Importantly, both the turbidity and increased ThT signal fell back to their original level within 15 min. Considering the two aspartic acid groups D3D, we doubled the fuel to 50 mM compared to the experiments carried out with 3D. Also, under these conditions, D3D underwent fuel-driven transient self-assembly (Figure S14A, C, E). These combined experiments showed that by increasing electrostatic repulsion in the molecular structure, we could change the peptide's behavior from a state where the precursors assembled to fuel-driven dissipative self-assembly.

We described earlier that 2D self-assembled transiently in response to 25 mM of EDC as fuel. In contrast, peptide D2D showed a small and short increase in turbidity after the addition of fuel (25 or 50 mM EDC (Figure 4D and Figure S14D)). Meanwhile, a ThT assay demonstrated that peptide D2D did not engage significantly in beta-sheet formation in response to EDC (Figure S14F). These experiments show that by increasing the electrostatic interactions between the peptides by the incorporation of an extra aspartic acid, the

behavior can be tuned from dissipative self-assembly to virtually no-assembly in response to fuel. Moreover, from the combined data set, we can conclude that the response of the peptide can be regulated by increasing electrostatic repulsion between peptides.

The combined experiments allow creating a phase diagram of the fuel-driven response of our peptides. In Figure 5A, on

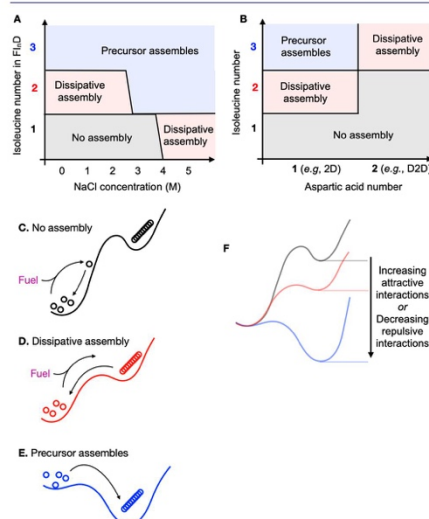


Figure 5. Phase diagrams and energy landscapes of chemically fueled assembly. (A) Possible peptide behavior with one, two, or three isoleucine residues in the peptide sequence Ac-FI_{*n*}-D-OH at different salt concentrations. (B) Possible peptide behavior with one, two, or three isoleucine residues and one or two charged residues in the peptide sequence. (C–E) Energy landscapes of the three scenarios: no assembly, dissipative assembly, and the precursor assemblies. (F) Combined energy landscape of the cases discussed in B–D.

the *y*-axis, we show the number of isoleucines in the peptide design (*n*), as a measure for attractive interactions, against the concentration of added salt, like an inverted measure for the repulsive interactions. With increasing attractive interactions and no added salt, the system behavior evolves from no assembly, through dissipative self-assembly, to a state where the precursor assembles. Similarly, the addition of salt decreases the electrostatic repulsion and thus evolves the system from no assembly to dissipative assembly to a state where the precursor assembles. In Figure 5B, on the *y*-axis, again, we show the number of isoleucines in the peptide design (*n*). On the *x*-axis, we show the number of aspartic acid groups; 1 or 2 corresponds, for example, to 2D or D2D, respectively. The *x*-axis is thus a measure for repulsive interactions. We found that on increasing that number, the behavior could be changed from dissipative assembly to no assembly or from a state where the precursor assembles to dissipative assembly.

The observed phase diagrams can be rationalized by the simplified energy landscapes of self-assembly (Figure 5C–E). These energy landscapes are characterized by at least two energy wells. One well represents the nonassembled precursor, and one represents the coassembled precursor and product state. The activation of the precursors pushes them up in the energy landscape, potentially in the next energy well, where self-assembly is favored. In the case of no assembly (Figure 5C), the energy gain upon activation is insufficient to drive the precursor into the next well, either because the attractive interactions are insufficient or the repulsive interactions are too great. In the case of dissipative assembly (Figure 5D), the energy gain upon activation can drive the precursor into the next well, where self-assembly takes place. Moreover, the energy barrier for disassembly is low; that is, disassembly takes place after deactivation without great delay. Finally, in the case where the precursor assembles, the energy well for assembly of the precursor is below the energy well for its nonassembled state (Figure 5E). The system thus favors the assembly of the precursor without the need for fuel.

In Figure 5F, we compare the three energy landscapes. In each of our experiments, the activation and deactivation are driven by the same chemical reaction cycle, and the energy gained upon activation is thus roughly similar. The difference in the behavior thus comes from the difference in the energy well of the self-assembled state relative to the energy well of the nonassembled state, which can be tuned by peptide designs. For example, when the number of attractive interactions is increased, the energy well corresponding to the self-assembled state is pushed downward relative to the nonassembled state. Similarly, when salt is added to the system, effectively decreasing the ionic repulsion between precursors, the energy well associated with the self-assembled state of the precursor and product is pushed down. We believe that these phase diagrams and their associated energy landscapes can be generalized to some degree for fuel-driven assemblies, provided that the design is based on a reaction cycle that uses charge abolishment as a mechanism to induce self-assembly.

CONCLUSION

We introduced a new family of peptides coupled to a well-known chemically fueled reaction cycle. The simplicity of the peptide design and reaction cycle allows creating some general rules for the self-assembly behavior in response to fuel. We find three possible behaviors: the peptide does not assemble, it assembles dissipatively, or it assembles without fuel. We can toggle between these behaviors with different peptide designs and environmental conditions. Future work should investigate further nuances in these energy landscapes to probe other dynamic behaviors such as kinetic trapping or dynamic instabilities.

ASSOCIATED CONTENT

Supporting Information

The Supporting Information is available free of charge at <https://pubs.acs.org/doi/10.1021/jacs.0c04203>.

Materials and methods description and additional turbidity data, fluorescence spectroscopy data, rheology data, NMR data, and cryo-TEM images (PDF)

AUTHOR INFORMATION

Corresponding Author

Job Boekhoven – Department of Chemistry and Institute for Advanced Study, Technical University of Munich, 85748 Garching, Germany; orcid.org/0000-0002-9126-2430; Email: job.boekhoven@tum.de

Authors

Kun Dai – Department of Chemistry, Technical University of Munich, 85748 Garching, Germany

Jennifer Rodon Fores – Department of Chemistry, Technical University of Munich, 85748 Garching, Germany; orcid.org/0000-0002-7472-1228

Caren Wanzke – Department of Chemistry, Technical University of Munich, 85748 Garching, Germany

Benjamin Winkeljann – Department of Mechanical Engineering and Munich School of Bioengineering, Technical University of Munich, 85748 Garching, Germany; orcid.org/0000-0002-6334-6696

Alexander M. Bergmann – Department of Chemistry, Technical University of Munich, 85748 Garching, Germany

Oliver Lieleg – Department of Mechanical Engineering and Munich School of Bioengineering, Technical University of Munich, 85748 Garching, Germany; orcid.org/0000-0002-6874-7456

Complete contact information is available at: <https://pubs.acs.org/10.1021/jacs.0c04203>

Notes

The authors declare no competing financial interest.

ACKNOWLEDGMENTS

K.D. thanks the financial support from the China Scholarship Council. J.R.F. thanks the Deutsche Forschungsgemeinschaft for project 411722921. J.B., W.B., and O.L. acknowledge funding from the Deutsche Forschungsgemeinschaft (DFG, German Research Foundation), SFB- 863, Project ID 111166240 (Project B11). C.W. is grateful for funding by the Deutsche Forschungsgemeinschaft (DFG, German Research Foundation), Project-ID 364653263, TRR 235. J.B. is grateful for funding by the Technical University of Munich, Institute for Advanced Study, funded by the German Excellence Initiative and the European Union Seventh Framework Program under grant agreement No. 291763.

REFERENCES

- (1) van Rossum, S. A. P.; Tena-Solsona, M.; van Esch, J. H.; Eelkema, R.; Boekhoven, J. Dissipative Out-of-Equilibrium Assembly of Man-Made Supramolecular Materials. *Chem. Soc. Rev.* **2017**, *46* (18), 5519–5535.
- (2) De, S.; Klajn, R. Dissipative Self-Assembly Driven by the Consumption of Chemical Fuels. *Adv. Mater.* **2018**, *30* (41), 1706750.
- (3) Sorrenti, A.; Leira-Iglesias, J.; Markvoort, A. J.; de Greef, T. F. A.; Hermans, T. M. Non-Equilibrium Supramolecular Polymerization. *Chem. Soc. Rev.* **2017**, *46* (18), 5476–5490.
- (4) Merindol, R.; Walther, A. Materials Learning from Life: Concepts for Active, Adaptive and Autonomous Molecular Systems. *Chem. Soc. Rev.* **2017**, *46* (18), 5588–5619.
- (5) Rieß, B.; Grötsch, R. K.; Boekhoven, J. The Design of Dissipative Molecular Assemblies Driven by Chemical Reaction Cycles. *Chem.* **2020**, *6* (3), 527.
- (6) Molla, M. R.; Rangadurai, P.; Antony, L.; Swaminathan, S.; de Pablo, J. J.; Thayumanavan, S. Dynamic Actuation of Glassy

Polymersomes through Isomerization of a Single Azobenzene Unit at the Block Copolymer Interface. *Nat. Chem.* **2018**, *10* (6), 659–666.

(7) Brouhard, G. J.; Rice, L. M. Microtubule Dynamics: An Interplay of Biochemistry and Mechanics. *Nat. Rev. Mol. Cell Biol.* **2018**, *19* (7), 451–463.

(8) Dogterom, M.; Koenderink, G. H. Actin–Microtubule Crosstalk in Cell Biology. *Nat. Rev. Mol. Cell Biol.* **2019**, *20* (1), 38–54.

(9) Wang, G.; Liu, S. Strategies to Construct a Chemical-Fuel-Driven Self-Assembly. *ChemSystemsChem.* **2020**, DOI: 10.1002/syst.201900046.

(10) Kim, B. J.; Yang, D.; Xu, B. Emerging Applications of Supramolecular Peptide Assemblies. *Trends in Chemistry* **2020**, *2* (1), 71–83.

(11) Ragazzon, G.; Prins, L. J. Energy Consumption in Chemical Fuel-Driven Self-Assembly. *Nat. Nanotechnol.* **2018**, *13* (10), 882–889.

(12) Pappas, C. G.; Sasselvi, I. R.; Ulijn, R. V. Biocatalytic Pathway Selection in Transient Tripeptide Nanostructures. *Angew. Chem., Int. Ed.* **2015**, *54* (28), 8119–8123.

(13) Boekhoven, J.; Brizard, A. M.; Kowligi, K. N. K.; Koper, G. J. M.; Eelkema, R.; van Esch, J. H. Dissipative Self-Assembly of a Molecular Gelator by Using a Chemical Fuel. *Angew. Chem., Int. Ed.* **2010**, *49* (28), 4825–4828.

(14) Leira-Iglesias, J.; Sorrenti, A.; Sato, A.; Dunne, P. A.; Hermans, T. M. Supramolecular Pathway Selection of Peryleneimides Mediated by Chemical Fuels. *Chem. Commun.* **2016**, *52* (58), 9009–9012.

(15) Leira-Iglesias, J.; Tassoni, A.; Adachi, T.; Stich, M.; Hermans, T. M. Oscillations, Travelling Fronts and Patterns in a Supramolecular System. *Nat. Nanotechnol.* **2018**, *13* (11), 1021–1027.

(16) Sorrenti, A.; Leira-Iglesias, J.; Sato, A.; Hermans, T. M. Non-Equilibrium Steady States in Supramolecular Polymerization. *Nat. Commun.* **2017**, *8*, 15899.

(17) Tena-Solsona, M.; Janssen, J.; Wanzke, C.; Schnitter, F.; Park, H.; Rieß, B.; Gibbs, J. M.; Weber, C. A.; Boekhoven, J. *ChemRxiv* **2019**, Preprint DOI: 10.26434/chemrxiv.9978539.V1.

(18) Tena-Solsona, M.; Wanzke, C.; Riess, B.; Bausch, A. R.; Boekhoven, J. Self-Selection of Dissipative Assemblies Driven by Primitive Chemical Reaction Networks. *Nat. Commun.* **2018**, *9* (1), 2044.

(19) Debnath, S.; Roy, S.; Ulijn, R. V. Peptide Nanofibers with Dynamic Instability through Nonequilibrium Biocatalytic Assembly. *J. Am. Chem. Soc.* **2013**, *135* (45), 16789–16792.

(20) Maiti, S.; Fortunati, L.; Ferrante, C.; Scrimin, P.; Prins, L. J. Dissipative Self-Assembly of Vesicular Nanoreactors. *Nat. Chem.* **2016**, *8* (7), 725–731.

(21) Heinen, L.; Walther, A. Programmable Dynamic Steady States in ATP-Driven Nonequilibrium DNA Systems. *Science Advances* **2019**, *5* (7), No. eaaw0590.

(22) Heuser, T.; Weyandt, E.; Walther, A. Biocatalytic Feedback-Driven Temporal Programming of Self-Regulating Peptide Hydrogels. *Angew. Chem., Int. Ed.* **2015**, *54* (45), 13258–13262.

(23) Panja, S.; Dietrich, B.; Adams, D. J. Chemically Fuelled Self-Regulating Gel-to-Gel Transition. *ChemSystemsChem.* **2020**, *2* (1), DOI: 10.1002/syst.201900038.

(24) Ragazzon, G.; Baroncini, M.; Silvi, S.; Venturi, M.; Credi, A. Light-Powered Autonomous and Directional Molecular Motion of a Dissipative Self-Assembling System. *Nat. Nanotechnol.* **2015**, *10* (1), 70–75.

(25) Grötsch, R. K.; Wanzke, C.; Speckbacher, M.; Angi, A.; Rieger, B.; Boekhoven, J. Pathway Dependence in the Fuel-Driven Dissipative Self-Assembly of Nanoparticles. *J. Am. Chem. Soc.* **2019**, *141* (25), 9872–9878.

(26) Grötsch, R. K.; Angi, A.; Mideksa, Y. G.; Wanzke, C.; Tena-Solsona, M.; Feige, M. J.; Rieger, B.; Boekhoven, J. Dissipative Self-Assembly of Photoluminescent Silicon Nanocrystals. *Angew. Chem., Int. Ed.* **2018**, *57* (44), 14608–14612.

(27) Wang, G.; Tang, B.; Liu, Y.; Gao, Q.; Wang, Z.; Zhang, X. The Fabrication of a Supra-Amphiphile for Dissipative Self-Assembly. *Chem. Sci.* **2016**, *7* (2), 1151–1155.

(28) Boekhoven, J.; Hendriksen, W. E.; Koper, G. J. M.; Elkema, R.; van Esch, J. H. Transient Assembly of Active Materials Fueled by a Chemical Reaction. *Science* **2015**, *349* (6252), 1075–1079.

(29) Tena-Solsona, M.; Rieß, B.; Grötsch, R. K.; Löhrer, F. C.; Wanzke, C.; Käs Dorf, B.; Bausch, A. R.; Müller-Buschbaum, P.; Lieleg, O.; Boekhoven, J. Non-Equilibrium Dissipative Supramolecular Materials with a Tunable Lifetime. *Nat. Commun.* **2017**, *8*, 15895.

(30) Wanzke, C.; Jussupow, A.; Kohler, F.; Dietz, H.; Kaila, V. R. L.; Boekhoven, J. Dynamic Vesicles Formed By Dissipative Self-Assembly. *ChemSystemsChem.* **2020**, DOI: 10.1002/syst.201900044.

(31) Rieß, B.; Wanzke, C.; Tena-Solsona, M.; Grötsch, R. K.; Maity, C.; Boekhoven, J. Dissipative Assemblies That Inhibit Their Deactivation. *Soft Matter* **2018**, *14* (23), 4852–4859.

(32) Kariyawasam, L. S.; Hartley, C. S. Dissipative Assembly of Aqueous Carboxylic Acid Anhydrides Fueled by Carbodiimides. *J. Am. Chem. Soc.* **2017**, *139* (34), 11949–11955.

(33) Sahoo, J. K.; Nazareth, C.; VandenBerg, M. A.; Webber, M. J. Aromatic Identity, Electronic Substitution, and Sequence in Amphiphilic Tripeptide Self-Assembly. *Soft Matter* **2018**, *14* (45), 9168–9174.

(34) Evans, D. F.; Wennerström, H. *The Colloidal Domain: Where Physics, Chemistry, Biology, and Technology Meet*, 2nd ed.; Advances in Interfacial Engineering Series; Wiley-VCH: New York, 1999.

Supporting Information for:

Regulating chemically fueled peptide assemblies by molecular design

Kun Dai,¹ Jennifer Rodon Fores,¹ Caren Wanzke,¹ Benjamin Winkeljann,² Alexander M. Bergmann,¹ Oliver Lieleg² & Job Boekhoven^{*1,3}

¹ Department of Chemistry, Technical University of Munich, Lichtenbergstrasse 4, 85748 Garching, Germany.

² Department of Mechanical Engineering and Munich School of Bioengineering, Technical University of Munich, Boltzmannstrasse 11, 85748 Garching, Germany.

³ Institute for Advanced Study, Technical University of Munich, Lichtenbergstrasse 2a, 85748 Garching, Germany.

Materials and Methods

Materials.

All reagents were purchased from Sigma-Aldrich and Alfa-Aesar and used without further purification unless otherwise indicated. The peptides used in this study were synthesized using solid-phase peptide synthesis.

Peptide synthesis and its purification.

Ac-FI_nD-OH (nD), Ac-FV_nD-OH

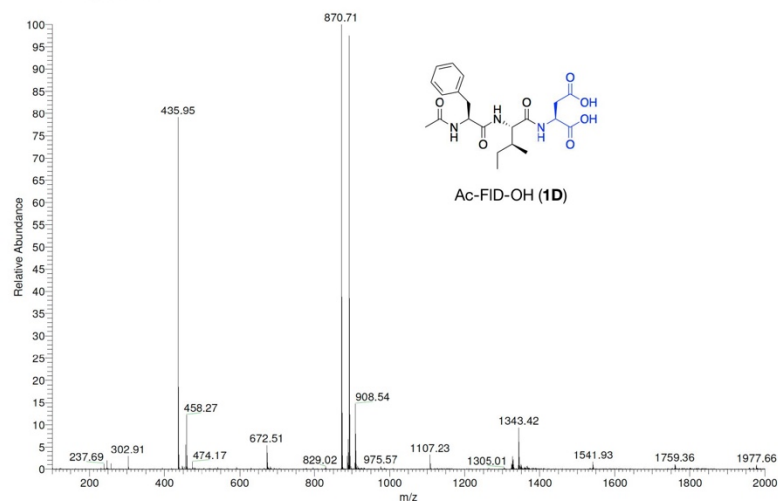
The peptide synthesis was performed on a CEM Liberty microwave-assisted peptide synthesizer. The first amino acid coupling to the resin was accomplished by using the symmetrical anhydride method. Briefly, a 0.2 M solution of the symmetrical anhydride was prepared by allowing the Fmoc-protected aspartic acid (FmocD(OtBu)OH, 12 mmol) and N,N'-diisopropylcarbodiimide (DIC, 6 mmol) to react in 30 mL N,N-dimethylformamide (DMF) for 60 min. The solution was placed in a freezer at -20 °C for 30 min, and the solid urea formed was filtered out before the next step. Loading of the resin was performed using the automated peptide synthesizer. The symmetrical anhydride solution (0.2 M, 12 mL) and 4-(dimethylamino)pyridine (DMAP) solution in DMF (20 mM, 2.5 mL) were added to the pre-swollen Wang resin (0.5 mmol, 1.1 mmol/g) and heated in the microwave (30 min, 75 °C). The coupling was repeated twice. The resin was then washed with DMF (2x10 mL). Following couplings were achieved using 4 equivalents (eq.) of Fmoc-protected amino acid in DMF, 4 eq. of DIC and 4 eq. of ethyl (hydroxyimino)cyanoacetate (Oxyma). The resin solution was then heated in the microwave (1x2 min, 90 °C). Fmoc removal was accomplished using a solution of 20% piperidine in DMF (1x2 min, 90 °C). The resin was washed with DMF (3x7 mL) between different steps. This procedure was repeated until the last chemical CH₃COOH was coupled. The resulting peptide was cleaved from the resin using a mixture of 95% trifluoroacetic acid (TFA), 2.5% water, and 2.5% triisopropylsilane (TIPS). The solvent was removed by co-distillation with DCM by rotary evaporation and dried under reduced pressure. The residue was extracted with diethyl ether one time and the organic phase was washed two times with water. The combined aqueous phase was purified using reversed-phase high-performance liquid chromatography (HPLC, Thermofisher Dionex Ultimate 3000, Hypersil Gold 250x4.8 mm) in a linear gradient of acetonitrile (ACN, 2% to 98%) and water with 0.1% TFA. The purified peptide was lyophilized and stored at -20 °C until further use. The purity of the peptide was analyzed by electrospray ionization mass in ESI-MS as well as analytical HPLC (See Supporting Table 1 for a summary of the analysis of the purity. See the section on Peptides characterization for the extensive data).

D*FlnD-OH (DnD)

The synthesis of the title compound was carried out similarly to the Ac-FIID-OH until the point of the phenyl alanine Fmoc-deprotection. After the deprotection, a 0.2 M solution of the succinic anhydride and DMAP solution in DMF (20 mM, 2.5 mL) was added to the previous deprotected peptides on Wang-resin and heated in the microwave (30 min, 75 °C). The procedure was repeated twice. The resin was then washed with DMF (2x10 mL). The final addition of L-aspartic acid, was achieved by using L-Aspartic acid di-tert-butyl ester hydrochloride. First, 4 eq. L-Aspartic acid di-tert-butyl ester hydrochloride was dissolved in DMF, and 1.5 eq. triethylamine was added. Then, after the filtration, to the solution, 4 eq. of DIC and 4 eq. of Oxyma were added to the resin. The resin solution was then heated in the microwave (1x2 min, 90 °C), and this coupling was repeated twice. The resulting peptide was cleaved from the resin using a mixture of 95% TFA, 2.5% water, and 2.5% TIPS. The solvent was removed by codistillation with DCM by rotary evaporation, and the sample was dried under reduced pressure. The residue was extracted with diethyl ether one time and the organic phase was washed two times with water. The combined aqueous phase was purified using reversed-phase high-performance liquid chromatography (HPLC, Thermofisher Dionex Ultimate 3000, Hypersil Gold 250x4.8 mm) in a linear gradient of acetonitrile (ACN, 2% to 98%) and water with 0.1% TFA. The purified product was lyophilized and stored at -20 °C until further use. The purity of the peptide was analyzed by electrospray ionization mass in ESI-MS as well as analytical HPLC HPLC (See Supporting Table 1 for a summary of the analysis of the purity. See the section on Peptides characterization for the extensive data).

Peptide characterization by ^1H NMR, MS and HPLC.**Ac-FID (1D):**

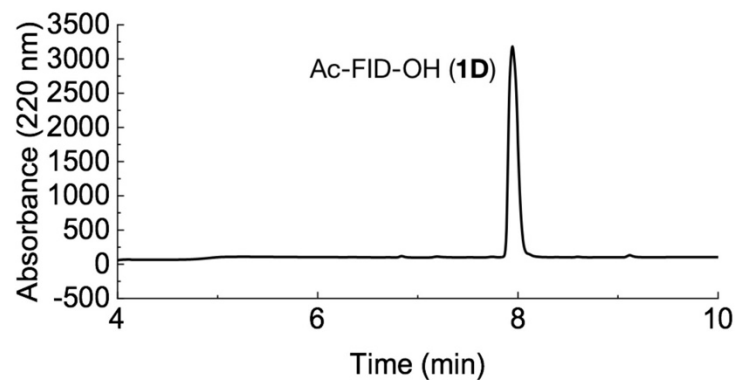
ESI-MS spectrum



NMR shifts:

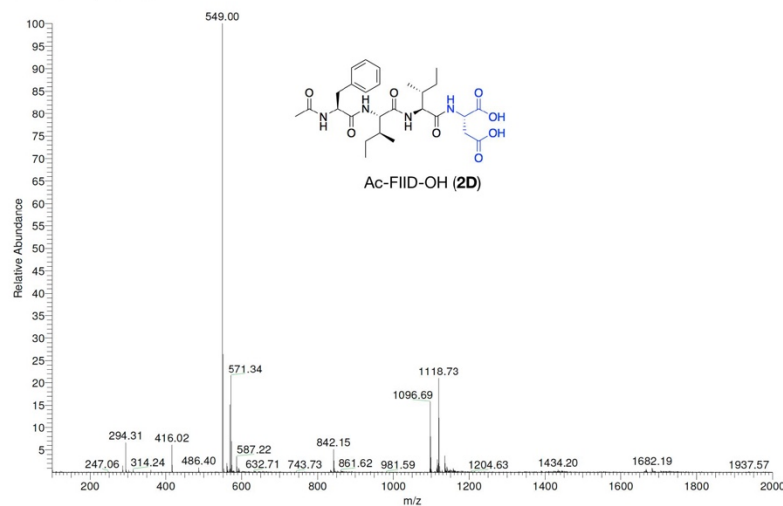
^1H NMR (500 MHz, DMSO) δ 8.27 (dd, $J = 29.4, 7.9$ Hz, 1H), 8.06 (dd, $J = 8.4, 4.7$ Hz, 1H), 7.88 (d, $J = 9.0$ Hz, 1H), 7.30 – 7.21 (m, 4H), 7.21 – 7.08 (m, 1H), 4.55 (dtd, $J = 14.6, 7.7, 6.8, 2.8$ Hz, 2H), 4.23 (dd, $J = 8.9, 6.9$ Hz, 1H), 3.05 – 2.94 (m, 1H), 2.69 (dd, $J = 6.5, 2.1$ Hz, 2H), 2.62 – 2.53 (m, 1H), 1.75 (s, 4H), 1.44 (td, $J = 7.5, 6.7, 3.4$ Hz, 1H), 1.06 (ddt, $J = 14.8, 12.2, 7.4$ Hz, 1H), 0.89 – 0.77 (m, 6H).

HPLC chromatogram measured at 220 nm



Ac-FIID (2D):

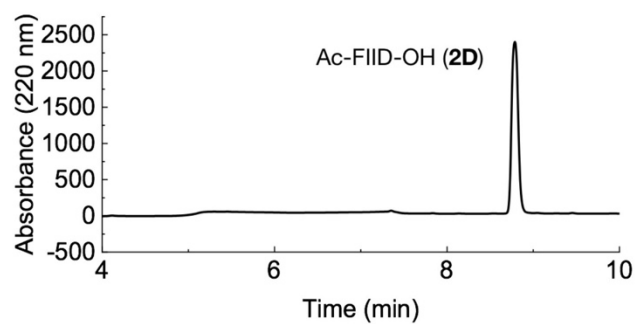
ESI-MS spectra



NMR shifts

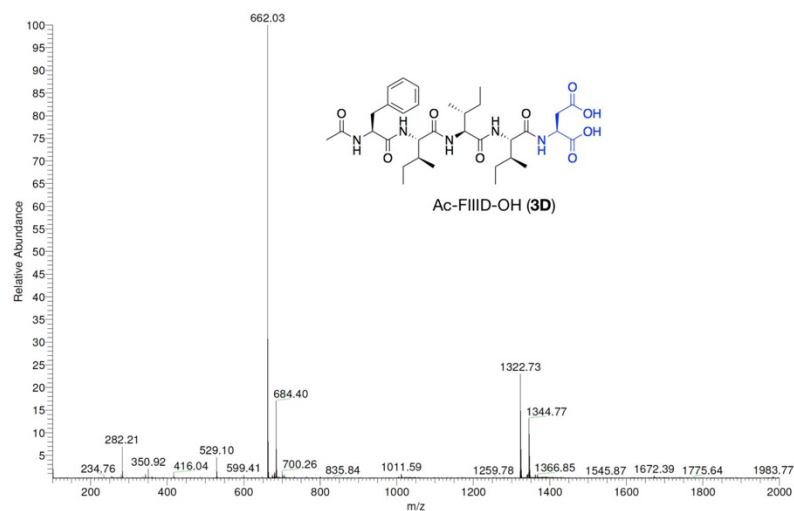
^1H NMR (500 MHz, DMSO) δ 8.23 (dd, $J = 35.8, 7.9$ Hz, 1H), 8.06 (d, $J = 8.4$ Hz, 1H), 7.99 (d, $J = 8.8$ Hz, 1H), 7.80 (d, $J = 9.0$ Hz, 1H), 7.25 (d, $J = 4.4$ Hz, 4H), 7.20 – 7.13 (m, 1H), 4.59 – 4.47 (m, 2H), 4.22 (dt, $J = 8.8, 7.1$ Hz, 2H), 2.96 (dd, $J = 13.9, 4.1$ Hz, 1H), 2.76 – 2.63 (m, 2H), 2.56 (dd, $J = 16.7, 6.8$ Hz, 1H), 1.74 (s, 5H), 1.44 (ddd, $J = 14.2, 7.4, 3.7$ Hz, 2H), 1.08 (dddd, $J = 13.4, 11.2, 9.1, 7.1$ Hz, 2H), 0.88 – 0.73 (m, 12H).

HPLC chromatogram measured at 220 nm



Ac-FIIID (3D):

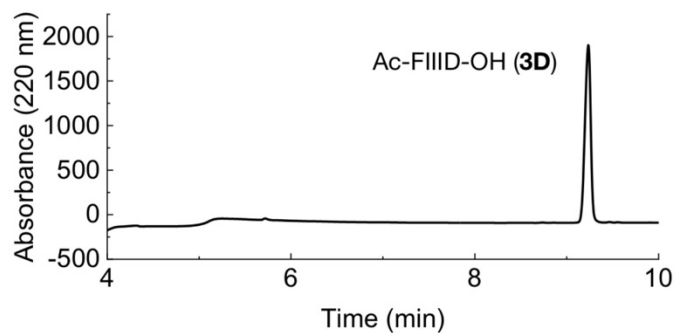
ESI-MS spectra



NMR shift

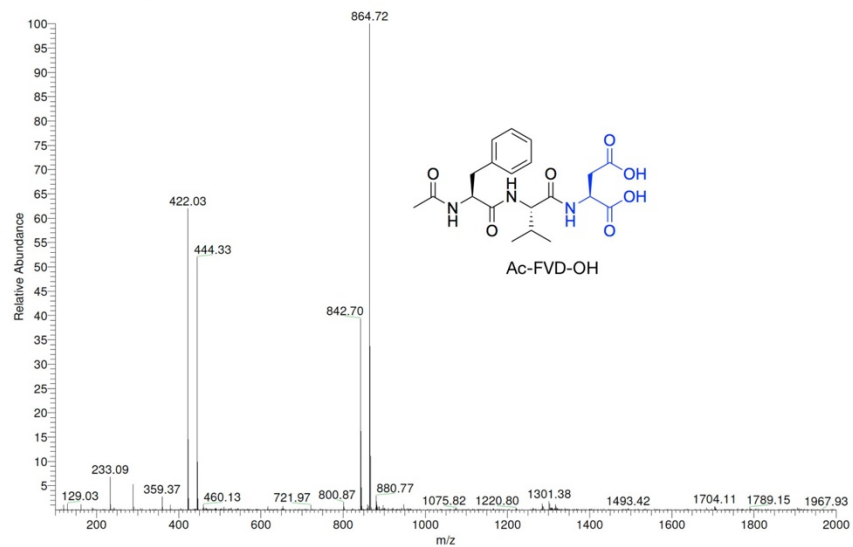
^1H NMR (500 MHz, DMSO) δ 12.64 (s, 1H), 12.37 (s, 1H), 8.17 (s, 1H), 8.05 (d, $J = 8.5$ Hz, 1H), 7.96 (d, $J = 8.8$ Hz, 1H), 7.91 (d, $J = 8.9$ Hz, 1H), 7.82 (d, $J = 8.7$ Hz, 1H), 7.25 (d, $J = 4.4$ Hz, 4H), 7.21 – 7.15 (m, 1H), 4.59 – 4.53 (m, 1H), 4.51 (d, $J = 6.9$ Hz, 1H), 4.23 (ddt, $J = 10.7$, 6.4, 2.7 Hz, 3H), 2.96 (dd, $J = 13.9$, 4.0 Hz, 1H), 2.70 (dd, $J = 14.0$, 10.2 Hz, 1H), 2.64 (d, $J = 5.1$ Hz, 1H), 2.56 (d, $J = 6.7$ Hz, 1H), 1.74 (s, 4H), 1.73 – 1.66 (m, 3H), 1.43 (s, 3H), 1.12 – 0.99 (m, 3H), 0.85 – 0.75 (m, 18H).

HPLC chromatogram measured at 220 nm

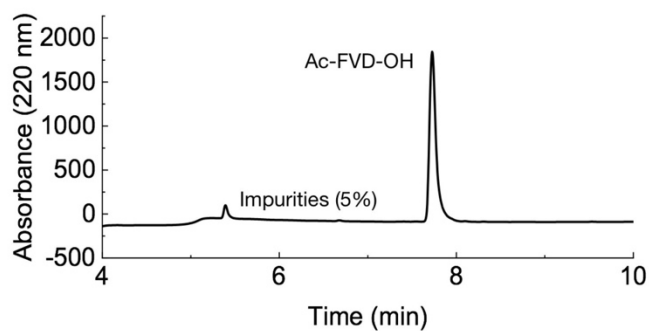


Ac-FVD:

ESI-MS spectra

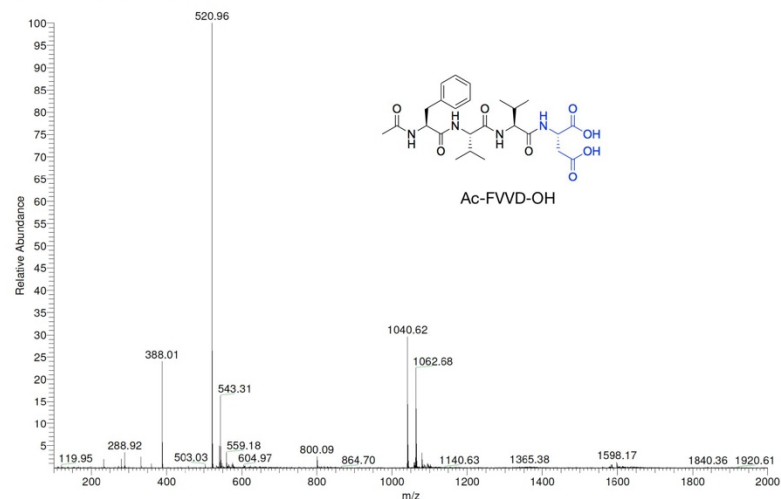
NMR shifts

^1H NMR (500 MHz, $\text{DMSO-}d_6$) δ 12.5 (s, 1H), 8.31 (dd, $^3J = 28.1, 7.9$ Hz, 1H), 8.09 (d, $^3J = 8.4$ Hz, 1H), 7.86 (d, $^3J = 8.9$ Hz, 1H), 7.25 (d, $^3J = 4.5$ Hz, 4H), 7.17 (s, 1H), 4.60 – 4.51 (m, 2H), 4.23 (dd, $^3J = 9.0, 6.2$ Hz, 1H), 3.01 (dd, $^3J = 13.9, 4.2$ Hz, 1H), 2.75 – 2.68 (m, 2H), 2.61 (dd, $^3J = 8.9, 4.5$ Hz, 1H), 2.02 – 1.94 (m, 1H), 1.74 (s, 3H), 0.86 (dd, $^3J = 13.3, 6.8$ Hz, 6H).

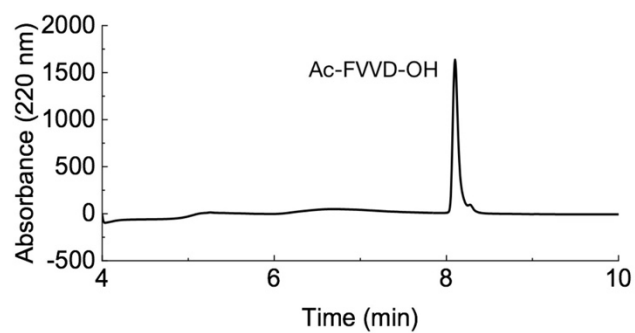
HPLC chromatogram measured at 220 nm

Ac-FVVD:

ESI-MS spectrum

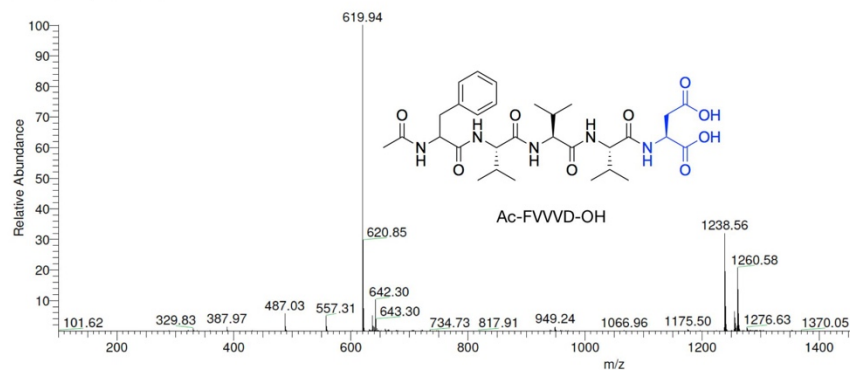
NMR shifts

^1H NMR (500 MHz, $\text{DMSO-}d_6$) δ 8.23 (dd, $^3J = 25.7, 7.9$ Hz, 1H), 8.08 (d, $^3J = 8.4$ Hz, 1H), 7.96 (d, $^3J = 8.8$ Hz, 1H), 7.78 (d, $^3J = 8.7$ Hz, 1H), 7.31-7.22 (m, 4H), 7.19 (dd, $^3J = 5.7, 3.0$ Hz, 1H), 4.62-4.48 (m, 2H), 4.22 (dt, $^3J = 9.0, 6.5$ Hz, 2H), 2.98 (dd, $^3J = 14.0, 4.1$ Hz, 1H), 2.82-2.63 (m, 2H), 2.57 (dd, $^3J = 16.7, 7.0$ Hz, 1H), 1.99 (ddd, $^3J = 11.7, 8.5, 5.8$ Hz, 2H), 1.75 (s, 3H), 0.93-0.77 (m, 12H).

HPLC chromatogram measured at 220 nm

Ac-FVVVD:

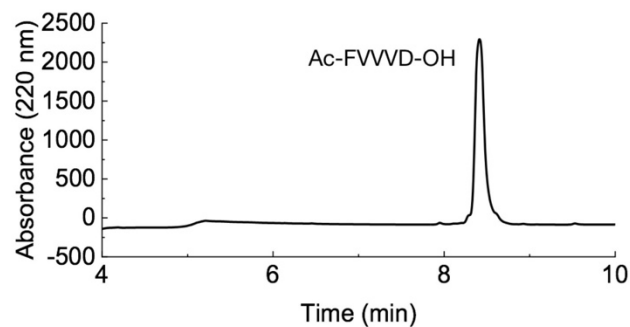
ESI-MS spectrum



NMR shifts

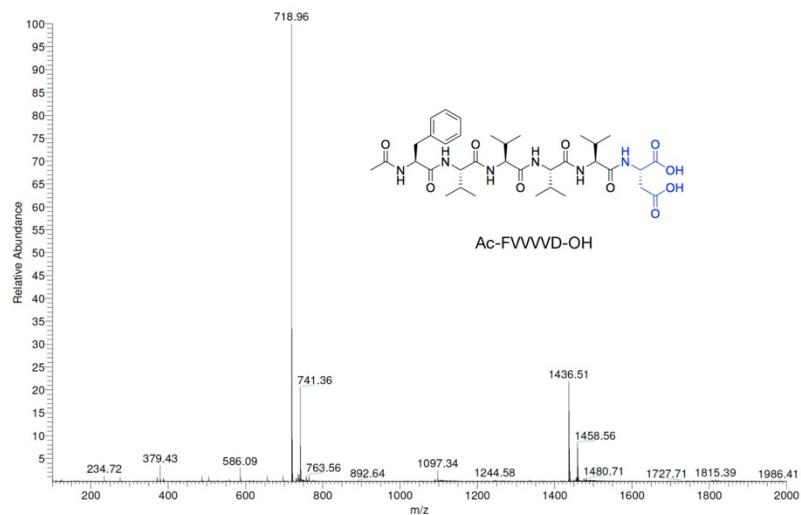
^1H NMR (500 MHz, $\text{DMSO}-d_6$) 8.72 (d, $J = 8.2$ Hz, 1H), 8.29 (d, $J = 8.8$ Hz, 1H), 8.07 (d, $J = 8.5$ Hz, 2H), 7.94 (d, $J = 8.8$ Hz, 2H), 7.88 (d, $J = 8.7$ Hz, 1H), 7.78 (d, $J = 9.0$ Hz, 1H), 7.32 – 7.15 (m, 9H), 4.74 (d, $J = 4.3$ Hz, 1H), 4.48 (s, 1H), 4.34 – 4.14 (m, 3H), 3.99 (s, 1H), 3.12 (dd, $J = 14.2, 4.4$ Hz, 1H), 3.03 (dd, $J = 14.1, 4.1$ Hz, 1H), 2.92 (dd, $J = 14.3, 8.1$ Hz, 1H), 2.83 (dd, $J = 14.0, 9.5$ Hz, 1H), 2.75 – 2.60 (m, 1H), 2.07 – 1.89 (m, 3H), 0.93 – 0.75 (m, 18H).

HPLC chromatogram measured at 220 nm



Ac-FVVVD:

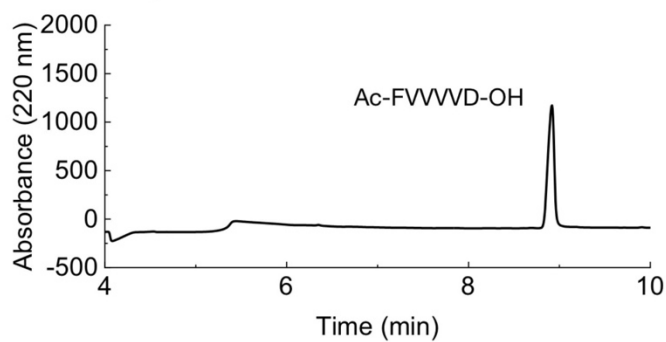
ESI-MS spectra



NMR shifts

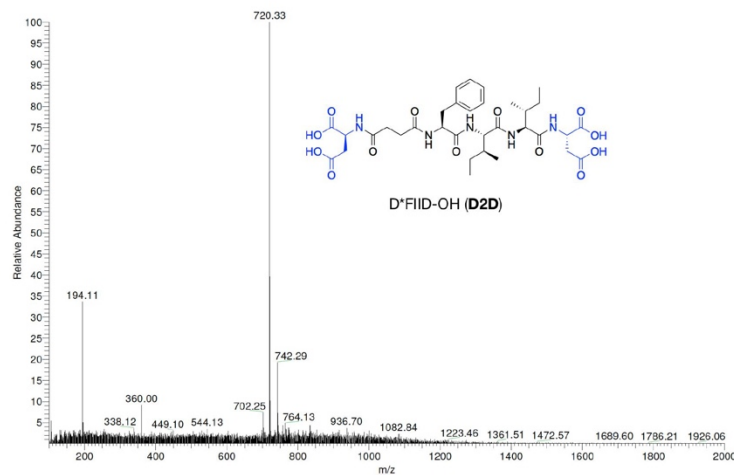
^1H NMR (500 MHz, DMSO) δ 12.51 (d, $J = 121.6$ Hz, 1H), 8.18 (d, $J = 7.8$ Hz, 1H), 8.07 (d, $J = 8.4$ Hz, 1H), 7.96 (d, $J = 8.8$ Hz, 1H), 7.88 (dd, $J = 8.8, 2.0$ Hz, 2H), 7.74 (d, $J = 9.0$ Hz, 1H), 7.25 (d, $J = 4.3$ Hz, 4H), 7.18 (q, $J = 4.2$ Hz, 1H), 4.58 (ddd, $J = 10.2, 8.5, 4.1$ Hz, 1H), 4.54 – 4.46 (m, 1H), 4.22 (ddd, $J = 15.7, 8.9, 6.6$ Hz, 4H), 2.98 (dd, $J = 13.9, 4.1$ Hz, 1H), 2.78 – 2.62 (m, 2H), 2.61 – 2.52 (m, 1H), 1.96 (dq, $J = 8.8, 6.7$ Hz, 4H), 1.74 (s, 3H), 0.90 – 0.76 (m, 24H).

HPLC chromatogram measured at 220 nm



D*FIID-OH (D2D):

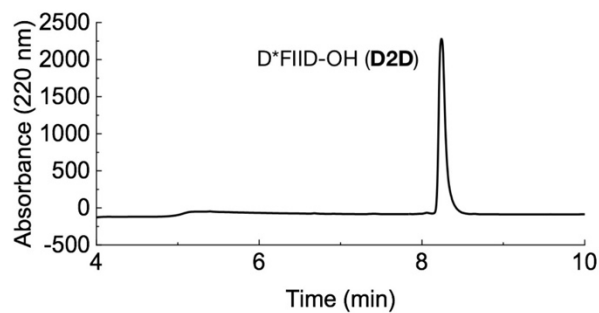
ESI-MS spectra



NMR shifts

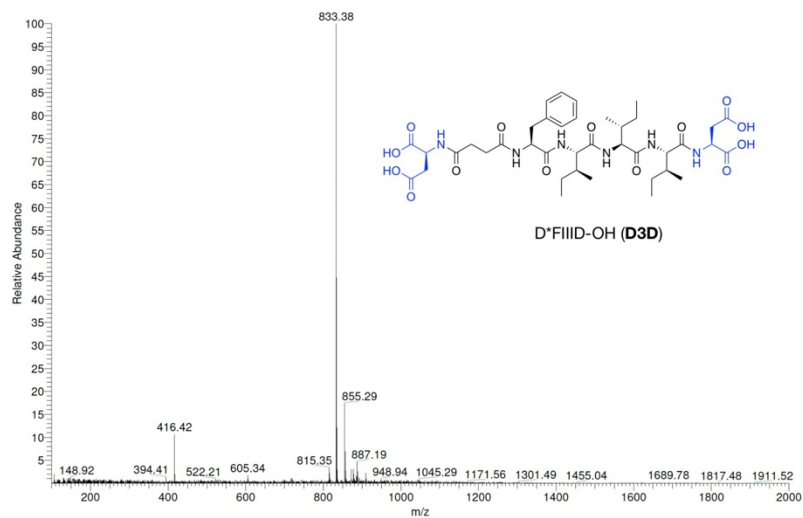
¹H NMR (500 MHz, DMSO) δ 12.50 (s, 3H), 8.18 (d, $J = 7.9$ Hz, 2H), 8.09 (d, $J = 8.3$ Hz, 1H), 7.95 (d, $J = 8.7$ Hz, 1H), 7.78 (d, $J = 9.0$ Hz, 1H), 7.24 (d, $J = 4.4$ Hz, 4H), 7.18 (d, $J = 4.3$ Hz, 1H), 4.52 (tdd, $J = 12.3, 8.7, 5.1$ Hz, 3H), 4.22 (td, $J = 9.5, 7.6$ Hz, 2H), 2.99 (dd, $J = 13.9, 4.1$ Hz, 1H), 2.72 (dd, $J = 14.1, 10.1$ Hz, 1H), 2.69 – 2.63 (m, 2H), 2.59 – 2.53 (m, 2H), 2.24 (dd, $J = 6.9, 4.6$ Hz, 4H), 1.73 (ddp, $J = 9.8, 6.6, 3.2$ Hz, 2H), 1.44 (ddq, $J = 15.1, 7.6, 3.8$ Hz, 2H), 1.07 (ddd, $J = 14.0, 11.3, 6.7$ Hz, 2H), 0.89 – 0.76 (m, 12H).

HPLC chromatogram measured at 220 nm



D*FIID-OH (D3D):

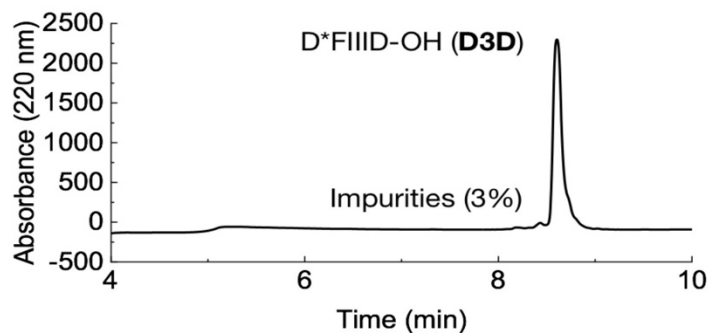
ESI-MS spectrum



NMR shifts

^1H NMR (500 MHz, DMSO) δ 12.45 (s, 4H), 8.17 (dd, J = 7.9, 4.2 Hz, 2H), 8.08 (d, J = 8.4 Hz, 1H), 7.91 (dd, J = 13.5, 8.8 Hz, 2H), 7.80 (d, J = 8.8 Hz, 1H), 7.24 (d, J = 5.3 Hz, 4H), 7.20 – 7.11 (m, 1H), 4.58 – 4.47 (m, 3H), 4.22 (t, J = 8.3 Hz, 3H), 2.98 (dd, J = 14.0, 4.1 Hz, 1H), 2.71 (dd, J = 13.8, 9.8 Hz, 1H), 2.68 – 2.63 (m, 2H), 2.56 (dd, J = 10.1, 6.9 Hz, 2H), 2.24 (dd, J = 8.5, 3.6 Hz, 4H), 1.72 (d, J = 10.4 Hz, 3H), 1.43 (dtd, J = 14.9, 7.5, 3.5 Hz, 3H), 1.07 (dd, J = 14.6, 7.2 Hz, 3H), 0.88 – 0.74 (m, 17H).

HPLC chromatogram measured at 220 nm



Methods.

Samples preparation. Stock solutions of the precursors were prepared by dissolving the peptides in 200 mM MES buffer or 200 mM MES buffer with different concentrations of salt, after which the pH was adjusted to pH 6.0. Stock solutions of EDC were prepared by dissolving the EDC powder in MQ water. These stock solutions were used freshly. The reaction cycles were initiated by the addition of the EDC to the precursor solution.

Analysis of the reaction kinetics by HPLC. The kinetics of the chemical reaction cycles were monitored by means of analytical HPLC (HPLC, Thermofisher Dionex Ultimate 3000, Hypersil Gold 250 x 4.8 mm). A 500 μ L sample was prepared (see general sample preparation) and placed into a screw cap HPLC vial. Every 15 minutes, samples of these solutions were directly injected without further dilution, and all compounds involved were separated using a linear gradient of acetonitrile (ACN, 2% to 98%) and water with 0.1% TFA in 15 min. In order to increase the data acquisition resolution, these experiments were repeated at least three times with a few minutes offset in the time in the cycle. For example, in one experiment, samples were injected at 1, 16, 31 minutes; in a next experiment, samples were injected at 3, 18, 33 minutes; in a next experiment, samples were injected at 6, 21, 36 minutes etc. Calibration curves for EDC ($\lambda = 220$ nm) and the precursor ($\lambda = 220$ nm) were obtained in order to quantify the compounds over time. The product absorption coefficient was assumed to be similar to the absorption coefficient of the corresponding precursor. Measurements were performed at 25 $^{\circ}$ C.

Kinetic model. A kinetic model was used to predict the evolution of the anhydride concentration over time. The model is described in detail in the Supporting Note 1. The rate constants we used in this work are given in Table S2. The Matlab-code we used is available here: <https://github.com/BoekhovenLab/Dynamic-vesicles/>

UV/Vis Spectroscopy. Turbidity measurements were carried out at 25 $^{\circ}$ C on a Microplate Spectrophotometer (Thermo Scientific Multiskan GO, Thermo Scientific SkanIt Software 4.0). Measurements were performed in a non-tissue culture treated 96-well plate (Falcon, flat bottom). Every minute, the absorbance of the 200 μ L samples was measured at 600 nm. All experiments were performed in triplicate (N=3).

ESI-MS. ESI-MS experiments were conducted on an LCQ Fleet Ion Trap Mass Spectrometer (Thermo Scientific). Interpretation of all recorded MS data was performed using the Thermo Xcalibur Qual Browser 2.2 SP1.48 software.

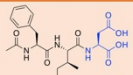
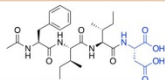
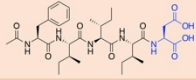
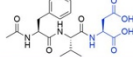
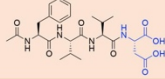
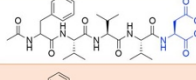
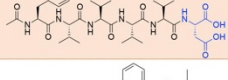
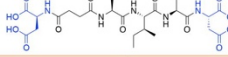
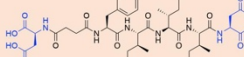
Rheology. Rheological measurements were carried out on a research-grade shear rheometer (MCR 302, Anton Paar, Graz, Austria) using a plate-plate geometry (PP25, Anton Paar, Graz, Austria) and a plate separation of 0.3 mm. Samples were prepared as previously mentioned and placed between the two plates. Storage moduli (G') and loss moduli (G'') were recorded over time in a torque-controlled measurement ($M = 1$ μ Nm for $G'_{\max} < 100$ Pa and $M = 5$ μ Nm

for $G'_{\max} > 100$ Pa, respectively) at a frequency of $f = 1$ Hz. A solvent trap was placed around the sample holder to avoid evaporation. Data was recorded at 25 °C.

Fluorescence spectroscopy. Fluorescence spectroscopy was performed on a Jasco (Jasco FP-8300) fluorescence spectrophotometer with an external temperature control (Jasco MCB-100). The ThT assay was performed on the same fluorescence spectrophotometer as described above. Samples were directly prepared in a 10 mm quartz cuvette (Precision Cells Inc.) by mixing precursor (15 mM in MES Buffer) with EDC and ThT (5 μ M). The fluorescence intensities were measured over time, every 1 minutes, at 485 nm with excitation at 450 nm.

Cryogenic-Transmission Electron Microscopy (cryo-TEM). Samples for TEM were prepared as described above. Shortly before imaging the samples were diluted a 10-fold to decrease the density of fibers in the micrographs. Cryo-TEM imaging was performed on a Jeol JEM-1400 plus operating at 120 kV. The images were recorded in a low-dose mode on a CCD camera. Quantifoil R2/2 on Cu-grid 400 mesh were used. The grids were freshly glow-discharged for 30 seconds prior to use. Preparation of the grids was performed in a FEI Vitrobot at 21 °C with the relative humidity set to 100% and the blotting force was set to -5. The sample (5 μ L) was incubated for 30 seconds, blotted twice for 3.5 seconds and then directly plunged into liquid ethane that was pre-cooled by liquid nitrogen. The cryo-TEM grids were transferred and stored in liquid nitrogen, and when needed, placed into a Gatan 625 cryo-specimen holder to insert into the microscope. The specimen temperature was maintained at -170 °C during the data collection.

Supplementary Table 1: Characterization of the peptides synthesized

Peptide sequence	Structure	Mass Calculated (g/mol)	Mass found	HPLC Retention time (min)	Yield	Purity
Ac-FID-OH (1D)		435.20	458.27 [Mw+Na] ⁺	7.93	60%	98%
Ac-FIID-OH (2D)		548.28	571.34 [Mw+Na] ⁺	8.79	75%	98%
Ac-FIIID-OH (3D)		661.37	684.40 [Mw+Na] ⁺	9.19	42%	98%
Ac-FVD-OH		421.18	444.33 [Mw+Na] ⁺	7.76	74%	95%
Ac-FVVD-OH		520.25	543.31 [Mw+Na] ⁺	8.12	76%	96%
Ac-FVVVD-OH		619.32	642.30 [Mw+Na] ⁺	8.41	57%	97%
Ac-FVVVD-OH		718.39	741.36 [Mw+Na] ⁺	8.78	40%	98%
D*FIID-OH (D2D)		721.32	720.33 [Mw-H] ⁻	8.23	51%	98%
D*FIIID-OH (D3D)		834.40	833.38 [Mw-H] ⁻	8.65	42%	97%

Supplementary Table 2: Rate constants used to fit the HPLC data with a kinetic model.

Peptide sequence	k ₀ (sec ⁻¹)	k ₁ (M ⁻¹ x sec ⁻¹)	k ₂	k ₃	k ₄ (sec ⁻¹)
Ac-FID-OH (1D)	1.35 x 10 ⁻⁵	0.8 x 10 ⁻²	2*k ₁	2*k ₁	1.5 x 10 ⁻²
Ac-FIID-OH (2D)	1.35 x 10 ⁻⁵	0.95 x 10 ⁻²	2*k ₁	2*k ₁	0.75 x 10 ⁻²

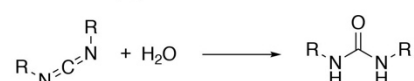
Supporting note 1: Description of the kinetic model

A kinetic model was written in Matlab that describes each reaction involved in the chemical reaction network except. The concentrations of each reactant were calculated for every second in the cycle. The model was used to fit the obtained HPLC data that described the evolution of the concentration of anhydride, EDC and acid over time. In all experiments, the concentration of the precursor was 15 mM.

The model described five chemical reactions:

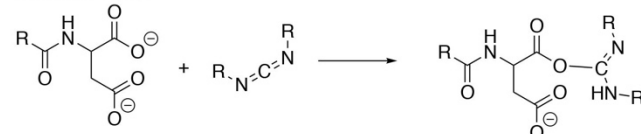
0) Direct hydrolysis of carbodiimide with a first order rate constant of $1.3 \times 10^{-5} \text{ sec}^{-1}$ as determined in previous work.

Reaction 0 (k_0)



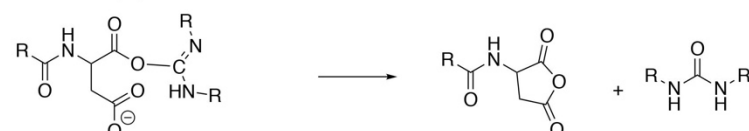
1) The formation of O-acylurea by reaction with EDC (k_1). This second order rate constant was dependent on the nature of the precursor. The rate constant was determined for each precursor by HPLC, by monitoring the EDC consumption.

Reaction 1 (k_1)



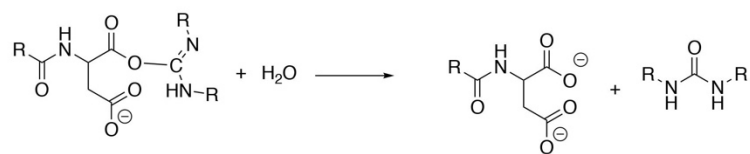
2) The formation of the anhydride with a first order rate constant. This rate constant could not be determined because the O-acylurea was never observed. It was therefore set to be twice the rate of k_1 . As a result, the O-acylurea did never reach concentrations over $1 \mu\text{M}$ in the model.

Reaction 2 (k_2)



3) Direct hydrolysis of O-acylurea (k_3). This reaction rate could not be obtained because the O-acylurea was not observed. The ratio of k_2 and k_3 (anhydride formation and competing direct hydrolysis of O-acylurea) was varied to fit the HPLC data for several concentrations of $[\text{fuel}]_0$ and $[\text{di-acid}]_0$.

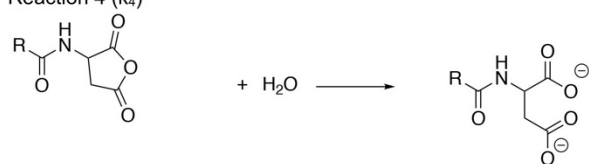
Reaction 3 (k_3)

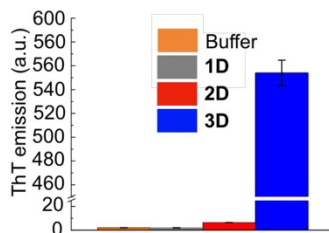


4) Hydrolysis of anhydride proceeded with a first order rate (k_4) The rate constant was determined by HPLC for kinetic experiments where no assemblies were reached.

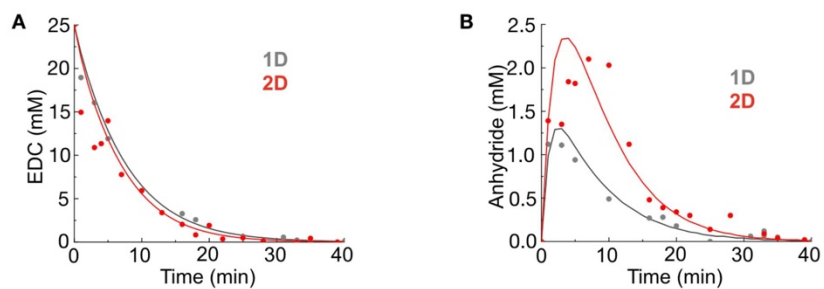
The rate of the hydrolysis reaction was calculated by multiplying the first order rate constant k_4 with the concentration of anhydride.

Reaction 4 (k_4)

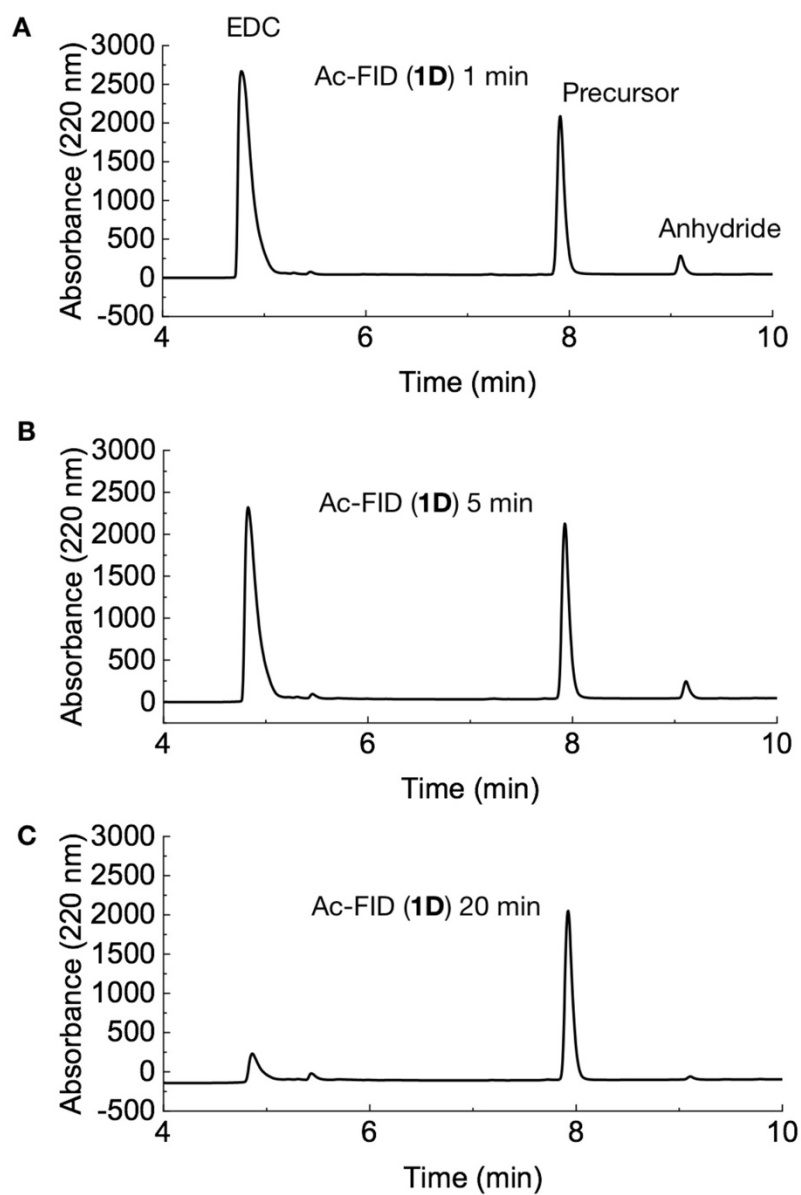




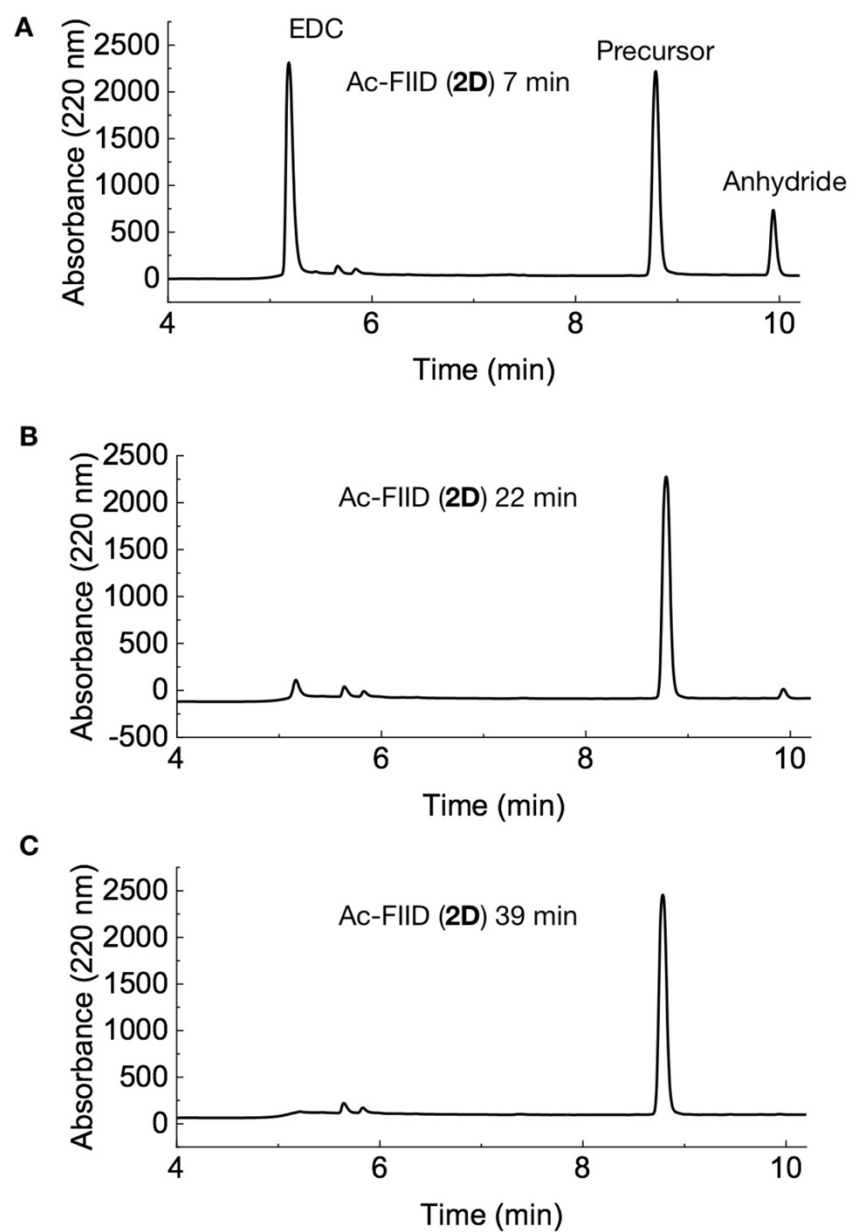
Supplementary Figure 1: Fluorescence emission at 485 nm by ThT as a measure for the presence of hydrogen bonding between peptides. The samples are buffer, and **1D**, **2D** and **3D** without EDC. It can be observed that 15 mM **1D** and **2D** do not form H-bonds leading to beta-sheets formation, while **3D** does. Error bars represent the standard deviation of the average ($n = 3$).



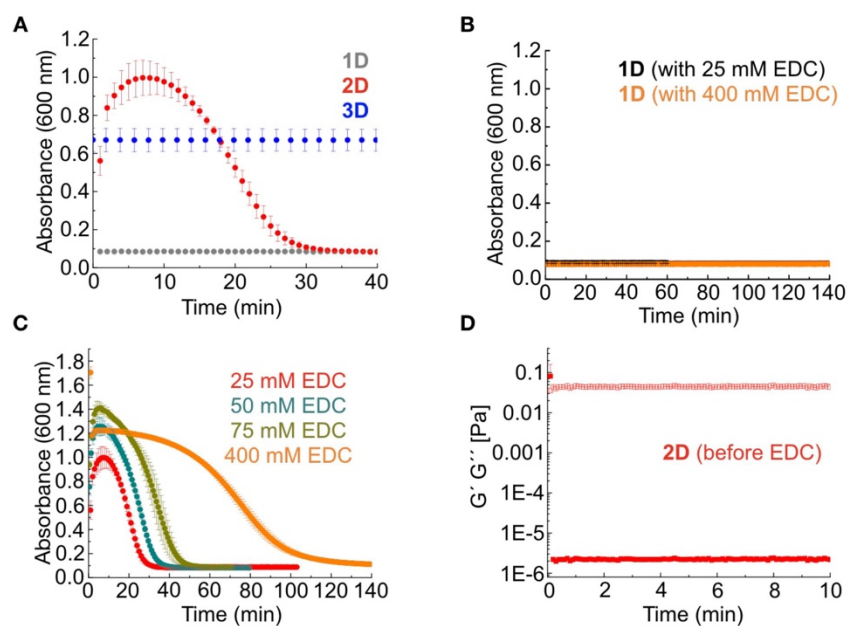
Supplementary Figure 2: Kinetic traces of 1D and 2D with fuel. The concentration of EDC (**A**) and anhydride product (**B**) as a function of time when 15 mM **1D** and **2D** are fueled with 25 mM EDC. The lines represent data from the kinetic model, whereas the markers represent HPLC data. The HPLC data is obtained from at least three experiments.



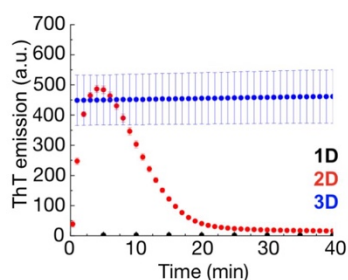
Supplementary Figure 3: HPLC chromatograms of 15 mM Ac-FID-OH (**1D**) solution reaction network at **A**) 1 min **B**) 5 min and **C**) 20 min after EDC addition measured at 220 nm.



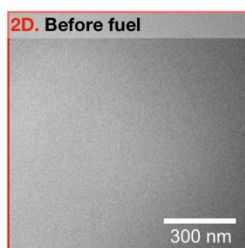
Supplementary Figure 4: HPLC chromatogram of 15 mM Ac-FIID-OH (**2D**) solution reaction network at **A**) 7 min **B**) 22 min and **C**) 39 min after EDC addition measured at 220 nm.



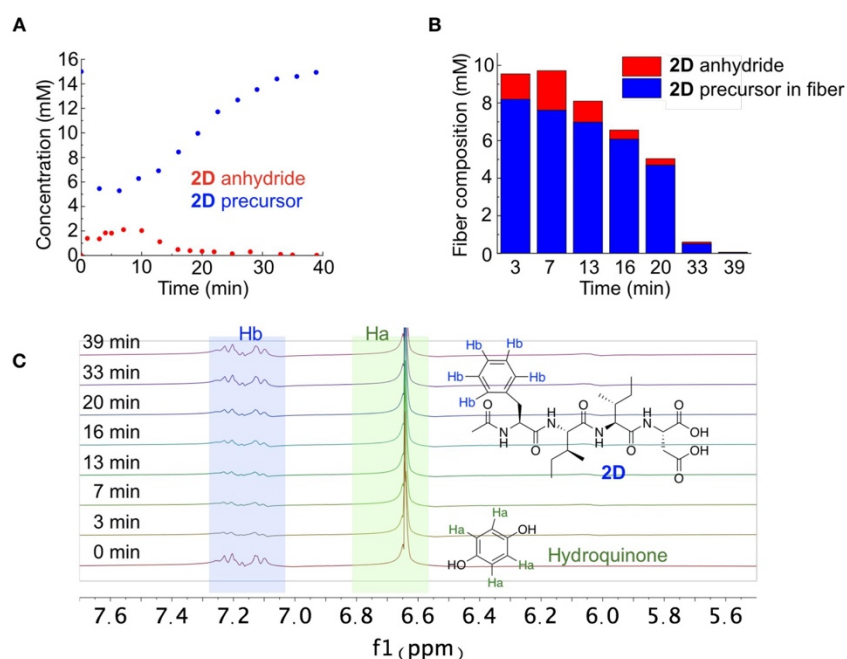
Supplementary Figure 5: Regulating the response to fuel by tuning the attractive interactions. **A)** Absorbance at 600 nm as a measure of turbidity of 15 mM **1D** with 25 mM EDC, 15 mM **2D** with 25 mM EDC, and 15 mM **3D** without EDC. **B)** Absorbance at 600 nm as a measure of turbidity of 15 mM **1D** with 25 mM and 400 mM EDC against time. **C)** Absorbance at 600 nm as a measure of turbidity of 15 mM **2D** with different concentration of EDC (25 mM, 50 mM, 75 mM and 400 mM) against time. **D)** Storage and loss modulus as a function of time as measured by a plate-plate rheometer of 15 mM **2D** without fuel. Solid squares represent the storage modulus (G'), open squares represent the loss modulus (G''). Error bars represent the standard deviation of the average ($n = 3$). One can observe a high signal of G'' for the first point, which is an artifact caused by the inertia of the measuring system.



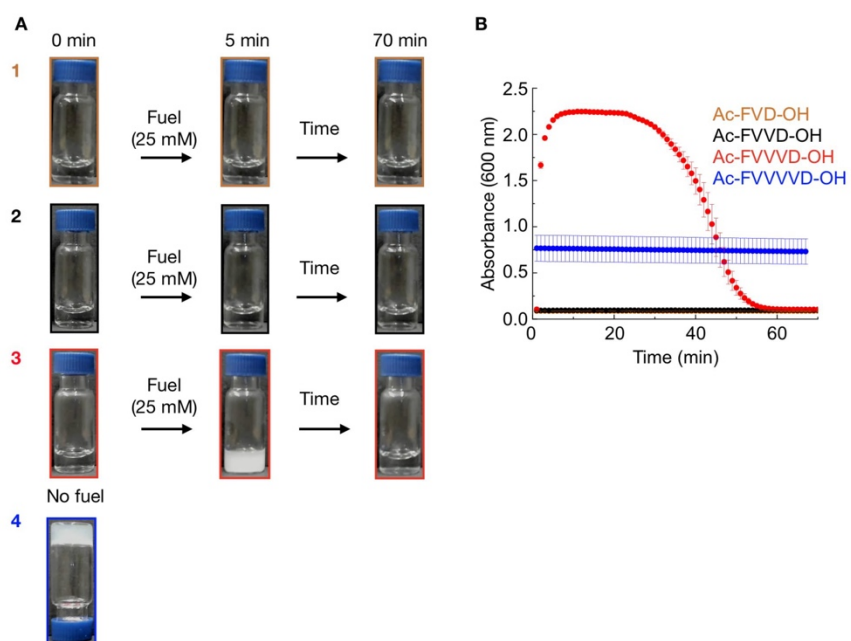
Supplementary Figure 6: Fluorescence emission at 485 nm by ThT as a measure for the presence of hydrogen bonding between peptides as a function of time of 15 mM **1D** with 25 mM EDC (black markers), 15 mM **2D** with 5 mM EDC (red) and 15 mM **3D** without EDC. We added only 5 mM EDC to **2D** because with the standard 25 mM EDC, the ThT signal cannot be accurately measured in the first minutes because the signal oversaturates the detector. The error bars represent the standard deviation of 1the average ($n = 3$).



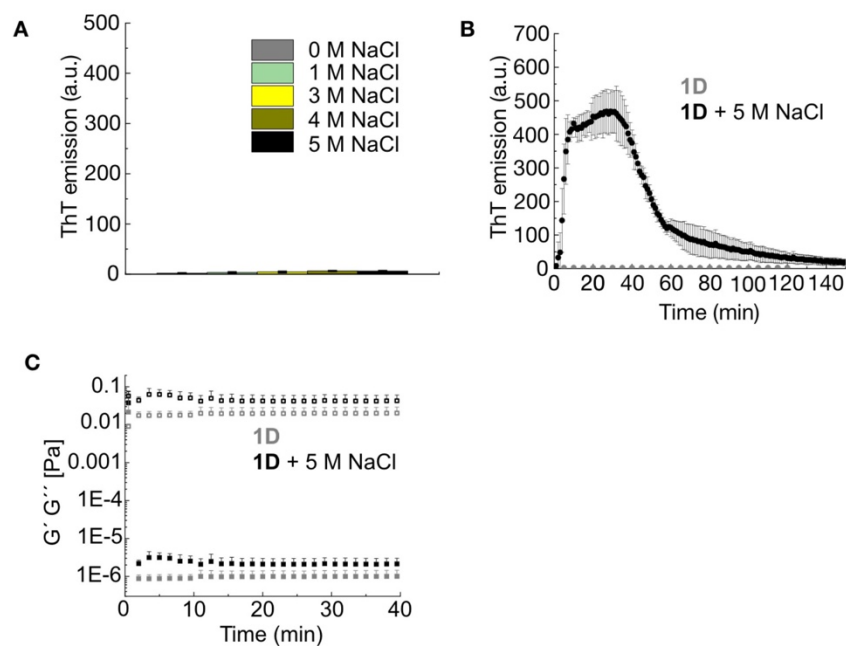
Supplementary Figure 7: *Cryo*-TEM micrograph of the solution of 15 mM **2D** before the addition of EDC.



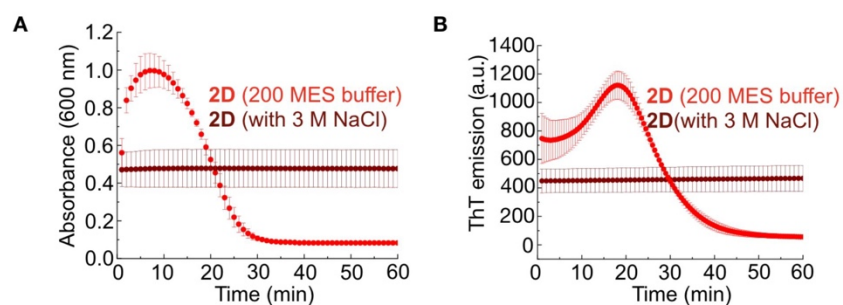
Supplementary Figure 8: 2D Fiber composition. **A)** The concentration of **2D** precursor in solution as measured by NMR (blue markers), and the concentration of **2D** anhydride product as measured by HPLC as a function of time (red markers) in response to 25 mM of EDC. **B)** The concentration of **2D** precursor and **2D** anhydride in the fibers as a function of time that we calculate from the data in **A**: $C_{\text{precursor in fibers}} = 15 \text{ mM} - C_{\text{precursor in the solution}} - C_{\text{anhydride}}$. In this calculation, we assume that all anhydride of **2D** is in the fibers. **C)** The concentration of **2D** precursor in solution against time measured by ^1H NMR. The concentration of **2D** is measured by the ratio of proton Hb in **2D** to proton Ha in one standard compound Hydroquinone in D_2O .



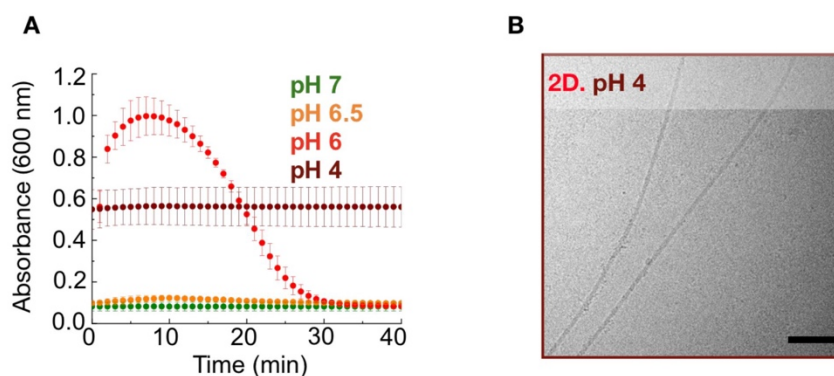
Supplementary Figure 9: Macroscopic properties of peptides 15 mM Ac-FV_nD-OH (n=1, 2, 3, 4) in response to fuel. A) Photographs of solutions of 15 mM Ac-FV_nD-OH (n=1, 2, 3, 4) before and after the addition of 25 mM fuel. **B)** Absorbance at 600 nm as a measure for turbidity for 15 mM Ac-FV_nD-OH (n=1, 2, 3, 4) with 25 mM fuel against time. The error bars represent the standard deviation of the average (n = 3).



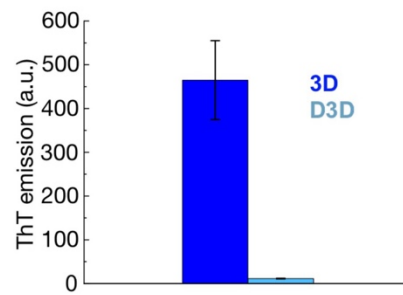
Supplementary Figure 10: Regulating the response to fuel by tuning repulsive interactions. **A)** Fluorescence emission at 485 nm by ThT as a measure for the presence of hydrogen bonding between peptides for **1D** without EDC with varying amounts of NaCl. No evidence of self-assembly was found. **B)** Fluorescence emission at 485 nm by ThT as a measure for peptide **1D** + 5 M NaCl in response to 25 mM EDC against time. **C)** Storage and loss modulus as a function of time measured by plate-plate rheology of a solution of 15 mM **1D** + 5 M NaCl with 25 mM fuel. Solid squares represent the storage modulus (G'), open squares represent the loss modulus (G''). The error bars represent the standard deviation of the average ($n = 3$).



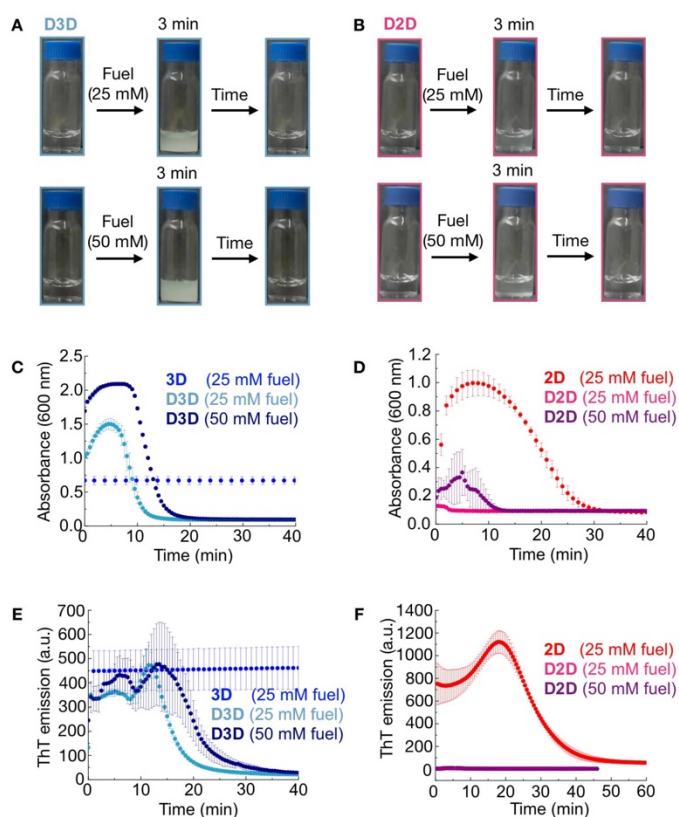
Supplementary Figure 11: Regulating the response to fuel by tuning repulsive interactions. **A)** Absorbance at 600 nm as a function of time as a measure for turbidity for 15 mM **2D** with 25 mM EDC (light red), and 15 mM **2D** + 3 M NaCl without EDC (dark red). **B)** Fluorescence emission at 485 nm by ThT as a measure against time for 15 mM **2D** in response to 25 mM EDC and 15 mM **2D** + 3 M NaCl without EDC. The error bars represent the standard deviation of the average ($n = 3$).



Supplementary Figure 12: Regulating the response to fuel of 2D by tuning pH. **A)** Absorbance at 600 nm as a function of time as a measure for turbidity for 15 mM **2D** with 25 mM EDC at pH 7, pH 6.5, pH 6, and 15 mM **2D** without EDC at pH 4. **B)** Cryo-TEM micrograph of the solution of 15 mM **2D** without the addition of EDC. The scale bar corresponds to 100 nm. The error bars represent the standard deviation of the average ($n = 3$).



Supplementary Figure 13: Fluorescence emission at 485 nm by ThT as a measure for the presence of hydrogen bonding between peptides, showed that without EDC, 15 mM **D3D** will not assemble compared with 15 mM **3D** leading to precursor assembly. The error bars represent the standard deviation of the average ($n = 3$).



Supplementary Figure 14: Regulating the response to fuel by tuning repulsive interactions in the molecular design. **A)** Photographs of solutions of peptide **D3D** (15 mM) before and after 25 mM fuel and 50 mM fuel addition. **B)** Photographs of solutions of peptide **D2D** (15 mM) before and after 25 mM fuel and 50 mM fuel addition. **C)** Absorbance at 600 nm as a measure of turbidity for 15 mM **D3D** in response to 25 mM and 50 mM fuel against time compared with **3D** without fuel. **D)** Absorbance at 600 nm as a measure of turbidity against time for 15 mM **D2D** in response to 25 mM and 50 mM fuel compared with **2D** in response to 25 mM fuel. **E)** Fluorescence emission at 485 nm by ThT as a measure against time for 15 mM **D3D** in response to 25 mM and 50 mM fuel EDC compared with **3D** without fuel. **F)** Fluorescence emission at 485 nm by ThT as a measure against time for 15 mM **D2D** in response to 25 mM and 50 mM fuel compared with **2D** in response to 25 mM fuel. The error bars represent the standard deviation of the average ($n = 3$).

4. Morphological transitions in chemically fueled self-assembly

Abstract

Molecular self-assembly has been a powerful bottom-up method for the construction of materials, so-called supramolecular materials. The liquid crystal display and hydrogels for biomedical applications are marvelous examples. Biology also uses molecular self-assembly for its structural components like the cytoskeleton and cell wall. The function of these structures is regulated through chemical reaction cycles. These operate out of equilibrium at the expense of chemical energy like ATP or GTP. In that kinetic regime, the structures have unique properties and could be of particular interest for the field of supramolecular materials. Therefore, fantastic progress has been made in the last five years to develop synthetic counterparts, and peptides have been particularly fruitful building blocks. However, most research has focused on how chemical reactions can induce self-assembly, and disassembly is expected to follow spontaneously. Spontaneous disassembly is not always the case.

This work demonstrated how disassembly in a chemically fueled reaction cycle varies between seemingly similar peptides and assemblies. Specifically, I present four similar peptides but with a different disassembly pathway, leading to different morphology transitions, Ac-FIVD-OH and Ac-FILD-OH assemble to colloids and disassemble to the solution, but Ac-FVVVD-OH and Ac-FIVVD-OH also assemble to the colloids and disassemble to fibers. Furthermore, the morphology transition time can be controlled by the fuel concentration. The mechanism is explained by the increasing of the β -sheet propensity of precursors and the decreasing tendency of solubility, which resulted in a different ratio of anhydride co-assembly with the precursor. Our findings demonstrate that assembly and disassembly should be taken into account in chemically fueled self-assembly. This is an important finding since disassembly is critical to creating dynamic assemblies but is not often considered in designing chemically fueled assemblies.

This work has been published:

Title: Morphological transitions in chemically fueled self-assembly

Authors: Kun Dai, Dr. Marta Tena-Solsona, Dr. Jennifer Rodon Fores, Alexander M. Bergmann, Prof. Dr. Job Boekhoven

First published: 8 November 2021

Journal: Nanoscale

Publisher: Royal Society of Chemistry

DOI: 10.1039/x0xx00000x

Link: <https://pubs.rsc.org/en/content/articlelanding/2021/nr/d1nr04954b>

Reprinted with permission from Nanoscale
Royal Society of Chemistry

I acknowledge the permission with this reprint from Royal Society of Chemistry.

This section states the individual work of each author in the publication above Kun Dai designed and conducted all experiments. Marta Tena-Solsona helped with scientific problems. Jennifer Rodon Fores helped with the confocal microscope. Alexander M. Bergmann imaged with a cryogenic transmission electron microscope. Kun Dai, Marta Tena-Solsona and J. Boekhoven wrote the manuscript. The work was performed under the supervision and guidance of J. Boekhoven.



Cite this: DOI: 10.1039/d1nr04954b

Received 30th July 2021,
Accepted 8th November 2021DOI: 10.1039/d1nr04954b
rsc.li/nanoscale

Morphological transitions in chemically fueled self-assembly†

Kun Dai,^a Marta Tena-Solsona,^b Jennifer Rodon Fores,^a Alexander M. Bergmann^a and Job Boekhoven^{a,b}

In chemically fueled self-assembly, a reaction cycle activates and deactivates molecules for self-assembly. The resulting assembly is dynamic and should be endowed with unique behavior in this kinetically controlled regime. Recent works have mainly focused on design rules for the activation of molecules for self-assembly, thereby assuming that disassembly upon deactivation inherently follows. However, that is not always the case. This work shows a family of peptides that assemble into colloids regulated through a chemical reaction cycle. Despite their similarity in assembly, we find that they follow a different disassembly pathway upon

deactivation. The colloids from several peptides completely disassemble as fuel depletes while others transition into fibers. Our findings demonstrate that assembly and disassembly should be taken into account in chemically fueled self-assembly.

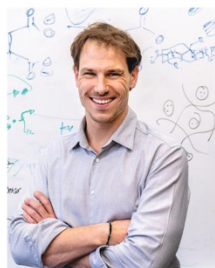
When molecules are held together through non-covalent interactions, nano-architectures arise with properties that differ from their non-assembled counterparts in a process referred to as molecular self-assembly.^{1,2} Particularly successful examples are amphiphiles that form micelles or peptides that form fibers.³ Decades of research have led to a fundamental understanding of the processes and resulted in design rules for molecular self-assembly.^{4–9} However, most of the experience is limited to self-assembly processes that occur in- or close-to-equilibrium.

Self-assembly is not limited to synthetic examples but is ubiquitously exploited in biology, for example, to form the cell wall or the cytoskeleton.^{10–12} In contrast to the examples of man-made self-assembly, molecular assembly in biology almost always occurs out of equilibrium. To sustain these assemblies in an out of equilibrium state, energy is converted by the hydrolysis of high-energy molecules like the phosphate anhydrides ATP or GTP. As a result of their non-equilibrium nature, these assemblies are regulated through the kinetics of their energy-consuming reaction cycle. Such kinetic control is vastly different than the thermodynamic control of self-assembly in- or close-to-equilibrium. A beautiful example of the stark contrast is evident from the lipid membrane in equilibrium versus the membrane of mitochondria which is highly dynamic and constantly undergoing fusion and fission that is tightly regulated by protein machinery fueled by chemical energy.

To create similar dynamic structures and to better understand the physicochemical mechanisms by which such systems are regulated, several studies have focused on the development of self-assembly regulated through kinetic processes. Inspired by the self-assembly of tubulin that is regulated through the hydrolysis of GTP,¹⁰ the process of chemi-

^aDepartment of Chemistry, Technical University of Munich, Lichtenbergstrasse 4, 85748 Garching, Germany. E-mail: job.boekhoven@tum.de^bInstitute for Advanced Study, Technical University of Munich, Lichtenbergstrasse 2a, 85748 Garching, Germany

† Electronic supplementary information (ESI) available. See DOI: 10.1039/d1nr04954b



Job Boekhoven

Job Boekhoven is developing tools to regulate the self-assembly of molecules the way biology does. He is best known for his work on chemically fueled reaction cycles that control the ability of molecules to assemble or phase separate. The resulting materials show exciting new properties, such as their intrinsic ability to self-heal or their controllable lifetime. Moreover, the chemically fueled assemblies manifest features we usually

associate with living cells, like the ability to emerge, decay, or even self-divide. Job holds a Ph.D. degree (2012) from Delft University of Technology and is currently an assistant professor at the Technical University of Munich.

Communication

[View Article Online](#)

Nanoscale

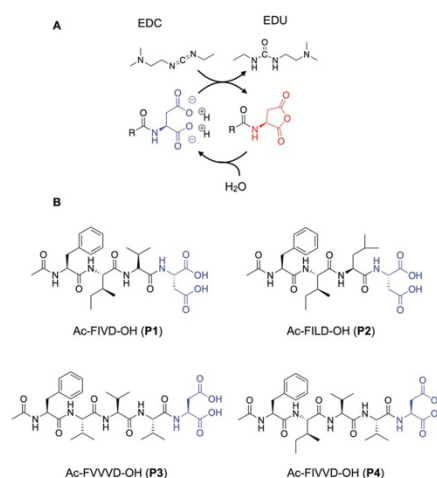
chemically fueled self-assembly was developed.¹³ In chemically fueled self-assembly, the assembly of molecules is coupled to a chemically fueled reaction cycle.^{14–18} The reaction cycle comprises two reactions, *i.e.*, an activation and deactivation reaction. In the activation reaction, a non-assembling precursor is activated for assembly by reaction with a chemical fuel. In the deactivation reaction, the activated product reacts to yield the original precursor. Notably, the activation and deactivation proceed through two different pathways and are thus not an equilibrium reaction. As a result, a molecule is temporarily activated for self-assembly at the expense of a molecule of chemical fuel. Examples of chemically fueled self-assembly include the formation of transient fibers driven by the hydrolysis of a methylating agent,¹⁹ oil droplets formed by the hydration of condensing agents,²⁰ vesicles that form by the hydrolysis of ATP²¹ and many others.^{22–25}

In the molecular designs of these chemically fueled assemblies, the precursor is well soluble, typically because it carries several ionic groups. The activation reaction converts these ionic groups, making the product more prone to assemble than the precursor. Upon deactivation, the electrostatic charges are reinstated, resulting in electrostatic repulsion and disassembly. While most of these studies have focused on the activation step resulting in self-assembly, the disassembly has not been studied in much detail.

In this work, we describe four peptides that assemble at the expense of a chemical fuel. The molecular designs of the peptides are chosen such that they vary in their propensity to form β -sheets and their solubility. We could toggle the peptide's assembly behavior, through molecular design, from almost no assemblies, formation of colloids that disassemble when fuel is depleted, to colloids that transition into fibers as fuel depletes. We qualitatively understand the underlying mechanism, which has to do with the degree of coassembly of the precursor. Our findings suggest that it is essential to consider the pathway of assembly but also the disassembly pathway when designing chemically fueled self-assembling systems. These results will aid the field in developing dynamic, chemically fueled assemblies that show behavior as observed in biological supramolecular architectures.

The chemical reaction cycle we used is based on the formation of a transient anhydride at the expense of the irreversible consumption of a high-energy molecule (fuel).^{26,27} The cycle comprises an activation and a deactivation reaction (Scheme 1A). In the activation, a precursor containing a C-terminal aspartic acid is converted into its corresponding cyclic anhydride at the cost of a carbodiimide-based fuel (1-ethyl-3-(3-dimethylaminopropyl)carbodiimide, EDC). In the deactivation reaction, a molecule of water hydrolyzes the anhydride to yield the initial precursor state. Due to the loss of the anionic charges of the precursor, the activated product can assemble.

We use short peptides containing a C-terminal aspartic acid as a precursor (Scheme 1B).²⁸ The loss of the anionic charges upon activation resulted in a product with a higher propensity to assemble. Directional intermolecular interactions, such as



Scheme 1 (A) A chemical reaction cycle that comprises an activation and deactivation reaction. Aspartic acid derivatives react with carbodiimide EDC in the activation reaction and are converted to their corresponding anhydride. In the deactivation reaction, the anhydride derivative is hydrolyzed in aqueous media. (B) Molecular structures of the precursors **P1**, **P2**, **P3**, and **P4**.

hydrogen bonds or aromatic interactions, are encoded in the remainder of the peptide sequence. By changing this part of the peptide segment, we aim to increase the β -sheet propensity of the products and modify their solubility and, therefore, influence the assembly and, ultimately, the disassembly process. We thus synthesized the precursors Ac-FIVD-OH (**P1**), Ac-FILD-OH (**P2**) and Ac-FVVVD-OH (**P3**), and Ac-FIVVD-OH (**P4**), where F stands for phenylalanine, I for isoleucine, L for leucine, V for valine, and D for aspartic acid.

We studied how the emergence and decay of the anhydride affected the macroscopic properties of a solution of 10 mM **P1**, **P2**, **P3**, and **P4** in MES buffer at pH 6.0. When these solutions were fueled with 25 mM EDC, we noticed that **P1** remained transparent while all other solutions turned turbid within 3 minutes and regained their original transparency after 35 min (**P2**), 70 min (**P3**), and 90 min (**P4**) (Fig. 1A). The transient emergence of turbidity was quantified by measuring the absorbance of 600 nm light in a plate reader (Fig. 1B). We monitored the anhydride and EDC concentration evolution by HPLC (high-pressure liquid chromatography) using a previously described quench method (ESI methods, Fig. S1–S4†).²⁹ We found that the amount of anhydride rapidly increased during the first minutes, explaining the quick change in turbidity for **P2**, **P3**, and **P4** previously mentioned (Fig. 1C). The concentration anhydride peaked at 10 min for **P1** and **P2** and 20 min for **P3** and **P4**, respectively. After 50 min and 60 min in the case of **P1** and **P2**, and after 70 min and

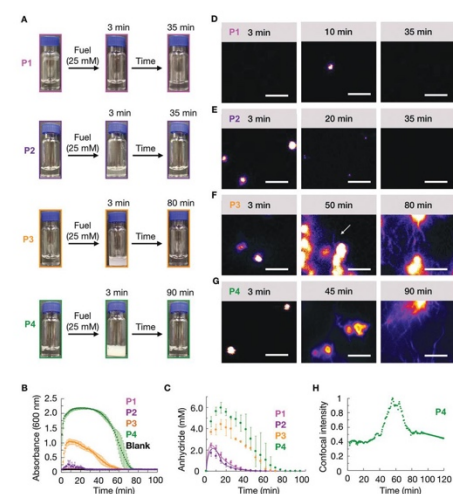


Fig. 1 (A) Timelapse photographs of compounds **P1**, **P2**, **P3**, **P4** (10 mM) in response to 25 mM of EDC. (B) Turbidity traces of 10 mM of **P1**, **P2**, **P3**, **P4** in response to 25 mM of fuel. (C) The concentration of anhydride over time of the same conditions described in B. The line represents data from the kinetic model, and the markers represent HPLC data. Confocal micrographs of 25 mM EDC addition to 10 mM **P1** (D), 10 mM **P2** (E), 10 mM **P3** (F) and 10 mM **P4** (G) at different times in the cycle. (H) The normalized intensity from confocal microscopy for 10 mM **P4** with 25 mM EDC as a function of time. All scale bars correspond to 5 μm . The dye used for confocal is 2.5 μM Nile red. White arrows point out the growth of fibers. All error bars represent the standard deviation ($n = 3$).

80 min in the case of **P3** and **P4** respectively, all the fuel was gone and, as expected, no more anhydride was present in the solutions (Fig. 1C).

We analyzed the morphology of the transient peptide assemblies using confocal microscopy. The solutions were stained with the hydrophobic fluorescent dye Nile Red (ESI methods[†]). In line with the lack of turbidity, the confocal microscopy showed only a few colloids, and all of which had disappeared within 35 minutes (Fig. 1D and Fig. S5[†]). We explain this behavior by the high solubility of the **P1** anhydride (2.2 mM, Fig. S6[†]). **P2**, which carries isoleucine (I) instead of a valine amino acid, has a lower solubility than **P1**. The addition of 25 mM fuel to **P2** resulted in the formation of transient colloids that disappeared after 35 min (Fig. 1E and Fig. S5[†]). A cryo-TEM analysis corroborated the formation of colloids right after the fuel addition and their disappearance when fuel depleted (Fig. S7[†]).

The timeframe of the emergence of the colloids and their disappearance coincided with the lifetime of the turbidity (Fig. 1B). With an increasing propensity to form β -sheets, **P3** and **P4** also assembled into transient colloids; however, unlike

P1 and **P2**, the colloids did not dissolve but transitioned into fibers at around 50 and 40 min, respectively (Fig. 1F and G). These fibers grow with time and remain kinetically trapped long after fuel depletes (Fig. 1F, and Fig. S5[†]). The morphological transition from colloids to fibers for **P4** was more acute. The transition occurred suddenly and was started by the collapse of the colloids into a donut-like structure. From this structure, fibers emerged and were growing for tens of minutes. Interestingly, the fibers did not disappear but remained kinetically trapped for hours (Fig. 1G and Fig. S5[†]), long after the fuel was gone. In order to better quantify when the morphological transition occurred, we took **P4** as an example, and we measured the total fluorescence intensity per micrograph and normalized it between experiments. We found it to rise rapidly after applying the fuel (Fig. 1H), after which it remained relatively constant for roughly 40 min. After 40 minutes, we observed a sharp increase in the total fluorescence intensity, which leveled off after around 15 min. This rapid onset coincided with the morphological transition from colloids to mainly fibers. After all the fuel had depleted, around 60 min, the intensity decreased somewhat, as we would expect due to the loss of anhydride. Cryo-TEM showed colloids after 3 minutes of fuel addition, few fibers around the transition time, and a clear fiber predominance after fuel depletes (Fig. S5[†]).

To better understand the origin of the different disassembly pathways, we analyzed the molecular composition of the assemblies by ¹H-NMR (proton nuclear magnetic resonance). We used the fact that self-assembled peptides have a reduced transversal relaxation time, resulting in long correlation times and a broadening of the signal that gets hidden in the baseline. This means that peptides that participate in the assembly become NMR-silent, while soluble peptides remain NMR-visible.

In the case of **P1**, as pointed out by the absorbance measurements and the macroscopy images, the number of assemblies formed after fuel addition was low. ¹H-NMR also confirmed that more than 95% of the peptide (either as precursor or product form) were in the solution state. The number of assemblies was within the error range of the technique, and therefore, we focused on the analysis of the composition of **P2–P4**.

P2 showed that the composition of the assemblies was mainly anhydride. For example, 5 minutes after the addition of 25 mM fuel to 10 mM of **P2**, we found that roughly 9.4 mM of the peptide (either as the product or as a precursor) was NMR-visible. In other words, 0.6 mM of the peptide was in the assembled state (Fig. S8[†]). This concentration value is lower than the 1.7 mM of anhydride observed by HPLC (Fig. 1C, the marker at 5 minutes), which means there was still 1.1 mM anhydride in the solution. This anhydride concentration value coincided with the solubility value determined for the anhydride of **P2** (ESI methods and Fig. S8[†]). Since the solubility of the precursor is much higher than the solubility of the anhydride, we assumed that, as long as there is still anhydride present in the solution, there is no or only a small amount of

Communication

[View Article Online](#)

Nanoscale

precursor in the assembly. The amount of anhydride in the assembled state was always below the concentration of anhydride determined by HPLC (Fig. S8†). Thus, the assemblies always comprised mostly anhydride until they disappeared at around 35 min (Fig. 2A).

The composition of the assemblies by **P3** and **P4** revealed a significantly different evolution compared to **P2**. In the first 35 minutes after adding 25 mM fuel to 10 mM of **P3**, there was only anhydride in the assemblies (Fig. 2B). For example, after 5 minutes, 6.6 mM of the peptide was NMR-visible, and there was 3.4 mM peptide in the assembled state (Fig. S9†), which was lower than the 3.7 mM anhydride detected from HPLC. In other words, 0.3 mM anhydride was in solution, and the assemblies are mainly composed of anhydride. After 45 minutes, the peptide concentration in the assemblies was higher than the anhydride concentration from HPLC. That means part of the precursor had coassembled with the anhydride. The ratio of anhydride to precursor continuously decreased until all anhydride had hydrolyzed. Even then, plenty of assemblies were present that comprised exclusively precursor.

In the case of **P4**, the more hydrophobic peptide, the coassembly between precursor and product occurred from the beginning of the cycle. The NMR signal after 5 minutes showed that the assemblies comprised a mixture of 80–20% anhydride-precursor, respectively (Fig. 2C and Fig. S10†). The maximum ratio of anhydride to precursor was found roughly after 15 minutes of fuel addition, after which it constantly decreased until all anhydride had gone. At that time, the assemblies comprised precursor exclusively and remained for at least 6 hours.

The data above suggests that for **P1**, there are almost no assemblies because of the high solubility of its anhydride. Of **P2**, with a lower solubility, the corresponding anhydride assembles into colloids that are composed of exclusively anhydride. Deactivation of the anhydride, through hydrolysis occurs predominantly in solution which is in line with previously described colloids.^{26,30} The hydrolysis results in the gradual dissolution of the colloids as evidenced by confocal microscopy. Peptide **P3** has a lower solubility, and also forms colloids composed of anhydride, but some coassembly with the precursor was also observed. After the first 30 minutes, the colloids of **P3** do not gradually dissolve when fuel is depleted.

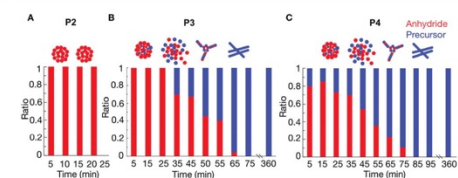


Fig. 2 The relative composition of the assemblies over time as determined by HPLC and NMR for 10 mM **P2** (A), 10 mM **P3** (B) and 10 mM **P4** (C) after the addition of 25 mM of fuel.

Instead, they transition into kinetically trapped fibers. The confocal images showed that the morphological transition occurred around 50 minutes. From the NMR experiments, we can conclude that at this time, almost 50% precursor is present in the assemblies.

Further decreasing the solubility from **P3** to **P4** results in more coassembly of the precursor with anhydride from the beginning, and the transition of the colloids to fibers occurred earlier at around 40 minutes. At that time also around 50% precursor is present in the assemblies.

For peptides **P3** and **P4**, we hypothesize that the hydrolysis can occur on the assembly, and that some of the precursors remains trapped in the colloids after hydrolysis. The fact that hydrolysis occurs on the colloids, as opposed to in solution, is further corroborated by the low solubility of **P3** and **P4** anhydride (0.4 mM, 0.2 mM, Fig. S5†). The accumulation of precursor results in an increase of the negative charges on the assembly. We hypothesize that when the fraction of anhydride in the assemblies falls around roughly 60%, the amount of negative charges induces a transition from colloids to fibers to redistribute the charges and increase the assembly's surface area.

To verify that the change in the assemblies' composition was responsible for the morphological transitions, we analyzed the samples of **P4** (10 mM) with confocal microscopy when fueled with various EDC concentrations (Fig. S11–S13†). We determined the time at which the colloids transformed into fibers for each experiment (the transition time) and plotted it as a function of the concentration of fuel added (Fig. 3A). From the plot, it became clear that the transition time increased with increasing fuel. For example, when we decreased the fuel concentration to 10 mM, the colloids transformed into fibers around 19 minutes (Fig. 3A and Fig. S12†). When we combined the transition time with the data of our HPLC and NMR-based experiments (Fig. 3A), an interesting correlation emerged, *i.e.*, the morphological transition in each experiment occurred at the time point where the ratio of anhydride to precursor in the assemblies was roughly 55%. In other

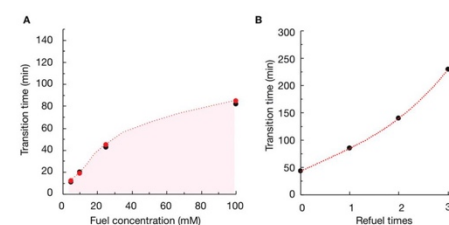


Fig. 3 (A) The time at which the anhydride to precursor ratio for **P4** in the assembled state is around 55% as measured by HPLC and NMR (red markers) in combination with the time where fibers appear from confocal microscopy (black markers) as a function of fuel concentration. (B) Morphology transition time from colloids to fibers observed with confocal microscopy for **P4** as a function of EDC refueling times. Refueling was done every 25 min up to 3 times with 25 mM of EDC.

words, when the majority of the peptides in the assemblies were in the anhydride state, colloids were stable. However, when the ratio reached a threshold, fibers emerged from the colloids, which kept on growing until the colloids had disappeared entirely. It is worth mentioning that the addition of new fuel to the colloids (*i.e.*, before the transition time) would extend the time for which the colloids were present (Fig. 3B and Fig. S14[†]). In other words, we could save the colloids from converting to the fibers by keeping the anhydride to precursor ratio high. However, the application of fuel after the transition occurred did not reverse the fibers to colloids (Fig. S15[†]).

From these combined results, we present a tentative mechanism that is responsible for the morphological transition of **P3** and **P4** and the formation of colloids of **P2**. Peptides **P2**, **P3**, and **P4** form colloids after the application of fuel. The anhydride of **P2** has a relatively high solubility that we determined to be 1.1 mM, whereas the solubility of anhydride of **P3** and **P4** is lower. In line with previous work, the colloids protect their anhydride building blocks from hydrolysis, and the hydrolysis thus occurs on the anhydride that remains in solution or on the surface of the colloids. We could fit the evolution of the anhydride of **P2** (and also of **P1**) well with a kinetic model that considers the hydrolysis occurring in solution (Fig. 1C and Fig. S2[†]). In other words, the hydrolysis occurs in solution, after which hydrolyzed anhydride is replaced with anhydride that disassembles from the colloids. Thus, disassembly is relatively fast compared to hydrolysis.

In contrast, the kinetic model that considers hydrolysis happening in solution could not fit the evolution of the anhydride profile of **P3** and **P4**. Part of the hydrolysis occurs in solution. However, the anhydride is not replaced by anhydride from the colloids. The energy barrier for disassembly is high due to its ability to form hydrogen bonds. Thus, the anhydride in the colloids hydrolyzes through a surface erosion mechanism. Because a surface erosion mechanism is drastically slower than an "in-solution-hydrolysis" mechanism, the lifetime of these colloids is much greater than those of **P2**. The high energy barrier for disassembly is further corroborated because the precursor also did not fully disassemble. NMR experiments showed a large amount of precursor present in the assemblies, which we did not see in the colloids of **P2**. We hypothesize that the accumulation of the precursor in the colloids also drives its morphological transition into the fibers. With the accumulation of the precursor, the colloid accumulates anionic carboxylates. When a threshold of charge density is reached, the charge-charge repulsion exceeds the attractive interactions forcing a rearrangement into fibers that can better accommodate the high charge density.

In conclusion, we designed a family of peptides that self-assemble at the expense of a chemical fuel addition into similar assemblies but show a different disassembly pathway. In one case, the colloids can disassemble and dissolve in water when fuel depletes. In the other case, the colloids transition into fibers that remain kinetically trapped long after fuel depletion. We propose a tentative mechanism that is related to the degree of coassembly between precursor and product.

Understanding the mechanism allows us to control when colloids transition into fibers by the amount of fuel added to the precursor solution. Our findings demonstrate the importance of considering the disassembly pathway when designing new chemically fueled self-assembling systems.

Conflicts of interest

There are no conflicts to declare.

Acknowledgements

K. D. thanks the financial support from the China Scholarship Council. J. B. and M. T. S. are grateful for funding by the European Research Council (ERC starting grant 852187). J. B. acknowledge funding from the Max Planck School Matter to Life supported by the German Federal Ministry of Education and Research (BMBF) in collaboration with the Max Planck Society.

Notes and references

- G. M. Whitesides and M. Boncheva, *Proc. Natl. Acad. Sci. U. S. A.*, 2002, **99**, 4769–4774.
- G. M. Whitesides and B. Grzybowski, *Science*, 2002, **295**, 2418–2421.
- H. Dong, S. E. Paramonov and J. D. Hartgerink, *J. Am. Chem. Soc.*, 2008, **130**, 13691–13695.
- C. J. Bowerman, W. Liyanage, A. J. Federation and B. L. Nilsson, *Biomacromolecules*, 2011, **12**, 2735–2745.
- C. J. Bowerman, D. M. Ryan, D. A. Nissan and B. L. Nilsson, *Mol. Biosyst.*, 2009, **5**, 1058–1069.
- G. L. Eakins, J. K. Gallaher, R. A. Keyzers, A. Falber, J. E. A. Webb, A. Laos, Y. Tidhar, H. Weissman, B. Rybtchinski, P. Thordarson and J. M. Hodgkiss, *J. Phys. Chem. B*, 2014, **118**, 8642–8651.
- C. Gribbon, K. J. Channon, W. Zhang, E. F. Banwell, E. H. C. Bromley, J. B. Chaudhuri, R. O. C. Oreffo and D. N. Woolfson, *Biochemistry*, 2008, **47**, 10365–10371.
- V. A. Kumar, B. K. Wang and S. M. Kanahara, *Exp. Biol. Med.*, 2016, **241**, 899–908.
- A. P. Schoen, B. Hommersom, S. C. Heilshorn and M. E. Leunissen, *Soft Matter*, 2013, **9**, 6781–6785.
- G. J. Brouhard and L. M. Rice, *Nat. Rev. Mol. Cell Biol.*, 2018, **19**, 451–463.
- M. Dogterom and G. H. Koenderink, *Nat. Rev. Mol. Cell Biol.*, 2019, **20**, 38–54.
- J. M. Neuhaus, M. Wanger, T. Keiser and A. Wegner, *J. Muscle Res. Cell Motil.*, 1983, **4**, 507–527.
- J. Boekhoven, A. M. Brizard, K. N. Kowgi, G. J. Koper, R. Eelkema and J. H. van Esch, *Angew. Chem., Int. Ed.*, 2010, **49**, 4825–4828.
- B. A. Grzybowski and W. T. Huck, *Nat. Nanotechnol.*, 2016, **11**, 585–592.

[View Article Online](#)
Communication
Nanoscale

- 15 R. Merindol and A. Walther, *Chem. Soc. Rev.*, 2017, **46**, 5588–5619.
- 16 S. De and R. Klajn, *Adv. Mater.*, 2018, **30**, 1706750.
- 17 B. Riefß, R. K. Grötsch and J. Boekhoven, *Chem*, 2020, **6**, 552–578.
- 18 A. Sorrenti, J. Leira-Iglesias, A. J. Markvoort, T. F. A. de Greef and T. M. Hermans, *Chem. Soc. Rev.*, 2017, **46**, 5476–5490.
- 19 J. Boekhoven, W. E. Hendriksen, G. J. Koper, R. Eelkema and J. H. van Esch, *Science*, 2015, **349**, 1075–1079.
- 20 M. Tena-Solsona, C. Wanzke, B. Riess, A. R. Bausch and J. Boekhoven, *Nat. Commun.*, 2018, **9**, 2044.
- 21 S. Maiti, I. Fortunati, C. Ferrante, P. Scrimin and L. J. Prins, *Nat. Chem.*, 2016, **8**, 725–731.
- 22 J. Leira-Iglesias, A. Sorrenti, A. Sato, P. A. Dunne and T. M. Hermans, *Chem. Commun.*, 2016, **52**, 9009–9012.
- 23 J. Leira-Iglesias, A. Tassoni, T. Adachi, M. Stich and T. M. Hermans, *Nat. Nanotechnol.*, 2018, **13**, 1021–1027.
- 24 L. Heinen and A. Walther, *Sci. Adv.*, 2019, **5**, eaaw0590.
- 25 E. A. J. Post and S. P. Fletcher, *Chem. Sci.*, 2020, **11**, 9434–9442.
- 26 M. Tena-Solsona, B. Riess, R. K. Grottsch, F. C. Lohrer, C. Wanzke, B. Kasdorf, A. R. Bausch, P. Muller-Buschbaum, O. Lieleg and J. Boekhoven, *Nat. Commun.*, 2017, **8**, 15895.
- 27 L. S. Kariyawasam and C. S. Hartley, *J. Am. Chem. Soc.*, 2017, **139**, 11949–11955.
- 28 K. Dai, J. R. Fores, C. Wanzke, B. Winkeljann, A. M. Bergmann, O. Lieleg and J. Boekhoven, *J. Am. Chem. Soc.*, 2020, **142**, 14142–14149.
- 29 F. Schnitter and J. Boekhoven, *ChemSystemsChem*, 2021, **3**, e2000037.
- 30 B. Riess, C. Wanzke, M. Tena-Solsona, R. K. Grottsch, C. Maity and J. Boekhoven, *Soft Matter*, 2018, **14**, 4852–4859.

Electronic Supplementary Material (ESI) for Nanoscale.
This journal is © The Royal Society of Chemistry 2021

Supporting Information for:

Morphological transitions in chemically fueled self-assembly

Authors: Kun Dai,^a Marta Tena-Solsona,^a Jennifer Rodon Fores,^a Alexander M. Bergmann,^a and Job Boekhoven^{*a,b}

Affiliations:

^a Department of Chemistry, Technical University of Munich, Lichtenbergstrasse 4, 85748 Garching, Germany.

^b Institute for Advanced Study, Technical University of Munich, Lichtenbergstrasse 2a, 85748 Garching, Germany.

Materials and methods

Materials. All reagents were purchased from Sigma-Aldrich and Alfa-Aesar and used without further purification unless otherwise indicated. The peptides used in this study were synthesized using solid-phase peptide synthesis.

Peptide synthesis and its purification.

Ac-FIVD, Ac-FILD-OH, Ac-FVVVD-OH, Ac-FIVVD-OH

The peptide synthesis was performed on a CEM Liberty microwave-assisted peptide synthesizer. The first amino acid coupling to the resin was accomplished by using the symmetrical anhydride method. Briefly, a 0.2 M solution of the symmetrical anhydride was prepared by allowing the Fmoc-protected aspartic acid (FmocD(OtBu)OH, 12 mmol) and N,N'-diisopropylcarbodiimide (DIC, 6 mmol) to react in 30 mL N,N-dimethylformamide (DMF) for 60 min. The solution was placed in a freezer at -20°C for 30 min, and the solid urea formed was filtered out before the next step. Loading of the resin was performed using the automated peptide synthesizer. The symmetrical anhydride solution (0.2 M, 12 mL) and 4-(dimethylamino)pyridine (DMAP) solution in DMF (20 mM, 2.5 mL) were added to the pre-swollen Wang resin (0.5 mmol, 1.1 mmol/g) and heated in the microwave (30 min, 75 °C). The coupling was repeated twice. The resin was then washed with DMF (2x10 mL). Following couplings were achieved using 4 equivalents (eq.) of Fmoc-protected amino acid in DMF, 4 eq. of DIC and 4 eq. of ethyl (hydroxyimino)cyanoacetate (Oxyma). The resin solution was then heated in the microwave (1x2 min, 90 °C). Fmoc removal was accomplished using a solution of 20% piperidine in DMF (1x2 min, 90 °C). The resin was washed with DMF (3x7 mL) between different steps. This procedure was repeated until the last chemical CH₃COOH was coupled. The resulting peptide was cleaved from the resin using a mixture of 95% trifluoroacetic acid (TFA), 2.5% water, and 2.5% triisopropylsilane (TIPS). The solvent was removed by co-distillation with DCM by rotary evaporation and dried under reduced pressure. The residue was extracted with diethyl ether one time and the organic phase was washed two times with water. The combined aqueous phase was purified using reversed-phase high-performance liquid chromatography (HPLC, Thermofisher Dionex Ultimate 3000, Hypersil Gold 250x4.8 mm) in a linear gradient of acetonitrile (ACN, 2% to 98%) and water with 0.1% TFA. The purified peptide was lyophilized and stored at -20 °C until further use. (See Supporting Table 1 for a summary of the analysis of the peptides).

Methods.

Sample preparation. Stock solutions of the precursors were prepared by dissolving the peptides in 200 mM MES buffer, after which the pH was adjusted to pH 6.0 with NaOH solution. Stock solutions of EDC were prepared by dissolving the EDC powder in MQ water.

These stock solutions were used freshly. The reaction cycles were initiated by the addition of the EDC to the precursor solution. We carried out all experiments at 21.5 (± 0.5) °C.

Analysis of the reaction kinetics by HPLC.

Analytical reversed-phase HPLC experiments were performed on a ThermoFisher Dionex Ultimate 3000 liquid chromatography setup (Dionex Ultimate pump, Dionex Ultimate Autosampler, Dionex Ultimate 3000 RS Variable Wavelength Detector, Hypersil Gold 250 x 4.6 mm, C18 column (5 μ m pore size)). The standard detection wavelengths were set to 220 and 254 nm. For quantification of the anhydride concentrations during the reaction cycle, a quenching method with benzylamine previously reported was used¹. Specifically, after the reaction cycle was started by the addition of EDC fuel, 10 μ L of the corresponding sample were pipetted on 30 μ L of a 500 mM benzylamine solution in Acetonitrile (ACN) in a 200 μ L HPLC vial inlet and mixed by pipetting and vortexing. The turbidity, vanished completely during the quenching and mixing process. Additionally, the pH of the quenched mixtures increased instantly to 9.3 which also inhibits further hydrolysis of the remaining EDC during the analysis and stops the reaction cycle. We used a linear gradient from 98:2 to 2:98 in 10 minutes followed by 2 minutes at 2:98 for the separation. The column was equilibrated for 2 minutes after each gradient. Retention times are given in Supporting Table S1. The peptide anhydride concentrations were quantified from the corresponding peptide-benzylamide peaks (Fig. S1 - Fig. S4). The calibration value for the **P1** peptide-benzylamide is 0.76, **P2** peptide-benzylamide is 0.75, **P3** peptide-benzylamide is 0.81, and **P4** peptide-benzylamide is 0.81.

Kinetic model. A kinetic model was used to predict the evolution of the anhydride concentration over time. The model is described in detail in the Supporting Note 1. The rate constants we used in this work are given in Table S2.

UV/Vis Spectroscopy. Turbidity measurements were carried out at 21.5 °C on a Microplate Spectrophotometer (Thermo Scientific Multiskan GO, Thermo Scientific SkanIt Software 4.0). Measurements were performed in a non-tissue culture treated 96-well plate (Falcon, flat bottom). Every minute, the absorbance of the 200 μ L samples was measured at 600 nm. All experiments were performed in triplicate (n=3).

ESI-MS. ESI-MS experiments were conducted on an LCQ Fleet Ion Trap Mass Spectrometer (Thermo Scientific). Interpretation of all recorded MS data was performed using the Thermo Xcalibur Qual Browser 2.2 SP1.48 software.

Confocal Fluorescence Microscopy. Confocal Fluorescence Microscopy. Confocal fluorescence microscopy was performed on a Leica TCS SP8 confocal microscope using a 63x water immersion objective. Samples were prepared as described above and transferred

into micro-well plates (ibidi, μ -Slide Angiogenesis Glass Bottom). 2.5 μ M *Nile red* was added as fluorescent dye. Samples were excited with 552 nm and imaged at 565-635 nm.

Determination of the solubility of the anhydride.

Samples of **P1** (10 mM), **P2** (10 mM) **P3** (10 mM) and **P4** (10 mM) were fuelled with different amounts of EDC and the mixtures were analysed over time by HPLC and UV-Vis (absorbance at 600 nm). When the amount of EDC was not enough to reach the value of the anhydride's solubility, no turbidity was observed. After a certain EDC concentration, turbidity appeared. The maximum concentration of anhydride obtained with this EDC concentration was compared with the maximum concentration of anhydride of the closest EDC concentration trace that did not show any turbidity over time. The solubility value for the anhydride was then established between these two maxima with the corresponding error.

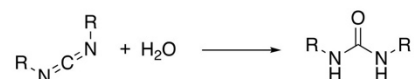
Supporting note 1: Description of the kinetic model

A kinetic model was written in Matlab that describes each reaction involved in the chemical reaction network except. The concentrations of each reactant were calculated for every second in the cycle. The model was used to fit the obtained HPLC data that described the evolution of the concentration of anhydride, EDC and acid over time. In all experiments, the concentration of the precursor was 10 mM.

The model described five chemical reactions:

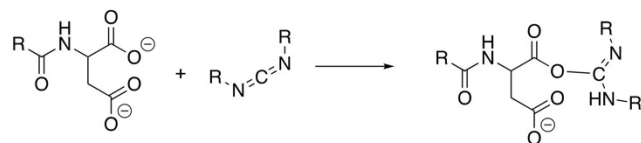
0) Direct hydrolysis of carbodiimide with a first order rate constant of $1.3 \times 10^{-5} \text{ sec}^{-1}$ as determined in previous work.

Reaction 0 (k_0)



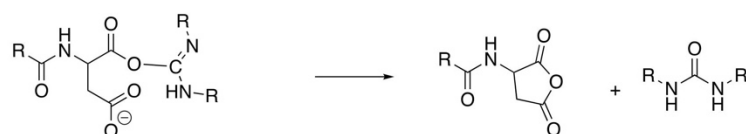
1) The formation of O-acylurea by reaction with EDC (k_1). This second order rate constant was dependent on the nature of the precursor. The rate constant was determined for each precursor by HPLC, by monitoring the EDC consumption.

Reaction 1 (k_1)



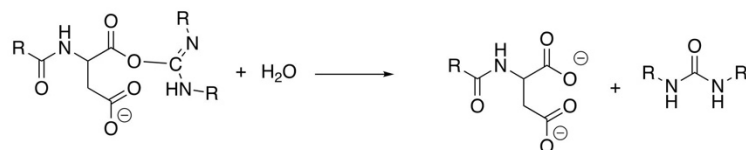
2) The formation of the anhydride with a first order rate constant. This rate constant could not be determined because the O-acylurea was never observed. It was therefore set to be twice the rate of k_1 . As a result, the O-acylurea did never reach concentrations over 1 μM in the model.

Reaction 2 (k_2)



3) Direct hydrolysis of O-acylurea (k_3). This reaction rate could not be obtained because the O-acylurea was not observed. The ratio of k_2 and k_3 (anhydride formation and competing direct hydrolysis of O-acylurea) was varied to fit the HPLC data for several concentrations of $[\text{fuel}]_0$ and $[\text{di-acid}]_0$.

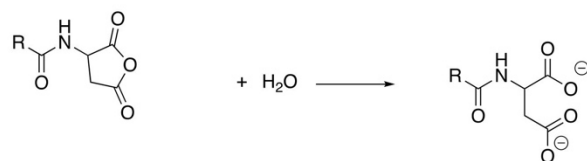
Reaction 3 (k_3)



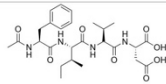
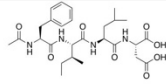
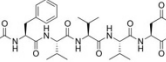
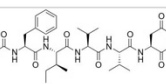
4) Hydrolysis of anhydride proceeded with a first order rate (k_4) The rate constant was determined by HPLC for kinetic experiments where no assemblies were reached.

The rate of the hydrolysis reaction was calculated by multiplying the first order rate constant k_4 with the concentration of anhydride.

Reaction 4 (k_4)



Supporting Table S1. Characterization of precursors

Name	Structure	Mass calculated [g/mol]	Mass observed [g/mol]	Retention time [min] @220nm	Purity
Ac-FIVD-OH (P1)		Mw = 534.27 $C_{26}H_{38}N_4O_8$	557.27 [Mw+Na] ⁺	6.167	96%
Ac-FILD-OH (P2)		Mw = 548.28 $C_{27}H_{40}N_4O_8$	571.32 [Mw+Na] ⁺	6.613	97%
Ac-FVVVD-OH (P3)		Mw = 619.32 $C_{30}H_{45}N_5O_9$	642.28 [Mw+Na] ⁺	6.175	95%
Ac-FIVVD-OH (P4)		Mw = 633.34 $C_{31}H_{47}N_5O_9$	656.28 [Mw+Na] ⁺	6.550	95%

Supporting Table S2. Rate constants used to fit the HPLC data with a kinetic model.

Name	k_0 (sec ⁻¹)	k_1 (M ⁻¹ x sec ⁻¹)	k_2	k_3	k_4 (sec ⁻¹)
Ac-FIVD(P1)	1.35×10^{-5}	9×10^{-2}	$1.7 * k_1$	$1 * k_1$	$6 * 10^{-3}$
Ac-FILD-OH (P2)	1.35×10^{-5}	7.5×10^{-2}	$1.7 * k_1$	$1 * k_1$	$1 * 10^{-2}$

Supporting Figures

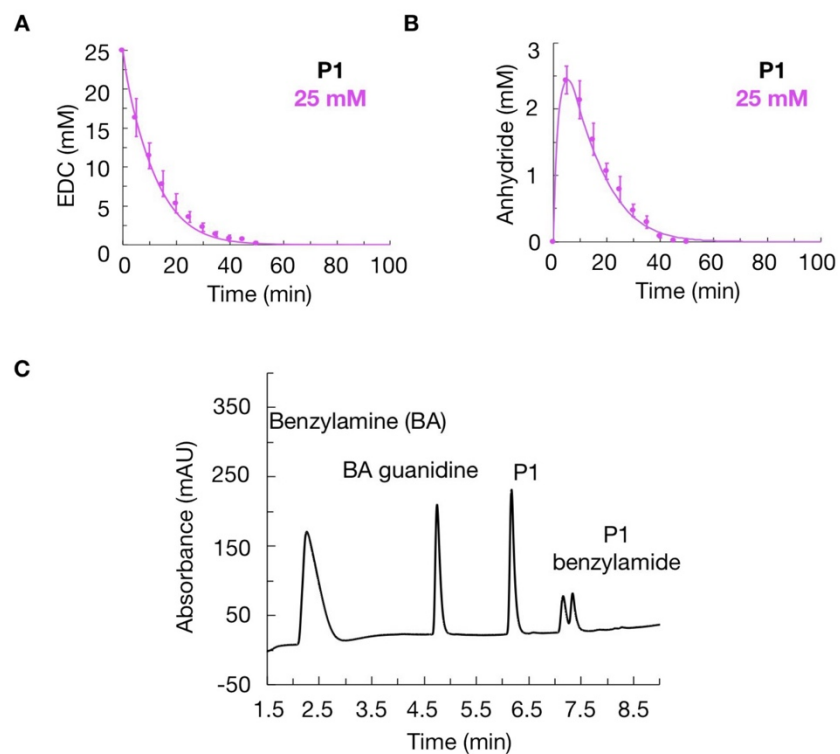


Figure S1. Kinetic traces of P1 in the presence of fuel. The concentration of EDC (A) and anhydride product (B) as a function of time when 10 mM P1 was fueled with 25 mM EDC. Error bars represent the standard deviation ($n=3$). The lines represent data from the kinetic model, whereas the markers represent HPLC data. The kinetic traces can be fitted with a kinetic model that takes into account the hydrolysis occurring in solution^{2, 3}. (C) Example of a chromatogram of 10 mM P1 with 25 mM EDC at 5 min after quenching with benzylamine (see Analytical HPLC Method).

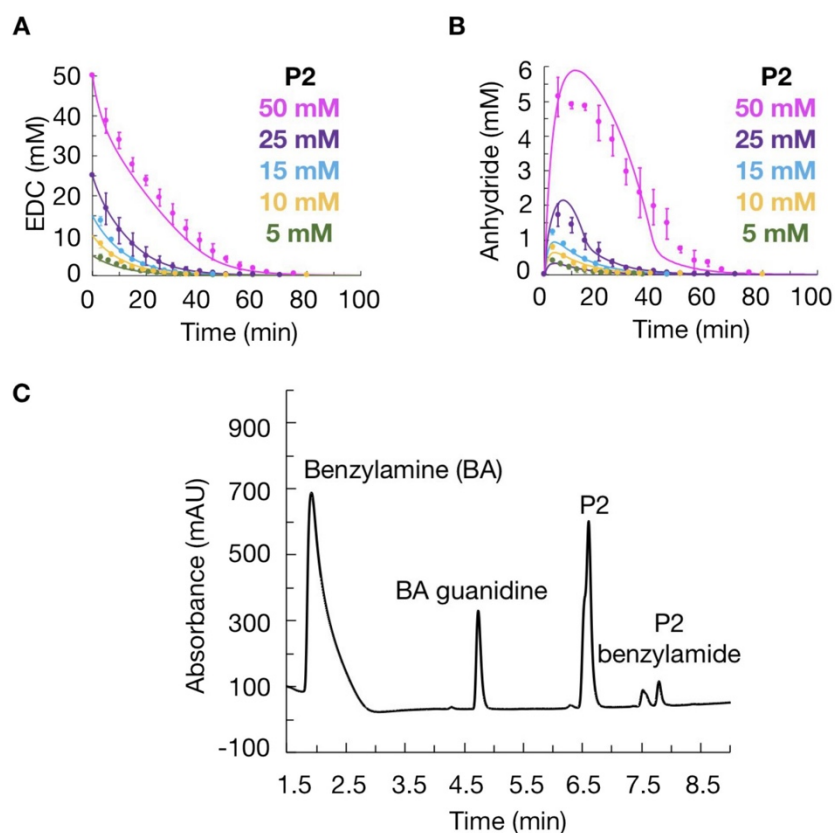


Figure S2. Kinetic traces of P1 in the presence fuel. The concentration of EDC (A) and anhydride product (B) as a function of time when 10 mM P1 was fueled with different concentrations of EDC. The kinetic traces can be fitted with a kinetic model that takes into account the hydrolysis occurring in solution^{2,3}. The lines represent data from the kinetic model, whereas the markers represent HPLC data. Error bars represent the standard deviation (n=3). (C) Example of a chromatogram of 10 mM P1 with 25 mM EDC at 10 min after quenching with benzylamine (see Analytical HPLC Method).

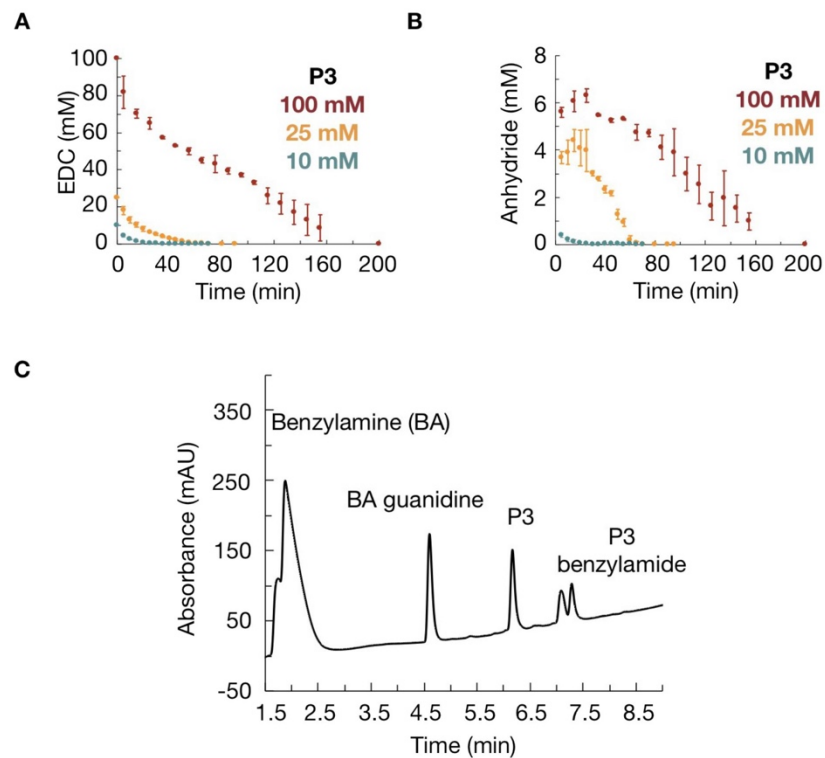


Figure S3. Kinetic traces of P3 in the presence of fuel. The concentration of EDC (A) and anhydride product (B) as a function of time when 10 mM P3 was fueled with different concentrations of EDC. Error bars represent the standard deviation ($n=3$). (C) Example of a chromatogram of 10 mM P3 with 25 mM EDC at 5 min after quenching with benzylamine (see Analytical HPLC Method).

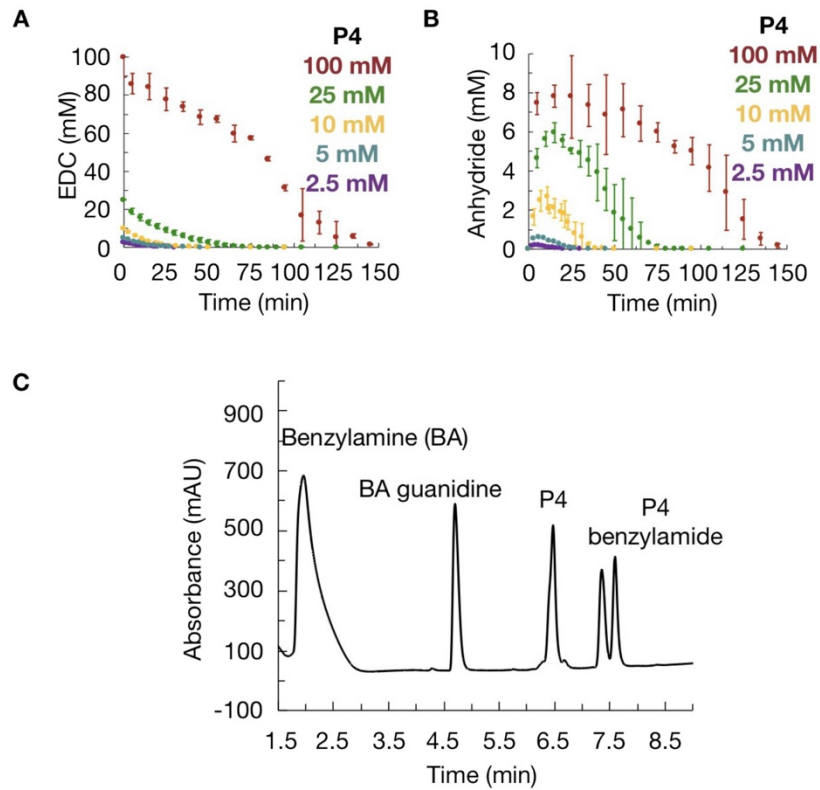


Figure S4. Kinetic traces of P4 in the presence of fuel. The concentration of EDC (A) and anhydride product (B) as a function of time when 10 mM P4 was fueled with different concentrations of EDC. Error bars represent the standard deviation ($n=3$). (C) Example of a chromatogram of 10 mM P4 with 25 mM EDC at 5 min after quenching with benzylamine (see Analytical HPLC Method).

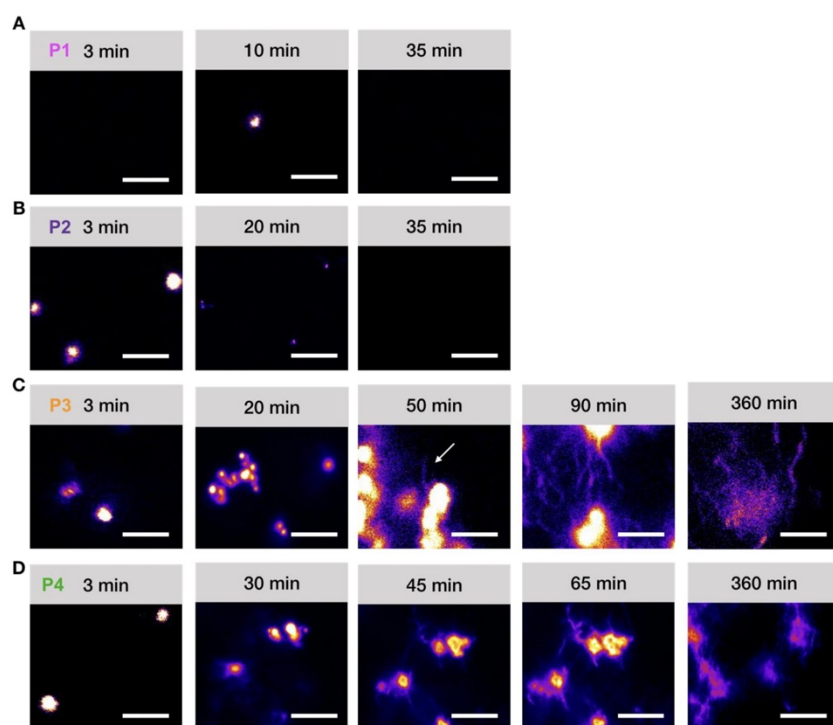


Figure S5. Confocal micrographs. Confocal micrographs corresponding to the addition of 25 mM EDC to 10 mM **P1** (A), 10 mM **P2** (B), 10 mM **P3** (C) and 10 mM **P4** (D) over time. All scale bars correspond to 5 μm . Samples were stained with 2.5 μM Nile red.

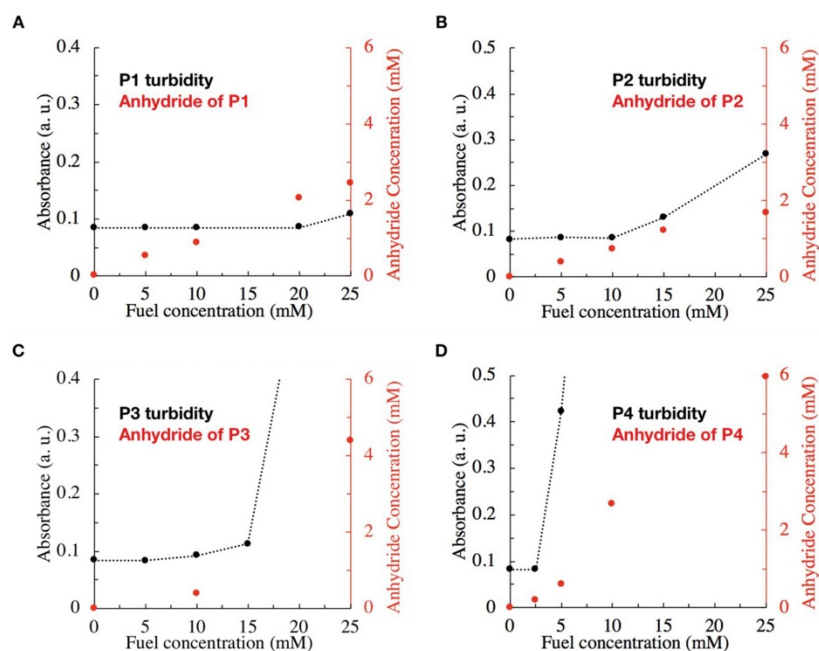


Figure S6. Determination of the solubility of the anhydride. (A) Anhydride concentration of **P1** and absorbance signal measured at 600 nm against fuel concentration. The solubility of the anhydride (2.2 mM) was averaged between the maximum anhydride concentration obtained with 25 mM fuel (first time turbidity was observed) and 20 mM of fuel (last time turbidity was not observed). (B) Anhydride concentration of **P2** and absorbance signal measured at 600 nm against fuel concentration. The solubility of the anhydride (1.1) was averaged between the maximum anhydride concentration obtained with 15 mM fuel (first time turbidity was observed) and 10 mM of fuel (last time turbidity was not observed). (C) Anhydride concentration of **P3** and absorbance signal measured at 600 nm against fuel concentration. The solubility of the anhydride (0.4 mM) was closed to the maximum anhydride concentration obtained with 10 mM fuel (first time turbidity was observed). (D) Anhydride concentration of **P4** and absorbance signal measured at 600 nm against fuel concentration. The solubility of the anhydride (0.2 mM) was averaged between the maximum anhydride concentration obtained with 5 mM fuel (first time turbidity was observed) and 2.5 mM of fuel (last time turbidity was not observed)

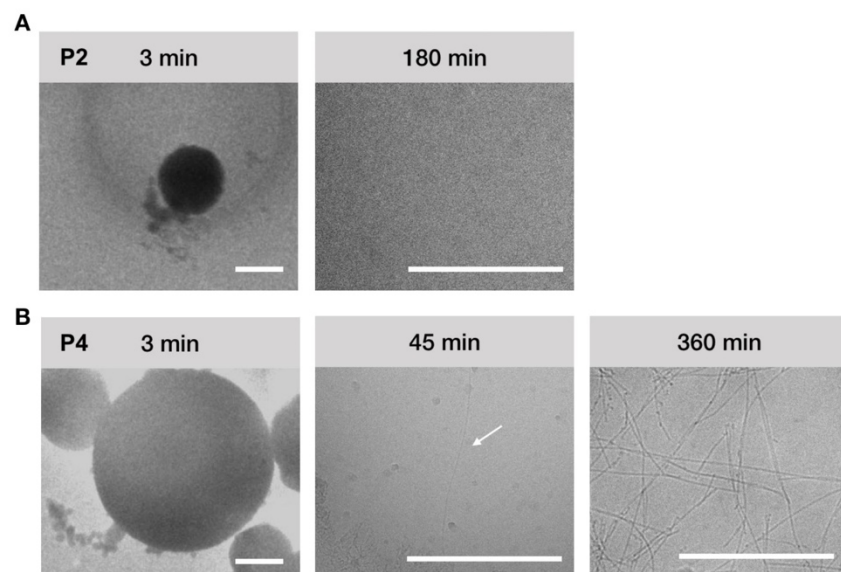


Figure S7. Cryo-TEM micrographs. All scale bars correspond to 100 nm. **Cryo-TEM micrographs** corresponding to the addition of 25 mM EDC to 10 mM **P2** (A) and 10 mM **P4** (B) over time. All scale bars correspond to 500 nm.

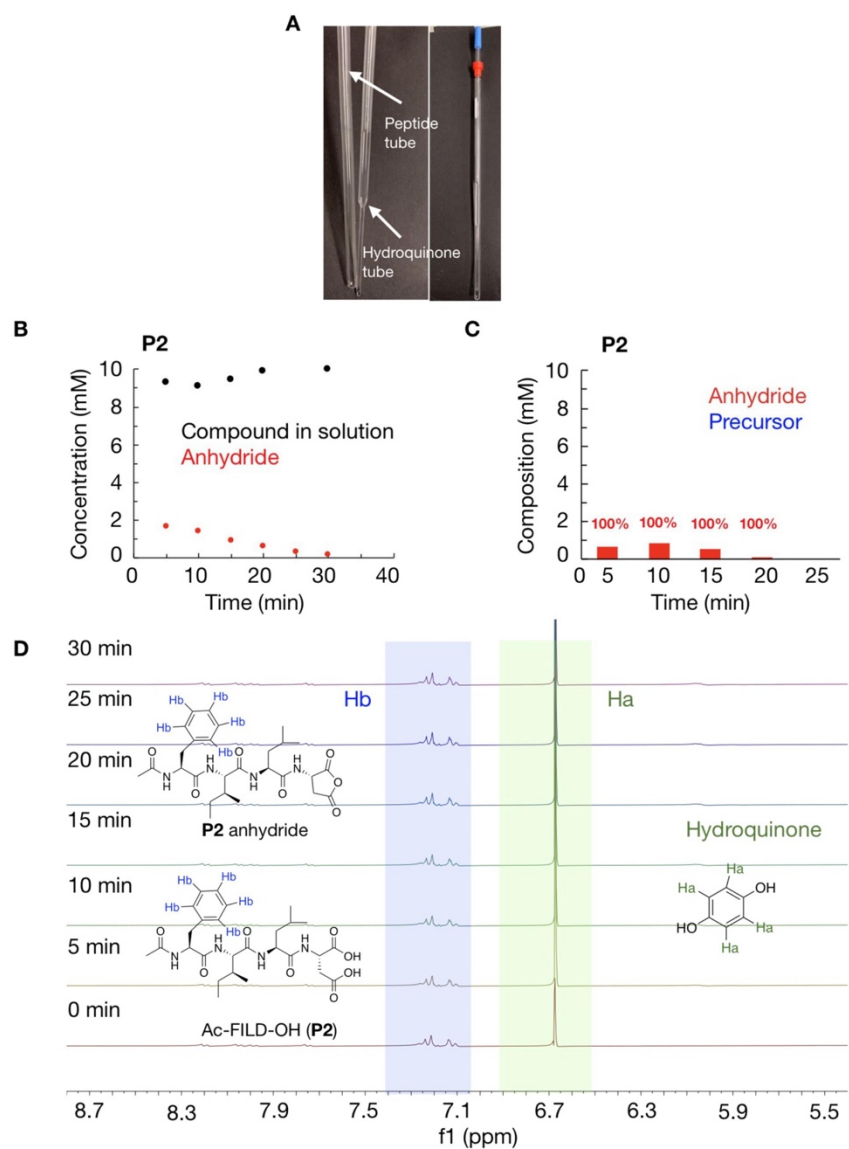


Figure S8: The assembly composition of P2. **A)** The scheme of NMR peptide tube and the inner tube with hydroquinone. **B)** The concentration of P2 precursor in solution as measured by NMR (black markers), and the concentration of P2 anhydride product as measured by

HPLC (red markers) as a function of time in response to 25 mM of EDC. **C)** The concentration of **P2** precursor and **P2** anhydride in the assembly as a function of time that we calculated from the data in **A**: $C_{in\ the\ assembly} = 10\ mM - C_{in\ the\ solution}$. We assumed that, as long as there is still anhydride present in the solution, it is likely that there is no or only small amount of precursor in the assembled state. **D)** 1H NMR kinetics of **P2** (10 mM) after the addition of 25 mM of fuel. To determine the concentration of **P2** precursor and **P2** anhydride an internal standard (hydroquinone 50 mM in D_2O) was used.

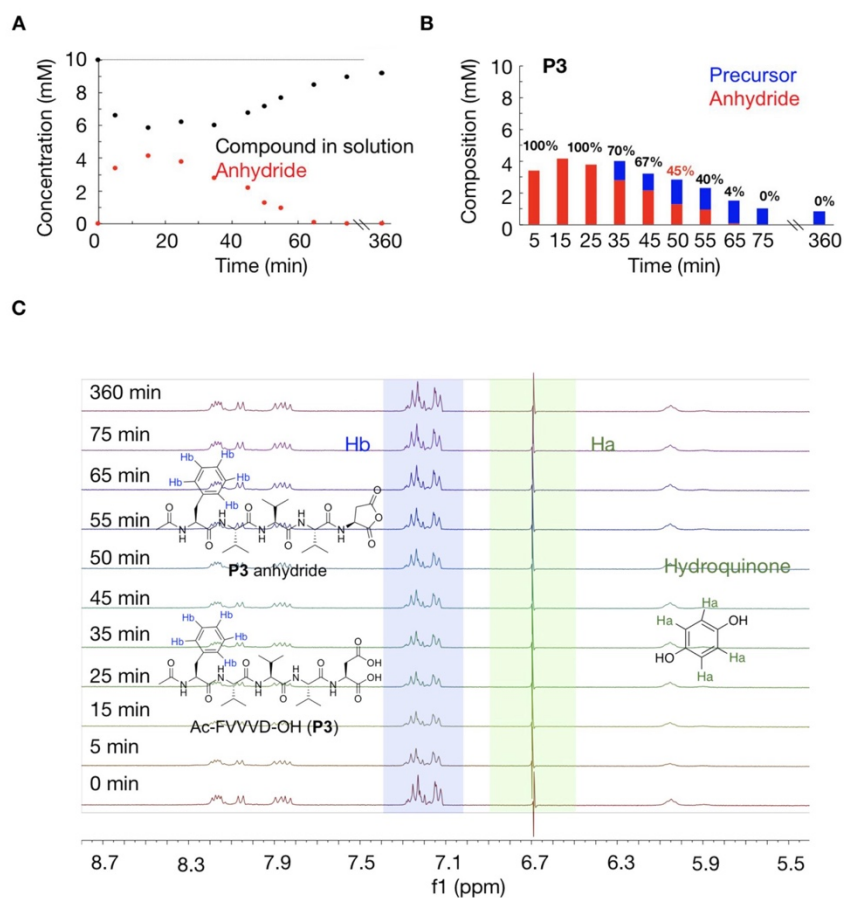


Figure S9: The assembly composition of P3. A) The concentration of **P3** precursor in solution as measured by NMR (black markers), and the concentration of **P3** anhydride product as measured by HPLC (red markers) as a function of time in response to 25 mM of EDC. **B)**

The concentration of **P3** precursor and **P3** anhydride in the assembly as a function of time that we calculated from the data in **A**: $C_{in\ the\ assembly} = 10\ mM - C_{in\ the\ solution}$. We assumed that, as long as there is still anhydride present in the solution, it is likely that there is no or only small amount of precursor in the assembled state. **C**) 1H NMR kinetics of **P3** (10 mM) after the addition of 25 mM of fuel. To determine the concentration of **P3** precursor and **P3** anhydride an internal standard (hydroquinone 50 mM in D_2O) was used.

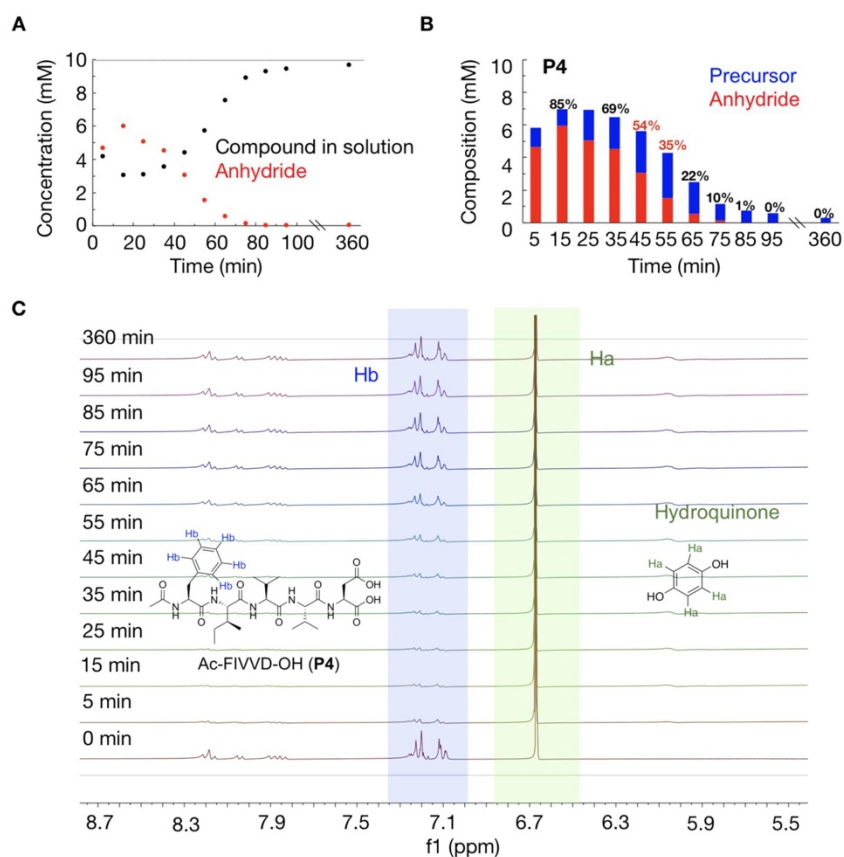


Figure S10: The assembly composition of P4. **A**) The concentration of **P4** precursor in solution as measured by NMR (black markers), and the concentration of **P4** anhydride product as measured by HPLC (red markers) as a function of time in response to 25 mM of EDC. **B**) The concentration of **P4** precursor and **P4** anhydride in the assembly as a function of time that we calculated from the data in **A**: $C_{in\ the\ assembly} = 10\ mM - C_{in\ the\ solution}$. **C**) 1H NMR kinetics of

P4 (10 mM) after the addition of 25 mM of fuel. To determine the concentration of **P4** precursor and **P4** anhydride an internal standard (hydroquinone 50 mM in D₂O) was used.

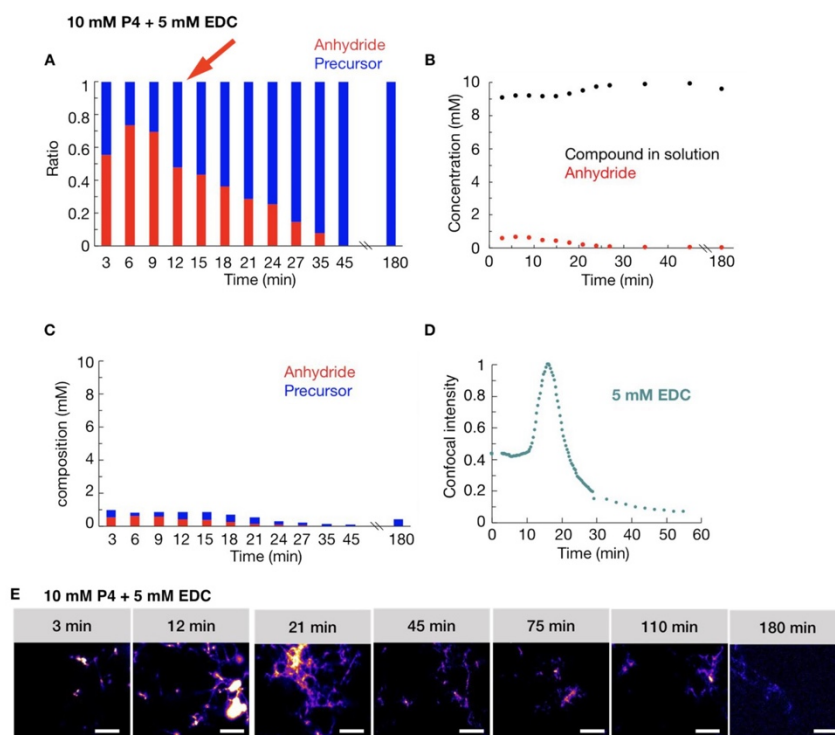


Figure S11: The assembly composition and the confocal microscopy for P4 with 5 mM Fuel. **A)** The ratio of anhydride and precursor in the assembly over time determined by HPLC and NMR for 10 mM **P4** after the addition of 5 mM of fuel. **B)** The concentration of **P4** precursor in solution measured by NMR (black markers), and the concentration of **P4** anhydride product measured by HPLC as a function of time (red markers) in response to 5 mM of EDC. **C)** The concentration of **P4** precursor and **P4** anhydride in the assembly as a function of time that we calculate from the data in **A**: $C_{in\ the\ assembly} = 10\ mM - C_{in\ the\ solution}$. We assumed that, as long as there is still anhydride present in the solution, it is likely that there is no or only small amount of precursor in the assembled state. **D)** The normalized intensity from confocal microscopy for 10 mM **P4** with 5 mM EDC as a function of time. **E)** Confocal micrographs of **P4** (10 mM) after the addition of 5 mM EDC over time. All scale bars correspond to 5 μ m. Samples were stained with 2.5 μ M Nile red. The red arrow indicates the point where around 55% of anhydride is in the assembly.

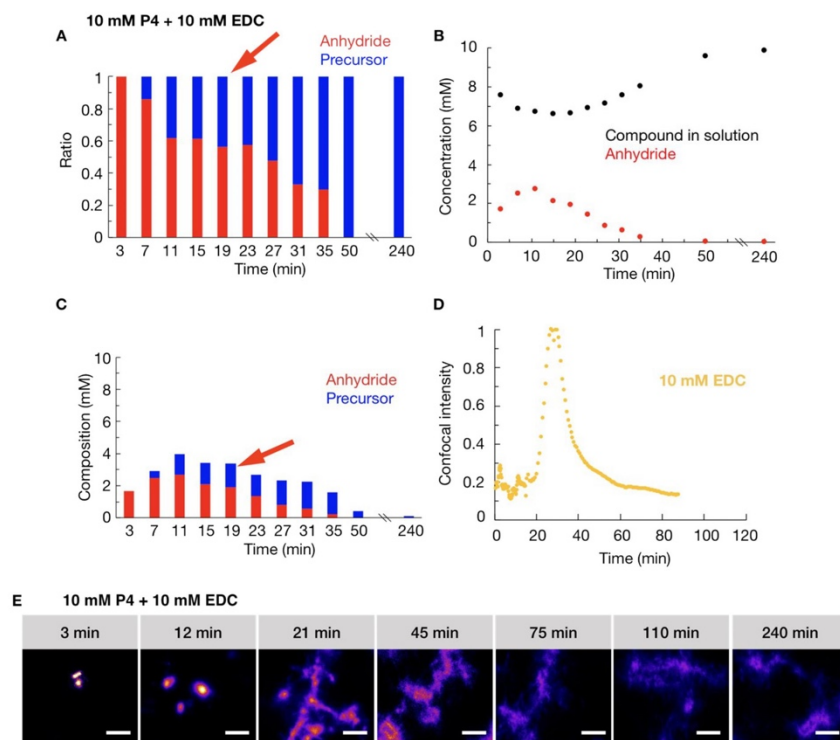


Figure S12: The assembly composition and the confocal microscopy for P4 with 10 mM Fuel. **A)** The ratio of anhydride and precursor in the assembly over time determined by HPLC and NMR for 10 mM P4 after the addition of 10 mM of fuel. **B)** The concentration of P4 precursor in solution measured by NMR (black markers), and the concentration of P4 anhydride product measured by HPLC as a function of time (red markers) in response to 10 mM of EDC. **C)** The concentration of P4 precursor and P4 anhydride in the assembly as a function of time that we calculate from the data in **A**: $C_{in\ the\ assembly} = 10\ mM - C_{in\ the\ solution}$. **D)** The normalized intensity from confocal microscopy for 10 mM P4 with 10 mM EDC as a function of time. **E)** Confocal micrographs of P4 (10 mM) after the addition of 10 mM EDC over time. All scale bars correspond to 5 μ m. Samples were stained with 2.5 μ M Nile red. The red arrow indicates the point where around 55% of anhydride is in the assembly.

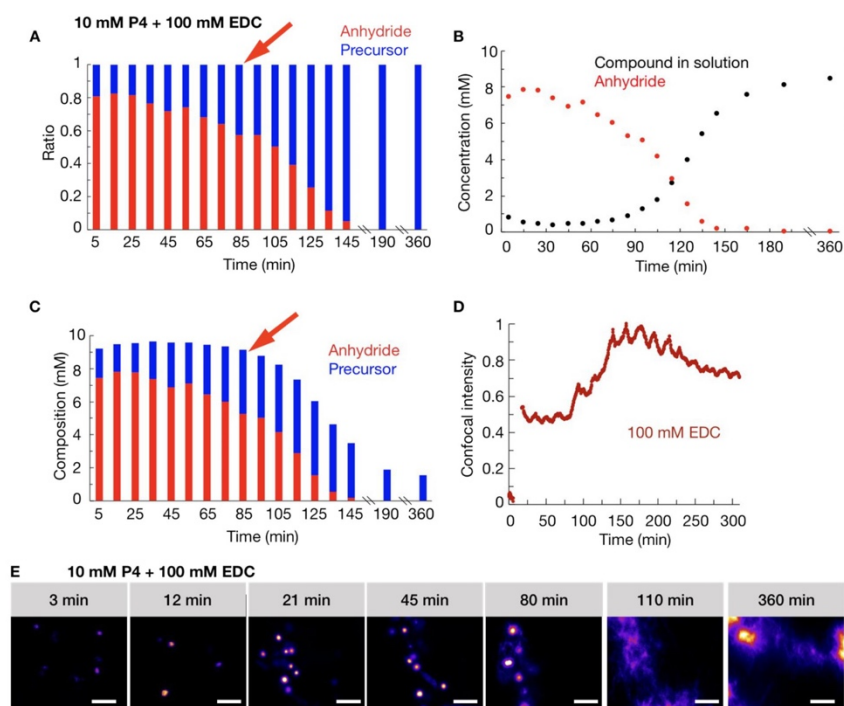


Figure S13: The assembly composition and the confocal microscopy for P4 with 100 mM Fuel. **A)** The ratio of anhydride and precursor in the assembly over time determined by HPLC and NMR for 10 mM P4 after the addition of 100 mM of fuel. **B)** The concentration of P4 precursor in solution measured by NMR (black markers), and the concentration of P4 anhydride product measured by HPLC as a function of time (red markers) in response to 100 mM of EDC. **C)** The concentration of P4 precursor and P4 anhydride in the assembly as a function of time that we calculate from the data in **A**: $C_{in\ the\ assembly} = 10\ mM - C_{in\ the\ solution}$. **D)** The normalized intensity from confocal microscopy for 10 mM P4 with 100 mM EDC as a function of time. **E)** Confocal micrographs of P4 (10 mM) after the addition of 100 mM EDC over time. All scale bars correspond to 5 μm . Samples were stained with 2.5 μM Nile red. The red arrow indicates the point where around 55% of anhydride is in the assembly.

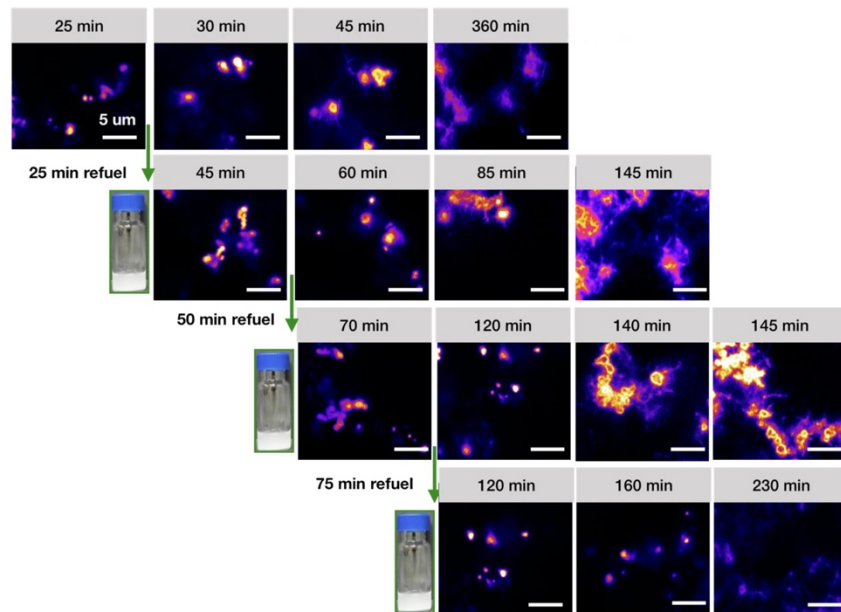


Figure S14: Confocal micrograph of P4 (10 mM) with EDC refueling (25 mM) every 25 minutes. All scale bars correspond to 5 μm. The dye for confocal is 2.5 μM Nile red.

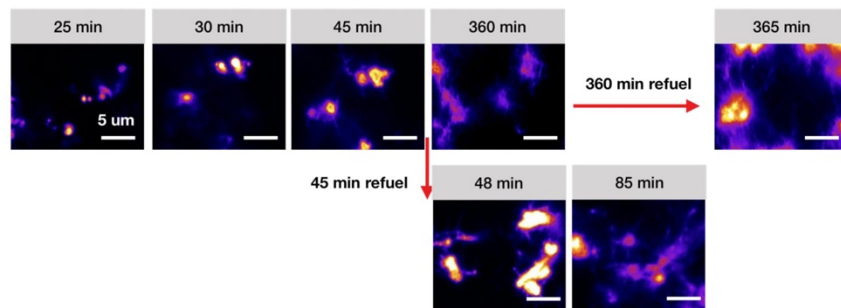


Figure S15: Confocal micrograph of 25 mM EDC refuel to 10 mM P4 with 25 mM EDC system after fiber formation. All scale bars correspond to 5 μm. Samples were stained with 2.5 μM Nile red.

1. F. Schnitter and J. Boekhoven, *ChemSystemsChem*, 2020, **3**.
2. B. Riess, C. Wanzke, M. Tena-Solsona, R. K. Grotsch, C. Maity and J. Boekhoven, *Soft Matter*, 2018, **14**, 4852–4859.
3. M. Tena-Solsona, B. Riess, R. K. Grotsch, F. C. Lohrer, C. Wanzke, B. Kasdorf, A. R. Bausch, P. Muller-Buschbaum, O. Lieleg and J. Boekhoven, *Nat Commun*, 2017, **8**, 15895.

5. Conclusion and Outlook

The overall aim of this thesis was to develop the design rules for a chemically fueled self-assembly with a focus on both the assembly and disassembly processes. The assembly behavior can be toggled between one chemically fueled reaction cycle without self-assembly, chemically fueled self-assembly, chemically fueled kinetically trapped self-assembly, and precursor self-assembles before the addition of fuel. I also introduced the notion that different disassembly pathways can induce morphological transitions.

In the first chapter, I introduced what chemically fueled self-assembly is and why I focus on it. Furthermore, I described how to design chemical reaction cycles and the strategies to couple these reaction cycles to assemblies. The general strategies are the charge abolishment and transient linker strategy. Finally, based on these strategies, I discussed unwanted outcomes that cannot be avoided in the design of chemically fueled self-assemblies. As a result, in chapter 3 and chapter 4, I specifically focus on the toggling of molecular assemblies from design rules.

In chapter 3, I demonstrate a new family of peptides coupled to the EDC-driven reaction cycle. The simplicity of the peptide design and reaction cycle allows creating general rules for the self-assembly behavior in response to fuel. Three possible behaviors are demonstrated: the peptide does not assemble, it assembles in a chemically fueled dynamic manner, or it assembles without fuel. In the molecular design of the peptide library I introduced, the attractive interactions can be controlled by the number of isoleucine (I) amino acids. In contrast, the repulsive interactions between peptides can be adjusted by introducing aspartic acid (D) amino acids in the peptide sequence or by adding salt to the system. As a result, the peptide's behaviors can be tuned by the ratio of attractive to repulsive interactions, and these design rules can be generalized to other peptide sequences. These behaviors can be understood by the context of the free energy landscape of self-assembly. Future work should investigate further nuances in these energy landscapes to probe other dynamic behaviors such as kinetic trapping or dynamic instabilities.

In chapter 4, four similar peptides are designed and their self-assembly is regulated by the EDC-driven reaction cycle. All peptides are assembled into colloids upon fuel addition but show a completely different disassembly pathway. In one case, the colloids disassemble and dissolve in water when the fuel depletes. In the other case, the colloids transition into fibers that remain kinetically trapped long after all fuel is depleted. The mechanism is explained by the increasing propensity to form beta-sheet and decreasing

solubility. Understanding the mechanism provides a chance to control the time that colloids transition into fibers by the amount of fuel added to the precursor solution. These findings highlight the importance of considering the disassembly pathway when designing new chemically fueled self-assembling systems.

In conclusion, this thesis demonstrates the development of design rules in the chemically fueled reaction cycle. With these design rules, I anticipate more chemically fueled self-assembly can be designed efficiently to help understand biological behaviors and develop more functional materials. Further research should pay more attention to the disassembly process in designing dissipative self-assembly.

6. Further publications

Besides the two publications reprinted above, I contributed to one more publication. The following is a full list of the publications during my Ph.D.

1. Patrick Schwarz, Marta Tena-Solsona, **Kun Dai**, Job Boekhoven. Carbodiimide-fueled catalytic reaction cycles to regulate supramolecular processes[J]. **Chem. Commun.** 2022
2. **Kun Dai**, Marta Tena-Solsona, Jennifer Rodon Fores, Job Boekhoven. Morphological transition regulated by chemical fuels[J]. **Nanoscale** 2021
3. **Kun Dai**, Jennifer Rodon Fores, Caren Wanzke, Benjamin Winkeljann, Alexander M. Bergmann, Oliver Lieleg, Job Boekhoven. Regulating Chemically Fueled Peptide Assemblies by Molecular Design[J]. **J. Am. Chem. Soc.** 2020, 142 (33), 14142-14149.

7. Acknowledgments

No one can walk the path of Ph.D. research alone. On the way, I definitely have the guidance, assistance, and even silent company from all of you!

First and foremost, I would like to express my sincere gratitude to Prof. Job Boekhoven. You gave me the opportunity to work in this great Lab and led me into the world of chemically fueled self-assembly. I enjoyed the topic very much, which gave me a chance to learn many new skills, techniques, and ways to think. You guided me to do experiments, personally taught me how to use the microscope, and discussed my project in the office, kitchen, online, and everywhere if I needed you. Thank you!

I want to thank the committee for accepting to review my work.

Without Boekhoven Lab's members, I would never finish my thesis so smoothly. Dr. Marta Tena-Solsona, thank you! I always receive excellent help from discussions with you. You taught me how to do research and how to write a paper.

Thanks to Dr. Jennifer Rodon-Fores, one very nice French postdoc. You helped me with my project and always patiently gave suggestions to me. You spent hours and hours with me in the 'cold' confocal room.

I would like to thank Michele Stasi, one gentleman with a broad knowledge of organic chemistry. No matter what organic questions I had, you always tried your best to solve them!

Fabian Schnitter, my lab-table mate. Thank you! You always shared your lab techniques and interesting stories with me, coloring the life in lab 2. I always enjoyed the football discussion with you.

Patrick (Pangzi?) and Michi, thank you for your tasty food before Corona! Thank you for taking me to the kick-off activity and introducing your friends and German culture to me! Of course, thank you for taking over the Lyo when I was not in Lab.

Alex, very similar to China's monkey-king Sunwukong, is impressed me a lot with your intelligence! More importantly, thank you for your beautiful Cryo-TEM pictures!

Laura, one tall girl who can speak some Chinese, is always very friendly. You tried to help me whenever I met any problems in experiments and life.

Xiaoyao, one 1-year younger than me to join our Lab. Thank you for your exist that I did not forget my mother tongue! I appreciate your help with my experiment.

Brigitte and Christine, finally I can recognize you two! Thank you for your earnestness!

I still remember when you did not know the answers to questions, you searched these and told me one day later. I also remember your kindly transferring your equipment time to me when I have some urgent experiments.

Judit! Thank you for your suggestions on my project and thoughtful discussions.

Thanks to Spabi, who is responsible for many instruments to keep everything going well in our Lab.

Especially, I want to thank Carsten. Thank you for organizing so many interesting activities and sharing different European cultures with me. It was you that the lab3 is not so boring!

Furthermore, I cannot forget some old guys, Dr. Benedikt Rieß and Dr. Raphael Grötsch shared lab1 with me when I came. As a fresh Ph.D. student, Dr. Caren Wanzke and these two guys introduced me to many new things for our Lab and taught me some important bad words in German. I enjoyed the nurf gun time! I enjoyed your spicy pepper!

Dear others of the group: Anna-Lena Holtmannspötter, Monika Wenisch, Dr. Oleksii Zozulia, Simone Poprawa, and some Canadine guys Michelle Ha, Yuning Liu, Chris. I enjoyed the time with you. I enjoyed every discussion, every BBQ, every game, every party with you. Thank you so much for your help!

I also want to thank my collaboration partners, Benjamin Winkeljann and Prof. Oliver Lieleg. Thank you for helping me with the rheology experiment.

For financial support I want to acknowledge the TUM as well as china scholarship council.

Of course, Thanks to my parents! You do not know English and cannot understand what 'chemically fueled self-assembly' is. However, you always try your best to support and encourage me. Without your constant support, I would never have had the chance to pursue my Ph.D. in TUM. It is a dream for me, but it is the yearning and worrying day and night for you. 谢谢你们，爸妈！

Thanks to my family, my grandma, my cousins, my uncles, and my aunts! Thank you for your help and trust. 感谢我的家人！

Thanks to all of my friends, You accompanied me through the pleasure time, we had a happy conversation! We had a party together! Thank you! All these are essential parts of my Ph.D. life.

8. References

1. E. Mattia and S. Otto, *Nat. Nanotechnol.*, 2015, **10**, 111-119.
2. C. Stoffelen and J. Huskens, *Small*, 2016, **12**, 96-119.
3. S. Yadav, A. K. Sharma and P. Kumar, *Frontiers in Bioengineering and Biotechnology*, 2020, **8**.
4. G. M. Whitesides and M. Boncheva, *Proceedings of the National Academy of Sciences*, 2002, **99**, 4769-4774.
5. A. Kajbafvala, H. Bahmanpour, M. H. Maneshian and M. Li, *Journal of Nanomaterials*, 2013, **2013**, 158517.
6. A. C. Mendes, E. T. Baran, R. L. Reis and H. S. Azevedo, *Wiley Interdiscip Rev Nanomed Nanobiotechnol*, 2013, **5**, 582-612.
7. B. Olenyuk, J. A. Whiteford, A. Fechtenkötter and P. J. Stang, *Nature*, 1999, **398**, 796-799.
8. A. Aggeli, I. A. Nyrkova, M. Bell, R. Harding, L. Carrick, T. C. B. McLeish, A. N. Semenov and N. Boden, *Proceedings of the National Academy of Sciences*, 2001, **98**, 11857.
9. T. Scheibel, R. Parthasarathy, G. Sawicki, X.-M. Lin, H. Jaeger and S. L. Lindquist, *Proceedings of the National Academy of Sciences*, 2003, **100**, 4527.
10. F. Di Maria, P. Olivelli, M. Gazzano, A. Zanelli, M. Biasiucci, G. Gigli, D. Gentili, P. D'Angelo, M. Cavallini and G. Barbarella, *J. Am. Chem. Soc.*, 2011, **133**, 8654-8661.
11. G. J. A. Sevink and A. V. Zvelindovsky, *Macromolecules*, 2005, **38**, 7502-7513.
12. T. M. Weiss, T. Narayanan, C. Wolf, M. Gradzielski, P. Panine, S. Finet and W. I. Helsby, *Phys. Rev. Lett.*, 2005, **94**, 038303.
13. A. H. Gröschel, F. H. Schacher, H. Schmalz, O. V. Borisov, E. B. Zhulina, A. Walther and A. H. E. Müller, *Nat. Commun.*, 2012, **3**, 710.
14. Y. Lu, J. Lin, L. Wang, L. Zhang and C. Cai, *Chem. Rev.*, 2020, **120**, 4111-4140.
15. D. J. Kraft, W. S. Vlug, C. M. van Kats, A. van Blaaderen, A. Imhof and W. K. Kegel, *J. Am. Chem. Soc.*, 2009, **131**, 1182-1186.
16. E. J. Foster, R. B. Jones, C. Lavigueur and V. E. Williams, *J. Am. Chem. Soc.*, 2006, **128**, 8569-8574.
17. T. L. Greaves and C. J. Drummond, *Chem. Soc. Rev.*, 2008, **37**, 1709-1726.
18. Y. Kim and N. Tamaoki, *Journal of Materials Chemistry C*, 2014, **2**, 9258-9264.
19. X. Li and X. Su, *Journal of Materials Chemistry B*, 2018, **6**, 4714-4730.
20. A. Akhmanova and M. O. Steinmetz, *Nat Rev Mol Cell Biol*, 2015, **16**, 711-726.

21. M. Fialkowski, K. J. M. Bishop, R. Klajn, S. K. Smoukov, C. J. Campbell and B. A. Grzybowski, *The Journal of Physical Chemistry B*, 2006, **110**, 2482-2496.
22. J. Babi, L. Zhu, A. Lin, A. Uva, H. El-Haddad, A. Peloewetse and H. Tran, *Journal of Polymer Science*, 2021, **59**, 2378-2404.
23. Y. Zhang, F. Fang, L. Li and J. Zhang, *ACS Biomaterials Science & Engineering*, 2020, **6**, 4816-4833.
24. X. Liu, B. Pi, H. Wang and X.-M. Wang, *Frontiers of Materials Science*, 2015, **9**, 1-13.
25. S. R. Batten, N. R. Champness, X.-M. Chen, J. Garcia-Martinez, S. Kitagawa, L. Öhrström, M. O'Keeffe, M. P. Suh and J. Reedijk, *CrystEngComm*, 2012, **14**.
26. H. Furukawa, E. Cordova Kyle, M. O'Keeffe and M. Yaghi Omar, *Science*, 2013, **341**, 1230444.
27. L. Li, R. Matsuda, I. Tanaka, H. Sato, P. Kanoo, H. J. Jeon, M. L. Foo, A. Wakamiya, Y. Murata and S. Kitagawa, *J. Am. Chem. Soc.*, 2014, **136**, 7543-7546.
28. B. A. Grzybowski, C. E. Wilmer, J. Kim, K. P. Browne and K. J. M. Bishop, *Soft Matter*, 2009, **5**, 1110-1128.
29. A. Patist, S. G. Oh, R. Leung and D. O. Shah, *Colloids and Surfaces A: Physicochemical and Engineering Aspects*, 2001, **176**, 3-16.
30. D. A. Fletcher and R. D. Mullins, *Nature*, 2010, **463**, 485-492.
31. T. Fukui, S. Kawai, S. Fujinuma, Y. Matsushita, T. Yasuda, T. Sakurai, S. Seki, M. Takeuchi and K. Sugiyasu, *Nat. Chem.*, 2017, **9**, 493-499.
32. F. Tantakitti, J. Boekhoven, X. Wang, R. V. Kazantsev, T. Yu, J. Li, E. Zhuang, R. Zandi, J. H. Ortony, C. J. Newcomb, L. C. Palmer, G. S. Shekhawat, M. O. de la Cruz, G. C. Schatz and S. I. Stupp, *Nature Materials*, 2016, **15**, 469-476.
33. L. S. Kariyawasam, M. M. Hossain and C. S. Hartley, *Angew. Chem. Int. Ed.*, **n/a**.
34. B. Rieß, R. K. Grötsch and J. Boekhoven, *Chem*, 2020, **6**, 552-578.
35. K. Das, L. Gabrielli and L. J. Prins, *Angew. Chem. Int. Ed.*, 2021, **60**, 20120-20143.
36. G. J. Brouhard and L. M. Rice, *Nature Reviews Molecular Cell Biology*, 2018, **19**, 451-463.
37. S. Chakraborti, K. Natarajan, J. Curiel, C. Janke and J. Liu, *Cytoskeleton (Hoboken)*, 2016, **73**, 521-550.
38. A. J. Matamoros and P. W. Baas, *Brain Research Bulletin*, 2016, **126**, 217-225.
39. K. H. Downing and E. Nogales, *Current Opinion in Structural Biology*, 1998, **8**, 785-791.
40. J. Al-Bassam and F. Chang, *Trends in Cell Biology*, 2011, **21**, 604-614.

41. S. A. P. van Rossum, M. Tena-Solsona, J. H. van Esch, R. Eelkema and J. Boekhoven, *Chem. Soc. Rev.*, 2017, **46**, 5519-5535.
42. T. Heuser, E. Weyandt and A. Walther, *Angew. Chem. Int. Ed. Engl.*, 2015, **54**, 13258-13262.
43. L. Heinen and A. Walther, *Chem. Sci.*, 2017, **8**, 4100-4107.
44. J. Boekhoven, A. M. Brizard, K. N. K. Kowligi, G. J. M. Koper, R. Eelkema and J. H. van Esch, *Angew. Chem. Int. Ed.*, 2010, **49**, 4825-4828.
45. A. Dasgupta and D. Das, *Langmuir*, 2019, **35**, 10704-10724.
46. Y. Deng, W. Zhan and G. Liang, *Advanced Healthcare Materials*, 2021, **10**, 2001211.
47. M. C. Branco, D. M. Sigano and J. P. Schneider, *Curr. Opin. Chem. Biol.*, 2011, **15**, 427-434.
48. S. Debnath, S. Roy and R. V. Ulijn, *J. Am. Chem. Soc.*, 2013, **135**, 16789-16792.
49. C. G. Pappas, I. R. Sasselli and R. V. Ulijn, *Angew. Chem. Int. Ed.*, 2015, **54**, 8119-8123.
50. C. Pezzato and L. J. Prins, *Nat. Commun.*, 2015, **6**, 7790.
51. S. Maiti, I. Fortunati, C. Ferrante, P. Scrimin and L. J. Prins, *Nat. Chem.*, 2016, **8**, 725-731.
52. S. Dhiman, A. Jain and S. J. George, *Angew. Chem. Int. Ed.*, 2017, **56**, 1329-1333.
53. A. Sorrenti, J. Leira-Iglesias, A. Sato and T. M. Hermans, *Nat. Commun.*, 2017, **8**, 15899.
54. P. Solís Muñana, G. Ragazzon, J. Dupont, C. Z.-J. Ren, L. J. Prins and J. L.-Y. Chen, *Angew. Chem. Int. Ed.*, 2018, **57**, 16469-16474.
55. L. Heinen and A. Walther, *Sci. Adv.*, 2019, **5**, eaaw0590.
56. M. A. Cardona and L. J. Prins, *Chem. Sci.*, 2020, **11**, 1518-1522.
57. D. Pei, B. Liu, S. Zhao, X. Shu, J. Nie and Y. Chang, *ACS Appl. Bio Mater.*, 2021, DOI: 10.1021/acsabm.1c00060.
58. M. J. Webber, C. J. Newcomb, R. Bitton and S. I. Stupp, *Soft Matter*, 2011, **7**, 9665-9672.
59. J. Leira-Iglesias, A. Sorrenti, A. Sato, P. A. Dunne and T. M. Hermans, *Chem. Commun.*, 2016, **52**, 9009-9012.
60. K. Jalani, S. Dhiman, A. Jain and S. J. George, *Chem. Sci.*, 2017, **8**, 6030-6036.
61. S. M. Morrow, I. Colomer and S. P. Fletcher, *Nat. Commun.*, 2019, **10**, 1011.
62. I. Maity, N. Wagner, R. Mukherjee, D. Dev, E. Peacock-Lopez, R. Cohen-Luria and G. Ashkenasy, *Nat. Commun.*, 2019, **10**, 4636.
63. W. A. Ogden and Z. Guan, *ChemSystemsChem*, 2020, **2**, e1900030.
64. M. Tena-Solsona, B. Rieß, R. K. Grötsch, F. C. Löhner, C. Wanzke, B. Käsdorf, A. R. Bausch, P. Müller-Buschbaum, O. Lieleg and J. Boekhoven, *Nat. Commun.*, 2017, **8**, 15895.

65. L. S. Kariyawasam and C. S. Hartley, *J. Am. Chem. Soc.*, 2017, **139**, 11949-11955.
66. B. Zhang, I. M. Jayalath, J. Ke, J. L. Sparks, C. S. Hartley and D. Konkolewicz, *Chem. Commun.*, 2019, **55**, 2086-2089.
67. M. M. Hossain, J. L. Atkinson and C. S. Hartley, *Angew. Chem. Int. Ed.*, 2020, **59**, 13807-13813.
68. I. M. Jayalath, H. Wang, G. Mantel, L. S. Kariyawasam and C. S. Hartley, *Org. Lett.*, 2020, **22**, 7567-7571.
69. L. S. Kariyawasam, J. C. Kron, R. Jiang, A. J. Sommer and C. S. Hartley, *J. Org. Chem.*, 2020, **85**, 682-690.
70. M. Cheng, C. Qian, Y. Ding, Y. Chen, T. Xiao, X. Lu, J. Jiang and L. Wang, *ACS Mater. Lett.*, 2020, **2**, 425-429.
71. F. Späth, C. Donau, A. M. Bergmann, M. Kränzlein, C. V. Synatschke, B. Rieger and J. Boekhoven, *J. Am. Chem. Soc.*, 2021, **143**, 4782-4789.
72. C. Wanzke, A. Jussupow, F. Kohler, H. Dietz, V. R. I. Kaila and J. Boekhoven, *ChemSystemsChem*, 2020, **2**, e1900044.
73. B. A. K. Kriebisch, A. Jussupow, A. M. Bergmann, F. Kohler, H. Dietz, V. R. I. Kaila and J. Boekhoven, *J. Am. Chem. Soc.*, 2019, **142**, 20837-20844.
74. R. K. Grötsch, C. Wanzke, M. Speckbacher, A. Angı, B. Rieger and J. Boekhoven, *J. Am. Chem. Soc.*, 2019, **141**, 9872-9878.
75. S. Bai, X. Niu, H. Wang, L. Wei, L. Liu, X. Liu, R. Eelkema, X. Guo, J. H. van Esch and Y. Wang, *Chem. Eng. J.*, 2021, **414**, 128877.
76. M. A. Würbser, P. S. Schwarz, J. Heckel, A. M. Bergmann, A. Walther and J. Boekhoven, *ChemSystemsChem*, **n/a**.
77. J. Heckel, S. Loescher, R. T. Mathers and A. Walther, *Angew. Chem.*, 2020.
78. J. Heckel, F. Batti, R. T. Mathers and A. Walther, *Soft Matter*, 2021, **17**, 5401-5409.
79. M. Tena-Solsona, C. Wanzke, B. Riess, A. R. Bausch and J. Boekhoven, *Nat. Commun.*, 2018, **9**, 2044.
80. P. S. Schwarz, S. Laha, J. Janssen, T. Huss, J. Boekhoven and C. A. Weber, *Chem. Sci.*, 2021, **12**, 7554-7560.
81. P. S. Schwarz, L. Tebcharani, J. E. Heger, P. Müller-Buschbaum and J. Boekhoven, *Chem. Sci.*, 2021, **12**, 9969-9976.
82. S. Bal, K. Das, S. Ahmed and D. Das, *Angew. Chem. Int. Ed.*, 2019, **58**, 244-247.
83. S. Bal, C. Ghosh, T. Ghosh, R. K. Vijayaraghavan and D. Das, *Angew. Chem. Int. Ed.*, 2020, **59**, 13506-13510.
84. C. Donau, F. Späth, M. Sosson, B. A. K. Kriebisch, F. Schnitter, M. Tena-Solsona, H.-S. Kang, E. Salibi, M. Sattler, H. Mutschler and J. Boekhoven, *Nat. Commun.*, 2020, **11**, 5167.
85. S. Mondal and D. Haldar, *New J. Chem.*, 2021, DOI: 10.1039/D0NJ05992G.

86. S. Panja, B. Dietrich and D. J. Adams, *ChemSystemsChem*, 2019, **2**, e1900038.
87. R. K. Grötsch, A. Angi, Y. G. Mideksa, C. Wanzke, M. Tena-Solsona, M. J. Feige, B. Rieger and J. Boekhoven, *Angew. Chem. Int. Ed.*, 2018, **57**, 14608-14612.
88. M. Tena-Solsona, J. Janssen, C. Wanzke, F. Schnitter, H. Park, B. Rieß, J. M. Gibbs, C. A. Weber and J. Boekhoven, *ChemSystemsChem*, 2021, **3**, e2000034.
89. A. J. Lomant and G. Fairbanks, *J. Mol. Biol.*, 1976, **104**, 243-261.
90. H. J. Goren and M. Fridkin, *Eur. J. Biochem.*, 1974, **41**, 263-272.
91. B. Rieß, C. Wanzke, M. Tena-Solsona, R. K. Grötsch, C. Maity and J. Boekhoven, *Soft Matter*, 2018, **14**, 4852-4859.
92. J. Boekhoven, W. E. Hendriksen, G. J. M. Koper, R. Eelkema and J. H. van Esch, *Science*, 2015, **349**, 1075-1079.
93. C. Wanzke, M. Tena-Solsona, B. Rieß, L. Tebcharani and J. Boekhoven, *Mater. Horiz.*, 2020, **7**, 1397-1403.